Long Span Bridges Under Wind Actions / A Non-Linear Fluid Force Model

Dissertation

submitted to and approved by the

Department of Architecture, Civil Engineering and Environmental Sciences
University of Braunschweig – Institute of Technology

and the

Faculty of Engineering
University of Florence

in candidacy for the degree of a
Doktor-Ingenieurin (Dr.-Ing.) /
Dottore di Ricerca in "Riduzione del Rischio da Catastrofi Naturali su Strutture ed Infrastrutture" *)

by
Laura Baro
Born 23.06.1981
from Padua, Italy

Submitted on	16 March 2011
Oral examination on	09 May 2011
Professorial advisors	Prof. A. Saetta Prof. U. Peil

2011

*) Either the German or the Italian form of the title may be used.

Abstract

Building new bridges is a primary factor in order to overcome obstacles and improve the connecting system of a site. The development of new technologies and materials has led to the construction of bridges characterized by high flexibility, low structural damping and lightness, thus very sensitive to wind actions. The importance of a careful analysis of wind effects on such kind of structures, in particular the assessment of the aerodynamic behaviour, is therefore reaffirmed.

In this thesis the vulnerability assessment of aeroelastic instability and buffeting oscillations are extensively investigated. The computation of self-excited force is usually performed through models based on coefficients evaluated by means of wind tunnel tests in smooth flow at a fixed value of the mean angle of attack. Several works have underlined how strong is the dependence of flutter derivatives with respect to the angle of attack. Furthermore flutter threshold is performed neglecting the effects due to the turbulent characteristics of the atmospheric flow. The development of a new force model able to predict the self-excited component of unsteady wind loads is here presented, taking into account also the effects produced by the presence of turbulence in order to investigate the above presented problems. The proposed time domain analysis framework is an improvement of the impulse response function load model that incorporates frequency dependent parameters of the load using the rational function technique.

A cable stayed bridge, recently built over the Adige river in Italy, is taken as a case study. Two different solutions of the deck section are designed and tested. A comparison between such solutions pointed out the important role played by the aerodynamic behaviour of the deck section. Furthermore, also the comparison between the response obtained with conventional linear approach and the one with the proposed nonlinear framework, outlined the importance of turbulence effects.

Abstrakt

Brücken sind ein wichtiger Bestandteil der Verkehrswege. Das Bestreben, immer schlankere Brücken mit immer größeren Spannweiten zu bauen, führt zu Brücken mit geringer Strukturdämpfung. Diese Entwicklung hat zur Folge, dass die Brücken sehr empfindlich auf Windlasten reagieren. Deshalb ist die sorgfältige Untersuchung der Windwirkung auf solche Bauwerke besonders wichtig.

In der hier vorgestellten Arbeit wird die Vulnerabilität von Brücken gegenüber aerodynamischer Instabilität und Flatterschwingungen untersucht. Zur Berechnung der selbsterregten Schwingungen werden in der Regel Rechenmodelle in Verbindung mit Windkanalversuchen verwendet. Die Flatterderivativa werden, bei diesen Versuchen, in glatter Strömung für einen festen, mittlernen Anströmwinkel ermittelt. Eine Vielzahl von Untersuchungen zeigt die große Abhängigkeit der Flatterderivativa vom Anströmungswinkel. Außerdem wird die Turbulenz des natürlichen Windes bei der Berechnung der Flatterwindgeschwindigkeit nicht berücksichtigt. Deshalb soll hier die Entwicklung eines neuen Modells zur Ermittlung der selbsterregenden, instationären Windkräfte vorgestellt werden, das auch die Turbulenz des Windes berücksichtigt. Der dafür vorgeschlagene Ansatz im Zeitbereich ist eine Weiterentwicklung des Impulsantwortfunktionsmodells, das mit Hilfe rationaler Funktionen den frequenzabhängigen Anteil der Windkräfte berücksichtigt.

Abschließend wird mit einer Fallstudie die Bedeutung der aerodynamischen Eigenschaften einer Brücke untersucht. Als Beispiel dient eine neue Schrägseilbrücke in Italien über den Adige. Für diese Brücke werden zwei unterschiedliche Brückenquerschnitte untersucht. Die Antwort beider Querschnitte auf die Windkräfte wird sowohl mit einem konventionellen, linearen Ansatz als auch mit dem hier vorgestellten nichtlinearen Ansatz berechnet. Die Untersuchung zeigt die Bedeutung der Turbulenz des natürlichen Windes auf das Flatterverhalten der Brückenquerschnitte.

Acknowledgments

First of all I would like to thank both Prof. Borri and Prof. Peil for their efforts as coordinators of the Graduate College; they give me the possibility of flying out of Italy for the first time in my life. Furthermore, I have really appreciated the internationality of the program which make me possible to get in contact with different people. This experience has enriched me a lot.

My gratitude also goes to the research group of Padua, first of all to my Italian tutor, Prof. Anna Saetta who has supported me and pushed my willingness to complete this work. Moreover, I would like to express my thankfulness to Prof. Vitaliani who introduced me to this research group. I am also very grateful to Giuseppe Olivato, who has accompanied me for these three years. He has been not only a great office mate but also a good friend who has taken particular care of me during my first experience in Braunshweig.

A special thank goes to Claudio Mannini, for his sustain and encouragement during this last year: “Claudio, I really appreciate the help you gave me!”.

I also would like to thank all the colleagues of the International Doctoral Course for their friendly companionship, in particular Enzo, Tobi, Arno, Silvio, Paola, Timm, Diego, Tommaso, Giovanni, Andrea e Laura. I enjoyed very much all the moments spent together.

Contents

List of figures

List of tables

Chapter 1

Introduction

1.1 Motivations

In recent years the awareness about the risk of natural (but also financial and political) disasters is highly increased among public, businesses and lawmakers. This have led to the growing of several organization for monitoring the international situations and promote researches in order to improve preparedness and responses in case of emergencies.

The "Centre for Research on the Epidemiology of Disaster" (CRED) every year furnishes a detailed statistical review of the annual disaster occurred worldwide. The database subdivides the events in the following 5 groups:

- **Geophysical**: Events originating from solid earth;
- **Meteorological**: Events caused by short-lived/small to meso scale atmospheric processes;
- **Hydrological**: Events caused by deviations in the normal water cycle and/or overflow of bodies of water caused by wind set-up;
- **Climatological**: Events caused by long-lived/meso to macro scale processes;
- **Biological**: Disaster caused by the exposure of living organisms to germs and toxic substances.

In Fig. 1 the natural disaster classification is reported, while in Table 1 the average values computed in the period between 2000 and 2008 about the number of natural disasters occurrence, related victims and damages are reported.

Looking at the data reported in Fig. 2, it can be observed that meteorological disasters account for about one third of all natural disasters throughout the world, but for more than one half if only the economical aspect is considered. Moreover, as reported in (Berz, 2005), windstorm disasters (including storm surges) account for more than two thirds of the insured losses and the trend analyses reveal that major windstorm disasters have increased drastically in recent decades, as well

as the losses they caused. This is mainly due to both climate change that is in act in last decades and the migration of people and goods towards wind hazardous area.

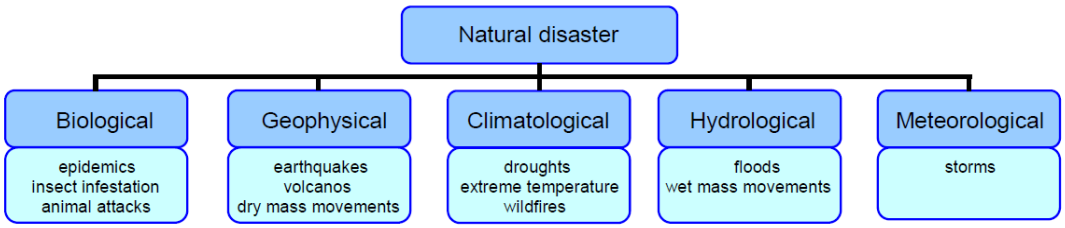

Fig. 1: Natural disaster classification (Vos, Rodriguez, Below, & Guha-Sapir, 2010)

	Number of occurrence	Number of victims (millions)	Damages (US$ billions)
Climatological	54	83.89	9.39
Geophysical	37	9.03	19.67
Hydrological	194	99.15	19.94
Meteorological	108	38.79	53.63

Table 1: Natural disaster occurrence and impacts (Vos, Rodriguez, Below, & Guha-Sapir, 2010)

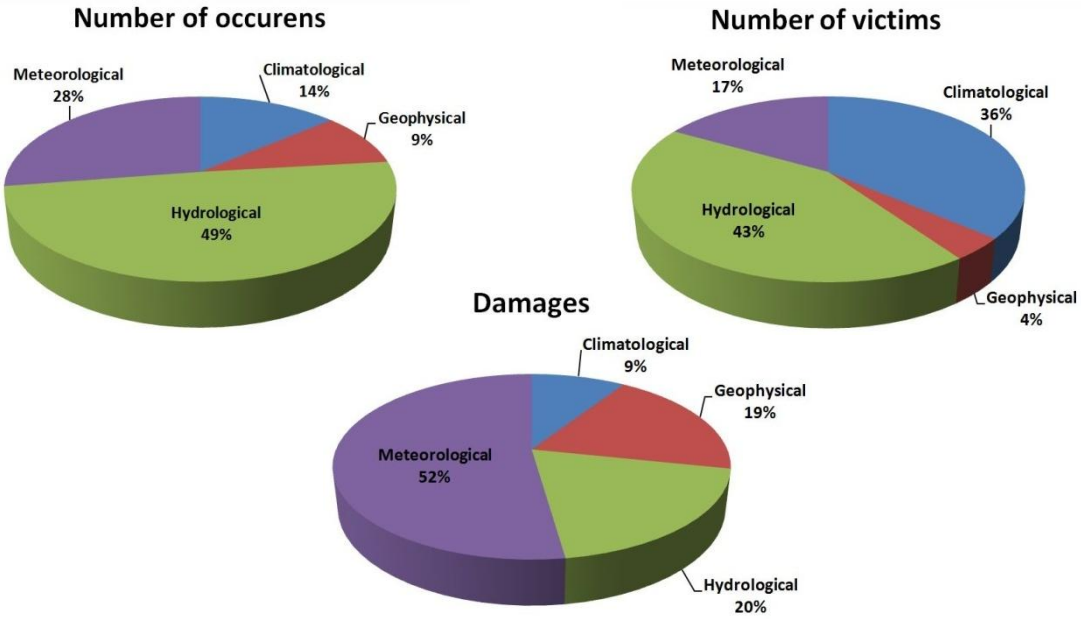

Fig. 2: Natural disaster occurrence and impacts (percentage values)

As reported in (Augusti, Borri, & Niemann, 2001) besides the heavy damages that can originate from windstorms, also other types of discomforts can be caused by moderate winds. Such type of hazardous events are classified with the name of dissatisfaction risk and include wind borne pollution, canyoning between buildings and pedestrian discomfort among the others. In particular, looking at civil structures, small storms can affect non-structural components giving rise to users discomfort and higher costly maintenance. Bridges, for example, plays a key role in the connection of two parts of a town and they are of crucial importance for evacuating areas in case of emergency. Moreover, the risk of their closure to traffic due to serviceability problem when moderate wind blow could happened several times a year, with highly economical and social impact.

Even if fluid-structure interaction has been studied since the infamous collapse of the Tacoma Narrows Bridge on November 1940, wind induced phenomena are still a topic of challenge. Let's think about the recent event occurs to St. Vitus bridge on the evening of May 20, 2010 when a gale-force winds induced structural deck vibrations with oscillations up to 1 metre (RIANOVOSTI, 2010), Fig. 3.

Fig. 3: St. Vitus bridge over Volga river

This bridge was built in the southern Russian city of Volgograd over the Volga river. The bridge have a total length of about seven kilometres and its deck is made of a concrete girder cross section. The structure was inaugurated on October 10, 2009 after 13 years of construction. When the event occurs drivers said that, because of the violently shaking conditions, their cars were literally thrown into the air sometimes causing vehicles to jump into the opposite lane and creating chaos. Some of them have also stated that seeing the deck moving in that manner makes themselves feeling afraid and, because of panic, they started to run faster in an unsafely manner.

Despite many years of experience with this particular deck design, this was the first time that such type of phenomena happened. This episode confirms that the wind-structure interaction knowledge needs to be deeply investigated.

1.2 Overview of the thesis

Within the general framework of risk management, the analysis of wind induced forces on bridges is the main focus of this thesis. It is well-known that wind forces are the most important loads which have to be considered in the designing process of long-span bridges. Both static and aerodynamic analysis must be performed to properly investigate the safety of these structures. In particular, static loads are responsible for structural displacements and may produced large stresses in all the elements. Furthermore, dynamic phenomena may be arisen due to aerodynamic effects. Among all of them a thoroughly study of self-excited forces is carried out. The literature shows that the hypothesis of linear structure and linear load are commonly accepted. For this reason several approaches in the frequency domain are considered the most suitable and effective tools for a correct evaluation of the instability threshold. However, the recent trend is to design structures with increasingly longer spans thanks to the development of high-performance materials and new construction technologies. This has lead toward the increase of bridge decks flexibility so that both structural and load nonlinearities are usually not anymore negligible. This is not only a matter of long span bridges, but also of smaller ones, like footbridges, because of their trend towards the design of lighter and more transparent structures. For these reasons in recent years more sophisticate wind load models have been developed in time domain. The main goal of this thesis is the development of a new and innovative force model for the simulation of loads nonlinearities.

This dissertation is organized as following reported:

In chapter 2 a general overview of the risk management framework will be provided. In particular it will be discussed how the work presented in this thesis fits into the risk chain.

Since buffeting analysis of rigid structures performed in time domain needs the knowledge of atmospheric turbulence features, in chapter 3 the mathematical modelling of the turbulent velocity field of natural wind is presented. Furthermore the procedures available in literature for the numerical generation of the wind field are examined.

Chapter 4 starts with a global review about various aeroelastic phenomena due to wind-structure interaction. In particular, a detailed studied of the literature about wind load models for the evaluation of self-excited and buffeting forces, which are two of the main aeroelastic forces acting on bridge decks, are extensively described. Both frequency and time domain approaches have been deeply reviewed and compared. Then a literature survey of nonlinear force models developed in recent years is given. It has been highlighted the different hypothesis on which they are based and how they take into account of aeroelastic nonlinearities. Finally, the development of a new and original nonlinear load approach is presented and discussed.

A finite element model for the structural discretization is presented in chapter 5. A general computational framework has been developed for the analysis of flutter instability and buffeting response in presence of self-excited forces. Both linearized quasi-steady and unsteady aerodynamic wind forces in time domain, described in section 4.3 and 4.4, have been implemented as well as the proposed nonlinear force model.

In chapter 6 the case study of the cable-stayed bridge recently built over the Adige river, in Italy, is investigated. In the preliminary design of the bridge deck, as first choice a box section was initially chosen, but just before its realizations, for economical reasons it was decided to open the bottom part of the cross-section. The aerodynamic behaviour of both sections have been investigated by means of wind tunnel tests. Furthermore, since the bridge has been already realized, an experimental campaign of the real structure has been performed. The knowledge of all these data allows the development of both sectional and full-order models in good agreement with structural and aerodynamic characteristics of the real bridge. By means of the developed computational framework, static and dynamic analysis have been performed. At first, the investigation of the flutter threshold has been conducted by means of classical linear force models. A comparison between results obtained using both sectional and full-order models has been addressed. Then, the same analysis have been repeated evaluating the self-excited force components by means of the new force model presented in section 4.7, so that the effects of load nonlinearities have been deeply investigated and discussed.

Finally, in chapter 7 the achievements of this research work are drawn and possible future developments in this field are discussed.

Chapter 2

The risk management

2.1 Risk management overview

Until few years ago, the design process of a structure, as well as of a complex systems, was performed following deterministic approaches based on the experience achieved in that field along the years. Even the prescriptions imposed by national codes were usually based on deterministic formulas. Modern codes, such as Eurocode, have introduced some probabilistic concepts and fixed some performance objectives providing a step forward in risk management practices. However, it is still impossible to speak of a design philosophy completely consistent with the risk management approach since the coefficients that these codes provide are based on empirical data and are not calibrated in a probabilistic way. Only with the recent development of the so called Performance-Based Design a general framework, focused on the optimization of specific performance objectives achieved in a probabilistic way, has been realized providing a tool for an integral structural design. This approach was initially developed in the seismic field; anyway, the fundamental concept on which it is based can be extended to any other context; in particular its implementation in case of wind loads is reported in (Paulotto, Ciampoli, & Augusti, 2004) and in (Petrini, 2009).

The field of risk analysis has assumed increasing importance in recent years, given the concern by both the public and private sectors in safety, health and environmental problems. In fact, because of the increasing number and the gravity of natural hazards which have been recorded in last decades (Parry, 2007), the concept of disaster risk management has been evolved over years. At the beginning, the focus was devolved only towards the improvement of all the operational activities for the disaster response in case of emergency, instead of reduction or prevention. Subsequently, also the monitoring, the maintenance and the early-warning of a system have become increasingly important until nowadays, where the concept of risk management encompasses all those pre-emptive actions based on the philosophy that it is irresponsible and wasteful waiting for an accident to happen and then figuring out how to prevent it from happening

again. The risk management framework has developed with the aim of providing a complete and effective tool for an optimized design and for the implementation of new protection systems.

An extensive use of this approach has been adopted by companies to satisfy their need to measure the financial impact of natural catastrophes on infrastructures. It is usually adopted with the purpose to anticipate the likelihood and severity of catastrophic events—like earthquakes, hurricanes, terrorism, crop failure and so on, so that companies, as well as governmental institutions, can properly get ready for their financial impact.

The probability that a hazardous event could cause damage to a given system, either because the adopted protection fails or because a rare event occurs, can never be equal to zero; this means that the presence of a residual risk is unavoidable. For this reason, early warning systems are nowadays a powerful forecasting tool based on modern technologies and sophisticate procedures.

Different procedures, definitions and terminologies are available in literature and each one is affected by the specific needs of the individual or the organization dealing with it. This can lead to misunderstandings and confusion. For this reason a common and unique framework has been developed and adopted within the IGC 802. It is able to fit the necessity of all different actors and can be applied to any field.

The Risk Management Chain proposed is a useful decision-making tool based on the systematic identifications of both risks and benefits, so that the best actions for any given situation can be determined. In Fig. 4 the risk management chain developed in (Pliefke, Sperbeck, Urban, Peil, & Budelmann, 2007) is reported.

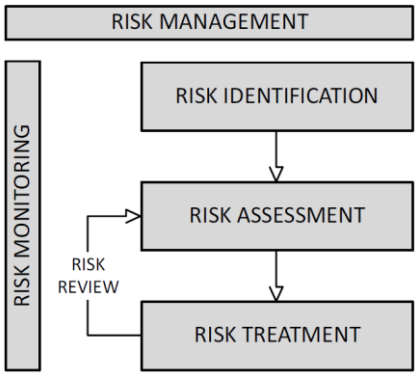

Fig. 4: The general risk management framework (Pliefke, Sperbeck, Urban, Peil, & Budelmann, 2007)

The flowchart above is composed by three main components that allow to go through the risk management chain: Risk Identification, Risk Assessment and Risk Treatment.

Trying to estimate potential future losses, the very first task is the risk identification, whose purposes is to create a catalogue of possible future harmful events. These will form the basis to reach appropriate conclusions about the perils (e.g. hurricanes) that may strike the system under analysis. Usually these are detected thanks to experience, common sense and specific analytical tools. The proper evaluations of risk sources depends on the time and costs of analysis efforts and the state of the technology involved.

The following step is the risk assessment. In this phase the level of risk associated with a specific hazards must be determined. The qualitative and quantitative measurements performed during the identification phase are fundamental for the risk quantification of any possible detrimental scenario. In other words this is the phase in which the likelihood and severity of an accident due to hazard events is defined. Its evaluation is based upon the exposure of the analyzed system. At this stage of the risk management process, engineers make their contribution to the risk evaluation through the continuous development of appropriate mathematical models. A deep insight on risk assessment will be addressed in the next section.

As final step, after all the risk sources have been detected and evaluated, the risk treatment focuses on the costs and benefits analysis of all the possible alternative remedial actions. The main task of this phase is the development of mathematical tools that support the identification of the appropriate decision-maker about how to address the risk. The main strategies that can be adopted are four: Risk Mitigation, Risk Transfer, Risk Acceptance and Risk rejection.

If a risk mitigation initiatives is implemented, three are the actions that can be adopted: reduction of the hazard, reduction of the exposure and reduction of the vulnerability. The hazard reduction can be addressed only when the hazard source is not by nature but rather a man-induced one. The exposure may be modified just choosing a different area to build the structure or the system under investigation. Anyway, this solution rarely can be adopted since the choice of the place usually is a fixed parameter that cannot be changed. Finally, the vulnerability mitigation can be performed looking for innovative technical solutions that better respond to the required needs. A deeper insight on these component will be afforded in the next section.

Each one of the presented three step constitutes the basis for the next one, and must be completed before proceeding further. Once the first run of the risk management chain is performed, controls strategies must be established and the process have to be periodically re-evaluated to ensure its effectiveness. These are the tasks of risk review and risk monitoring processes. Workers and managers at every level must fulfil their respective roles to assure that the controls are maintained over time. The risk management process continues throughout the life cycle of the system, mission or activity. The plan to apply the selected control system, as well as the time, materials and personnel that need to put these measures in place, has to be formulated in detail.

2.2 Risk assessment

Risk assessment phase is the basis of the risk mitigation planning. This step represents the main task for engineers and others professional subjects, since it concerns the development of mathematical models suited to the simulate every possible scenarios and to evaluate the relative risk.

As it is shown in Fig. 5, risk assessment essentially splits into two components: the risk analysis and the risk evaluation. The first is the process that allows the assessment of consequences suffered by the system under analysis once the hazard is completely defined. The second, as principal target, has the definition of parameters useful to build an appropriate grading of the

consequences on the analysed system, so that the comparison with other competing risks could be performed. The risk evaluation provides an effective tool for those who will make the choice of which type of risk treatment must be adopted.

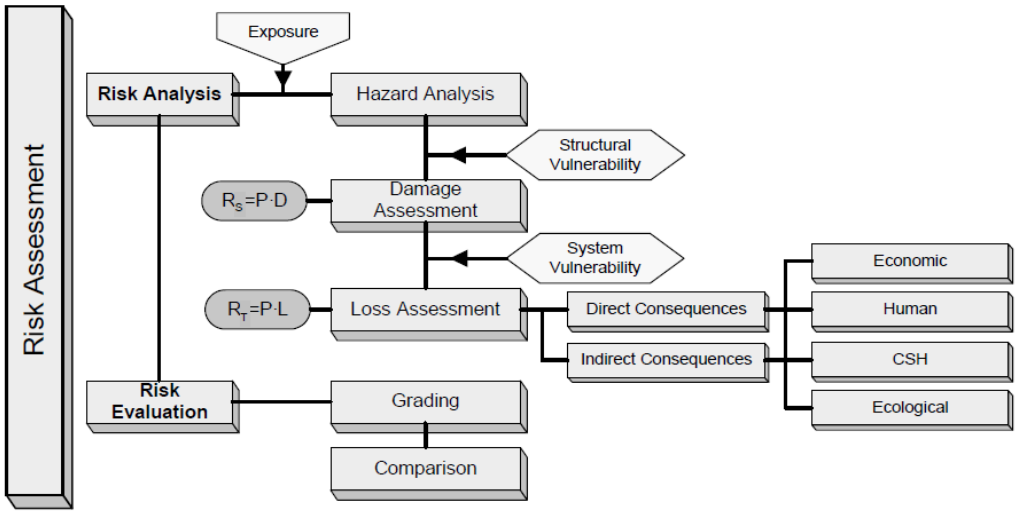

Fig. 5: Risk Assessment phase (Pliefke, Sperbeck, Urban, Peil, & Budelmann, 2007)

Before going on talking about risk analysis, it is fundamental to define what the word "risk" is referred to. Lots of definitions are available in literature, each one developed to better fit into the needs of a specific case study. Although it is often possible to understand from the discussion context what is the exact meaning of the used words, the lack of a common language may create confusion, generating difficulties in the relationship between different subjects involved in the process. In (Pliefke, Sperbeck, Urban, Peil, & Budelmann, 2007) a definition of risk which can be easily applied in any context is provided. The word "risk" indicates the product between the probability of an event to occur and the given consequences when the event really occurs. The total risk associated with an activity can be computed as the sum over all possible events of the risk concerning each event, as reported in (2.1).

$$\text{Risk} = \sum_{\text{events}} \text{Probability} * \text{Consequences} \tag{2.1}$$

The product, actually, is a convolution integral since it has to be extend over all the event probabilities or, in other words, over all the hazard levels. The probability in (2.1) has to be represented by the intensity of one parameter which must satisfy the requirements of sufficiency, computability and efficiency. It is quite common to represent the probability of an event occurrence by means of the so-called "Exceedance Probability curve" which describes the probability that different levels of the parameter magnitude will be exceeded. These statistical curves are usually based on a large catalogue of events. Since the past is not always indicative of the future, the catalogue therefore can include events more or less extreme than those that could occur. Particular attention should be paid when the intensity of an event relating to a long period has to be extrapolated from data relating to a shorter one.

Looking at the consequences term, as shown in Fig. 5, they could be direct or indirect, where the firsts refer to those effects caused immediately by the event, and the others consider all the long-term secondary effects. Moreover, losses can be catalogued in four different categories, not all quantifiable in monetary terms. Anyway, economic losses can be related to human losses even though not by a perfect correlation.

As previously observed, in the Risk Management Framework there is a sort of confusion about the different meaning that some words can have in various literature approaches. In particular, (Olivato 2010) proposed a different meaning of the word “exposure” and it will be later reported.

Furthermore, (Olivato 2010) proposed a new Risk Analysis Chain. In this approach, the meaning of the word “Chain” is stressed giving to the graph a linear shape, where the output of one phase is the input for the next one.

As previously stated, the risk analysis phase starts with the identification and definition of a possible hazardous event, so called hazard analysis, and ends with the evaluation of damages and financial losses. Defined the starting point of the analysis process, several steps, or chain rings, must be followed in order to establish the amount of losses incurred by the system. A detailed description of all the possible rings and their interdependencies is reported in Fig. 6. The chain has been developed considering meteorological events as promoters of catastrophic events; for this reason the Hazard at the beginning of the chain is supposed to be the “Nature”.

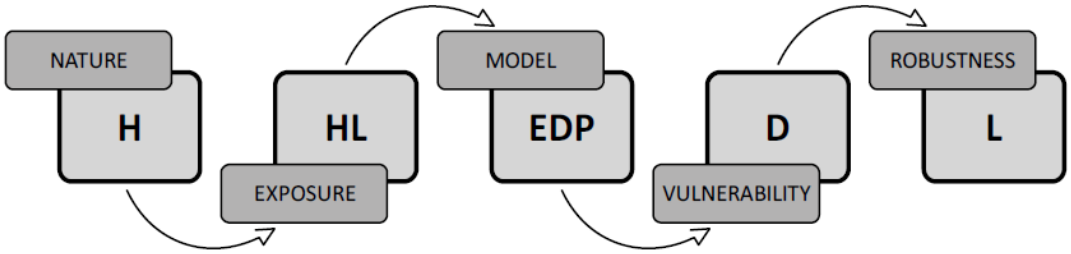

Fig. 6: Risk Analysis chain (Olivato, 2010)

Then the “Exposure” of the investigated system must be evaluate. It consists in the evaluation of the probability that the hazardous event meets something to damage. In case of a complex system, it is useful to subdivided it in several element at risk. In this way it is possible to create an inventory of those artefacts that are exposed to the hazard. The Exposure can be measured as a dimensionless factor ranged between 0 and 1. If just one structure is considered and nothing can be changed of the system under analysis, then the exposure is equal to the unity. Starting from the exposure knowledge it is possible to evaluate the Hazard Load. It represents how the harmful source is acting on the structure, for example how much it is the force acting on the bridge deck when hit by a specific value of the wind speed. Its physical size is one of those typically assumed by loads, like forces, pressures, accelerations. Then it is possible to calculate the structural response, also known as Engineering Demand Parameter. In the civil engineering field FEM models are widely used to simulate the structural behaviour and so obtain the response information as stress resultants, displacements, vibrations. The numerical model adopted may be more or less accurate depending on the level of details achieved by the structural discretization. The numerical codes

usually implemented do not support any type of uncertainties in the computed results, in the sense that given a specific set of input data the response is calculated in a deterministic way. Anyway some probabilistic numerical models have been recently developed, but their complexity are normally extremely high even when a limited number of parameters are considered.

The next step is the evaluation of the damage level by means of the structural vulnerability assessment or, in other word, the physical consequences suffered by the structure due to an hazard load. The structural damage can be represented in a scale of percentages (0% no damage; 100% totally destroyed), or by means of a classification as: none, slight, moderate, extensive, or complete damage. As a matter of fact, the definition of the damage level through the knowledge of the structural response is difficult to perform. Sometimes it is more convenient starting from the knowledge of the hazard intensity and directly estimate the probability of exceeding a specific damage level. This type of information are efficiently resume by means of the so called fragility curves. Their construction is usually performed by means of statistical methods once the knowledge of a sufficient amount of data is available. Also individualized fragility curves based on extensive computational simulations may be drawn instead of the classical empirical or experiential ones.

The vulnerability analysis allows to quantify the physical effect of a specific catastrophic event in terms understandable by any person. This is a fundamental aspect since the next step, the Loss assessment, is generally performed by economists who have no training in the engineering field. As final result it is obtained the evaluation of the amount of expected losses expressed in: losses/time [euros/year]. The opportunity to assess the risk of any problem through the use of a unique and homogeneous parameter gives to the decision maker a useful tool for the development of an appropriate decision plan.

As previously stated, the most efficient approach to mathematically perform the risk analysis is by means of the Performance Based Design method whose implementation can be performed in many different field since it is based on general principles that can be adapted to any context, even if not always in an easy way.

Referring to the nomenclature adopted in the risk chain of Fig. 6, the total risk of the system under analysis can be evaluated by the following convolution integral:

$$\mathrm{R} = \int \mathrm{L}\ \mathrm{f(L|D)}\ \mathrm{f(D|EDP)}\ \mathrm{f(EDP|HL)}\ \mathrm{f(HL|H)}\ \mathrm{dH}\ \mathrm{dHL}\ \mathrm{dEDP}\ \mathrm{dD}\ \mathrm{dL} \tag{2.2}$$

where the generic term $f(\cdot \mid \cdot)$ is the conditional probability density function.

The integral is extended over all the possible Hazard whose probabilities of exceedance have been determined through the hazard analysis.

The equation (2.2) takes into account all the chain rings presented in the analysis risk stage. It is evident that, when one of the steps is performed in a deterministic way, some simplifications have to be introduced also in the proposed formula since it is not considered any kind of uncertainty. For example, if fragility curves are adopted to perform the risk analysis of a specific structure, then the

vulnerability analysis is performed just in one single step, given that the probability of a damage to occur can be directly evaluated starting from the assessment of the hazard intensity: $f(D|H)$.

In the particular case of bridges subject to wind load, the mean wind velocity value is usually chosen as input hazard parameter while two different limit states can be adopted as performance objectives: a low performance level which only looks at the structural collapse, and a high performance level to ensure the comfort and the structural serviceability behaviour.

2.3 Thesis contribution

The interaction between a fluid flow and a bluff body is a complex phenomenon whose simulations is of critical importance for the proper evaluation of the dynamic response of a long-span bridge. A great number of research in this field have been performed starting from the collapse of the Tacoma Narrows Bridge in 1940. Despite that, current theories are not always capable to correctly predict the aeroelastic behaviour of a structure, as recently pointed out by the episode of St. Vitus bridge over the Volga river. This is a recent example of the crucial role of an accurate simulation of the structural response due to the action of site winds, which stresses the need for improved analytical and numerical models to better simulate such complex phenomena. Since the current trend of designers is towards a progressive increase in the main span length, the importance of a careful analysis of wind effects on these structures is reaffirmed.

The main focus of this research work is on flutter instability and buffeting response, two of the predominant types of wind-induced vibration sources of long-span bridges. In current practise, it is quite common to neglect buffeting terms for the study of instability analysis. The interaction of the load mechanism of both turbulence-related forces and self-excited component must be investigated to achieve an optimal bridge deck design. In fact, the understanding of turbulence effects on long-span bridge stability is a topic of the current investigation.

An important point to take well-informed decisions regarding risk management is a correct assessment of the structural vulnerability. In other words, improving the comprehension of aeroelastic phenomena leads to their better simulations and consequently towards a more efficient design. The main contribution of this work concerns the better evaluation of the Hazard Load. With this aim, a refine and innovative model for the evaluation of self-excited forces have been developed considering the nonlinearities due to both reduced frequency and effective angle of incidence.

Chapter 3

Wind field description

3.1 Introduction

One of the primary purposes of wind engineering research is to predict the random response of a structure when immersed in a flow. The associated fluctuating pressure is the effect of the complex interaction between the flow field and the structural motion. Its knowledge is basic to the study of wind loading. In particular, wind-induced forces have to be evaluated as function of the turbulent field acting around the body. The resulting loads depend on structural shape, location on the structure, and the characteristics of wind (such as wind speed and angle of attack). So, the numerical simulation of the wind velocity field can be considered as the starting point to investigate in a complete and comprehensive way the wind-structure interaction.

In this chapter the fundamental properties of the flow in the atmospheric boundary layer are recalled. At first a mathematical description of the velocity field is given. As the case study presented in chapter 6 is about an Italian bridge, the numerical parameters used by the Italian code to characterize the mathematical wind model in this zone are reported as reference values. In the second part of the chapter a brief review of the most commonly used numerical models for the wind field simulation and an exhaustive description of one of them are provided.

3.2 Mathematical model

In a macro-meteorological sense, winds are movements of air masses in the atmosphere mainly originated by temperature differences. The flow that is of interest in structural design is the one located in the lower layer of the atmosphere known as the atmospheric boundary layer. This is the region where the characteristics of the flow are directly influenced by the presence of the Earth's surface, so that the flow field is not constant with height. The depth of the boundary layer generally ranges from a few hundred meters to several kilometres, and on it, the influence of the frictional forces becomes increasingly important as the earth's surface is approached. Within the atmospheric boundary layer, the wind is studied as a multidimensional stochastic process, function

of both time and space. At the top of the atmospheric boundary layer the magnitude of the wind velocity is often referred to as the gradient speed and can be assumed as horizontally homogeneous and stationary; while in the lowest 10% the shear is approximately constant and the production of turbulence is high: this region is called the atmospheric surface layer. An overview of the parameters for the description of the flow in this region is addressed in this section. The models here presented are valid only for neutral stability, this means that vertical heat transfer is negligible. An interesting characterisation of these surface winds is their kinetic energy distribution in the frequency domain, which is known as Van der Hoven spectrum (Van der Hoven, 1957), whose typical spectrum is illustrated in Fig. 7. Note that the figure shows the power spectral density S_V multiplied with the angular frequency ω, to highlight the value in the right hand side of the diagram.

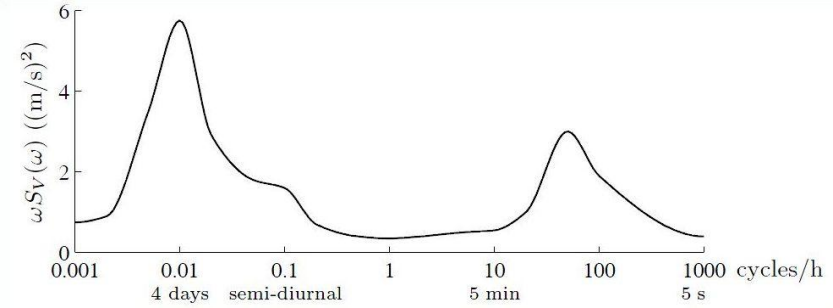

Fig. 7: Van der Hoven spectrum

Although there are differences in some details, the spectra measured in different sites follow almost the same pattern. Independently of the site, the spectrum exhibits two mesometeorological peaks, one approximately at 0.01 cycles/h (4-days cycles), associated with the passage of a typical weather system past a fixed point, and one at 0.1 cycles/h (1 day cycles), referred to the frequency of daily wind, and a micrometeorological peak at 50 cycles/h referred to a period of about one minute due to local gust. The low frequency side of the spectrum corresponds to geostrophic winds whereas the high frequency side represents the turbulence associated to local winds, these two sides are separated by the so called spectral gap, where the amount of variance in periods between approximately 10 minutes and about 5-10 hours is very low. The spectral gap means that the wind climate and the turbulence in the atmospheric boundary layer are mutually independent, so the mean wind velocity U is separately considered from $u(t)$ which is the fluctuating component of the wind that is usually treated as a stationary stochastic process because it arises as the effects of turbulence.

The wind turbulent component observed at one point in space can be defined by three orthogonal components: u is the instantaneous wind velocity along the mean wind direction, v the horizontal component, normal to u, and w the vertical component. If a right hand Cartesian system oriented with the X-axis in the direction of the mean wind velocity is considered, the velocity at time t can be written as:

$$\begin{aligned} U(z) + u(x,y,z,t) &\quad \text{in X-direction (along wind)} \\ v(x,y,z,t) &\quad \text{in Y-direction (across wind)} \\ w(x,y,z,t) &\quad \text{in Z-direction (vertical)} \end{aligned} \tag{3.1}$$

where $U(z)$ is the mean wind velocity, which depends on the height z above the ground, u, v and w are the zero mean fluctuating components of the wind velocity field, treated as stationary stochastic processes.

3.2.1 Mean wind velocity

The mean wind velocity in built-up terrain is calculated starting from meteorological data obtained by means of measurements at weather stations, under standard meteorological circumstances, measured at 10 m over relatively smooth grass land, conventionally calculated over a time intervals of 10 minutes. In codes and standards this reference velocity is usually provided with reference to a return period of 50 years. Because the annual extreme wind velocity usually fits the extreme value distribution of Type 1 (Gumbel distribution), it is possible to calculate the reference mean wind velocity for any others different return periods.

The probability of occurrence of a given mean wind velocity is not the same in all directions, since predominant wind directions may be present. Only by means of on-site measurements it is possible obtain such information, usually represented through directional probability diagrams called wind speed rosettes.

It is possible to evaluate the mean wind velocity value in any places if the roughness length of the terrain, the height of the point respect to the ground and the mean wind reference velocity for that specific area are known. The mathematical models widely used at this purposes are following reported.

Roughness length

The roughness length is a parameter that affects the intensity mechanical turbulence above the surface and it is used to model the horizontal mean wind speed near the ground. It can be interpreted as the size of a characteristic vortex, which is form as a result of friction between the air and the ground surface, and represent the height above ground at which the mean wind velocity is zero. An illustration of the roughness length z_0 is reported in Fig. 8.

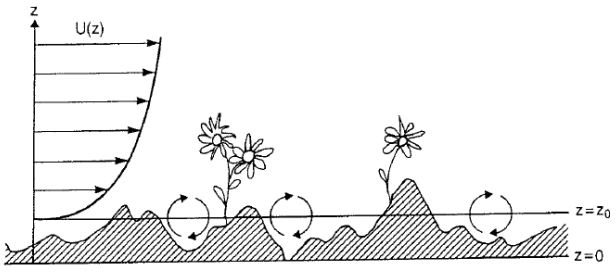

Fig. 8: Roughness length representation

The roughness of a particular surface area is determined by the size and distribution of the roughness elements it contains; for land surfaces these are typically vegetation, built-up areas and the soil surface, while over water it depends on the wind velocity since the wind interacts with the water surface by inducing waves that increase the roughness. Codes and standards report tables which associate roughness length values to terrain categories. The values of z_0 range from few microns (for plane ice) up to some meters (for urban areas).

Wind profile models

Close to the ground the velocity gradient depends upon the friction velocity, the air density and the height z above ground. The friction velocity $u_*$is a parameter that depend on the roughness of the ground in function of the shear surface stress τ_0:

$$u_* = \sqrt{\tau_0/\rho} \tag{3.2}$$

Usually it is in the order of magnitude between 1-2 m/s.

Based upon a dimensional analysis, a differential equations for the mean wind velocities can be formulated and, if there is a long flat terrain upstream, its solution leads to the following expression of the logarithmic profile:

$$U(z) = \frac{u_*}{k} \ln \frac{z-d}{z_0} \tag{3.3}$$

where k is the von Karman's constant ($k \cong 0.4$), d is a corrected height of the surface level between densely built obstacles, and z_0 is the roughness length that characterized the surface texture.

The logarithmic law is valid for homogeneous and stationary flow under neutral conditions and it is not valid close to build at windward side.

The different shape assumed by the logarithmic profile in function of the value of the roughness length is reported in Fig. 9.

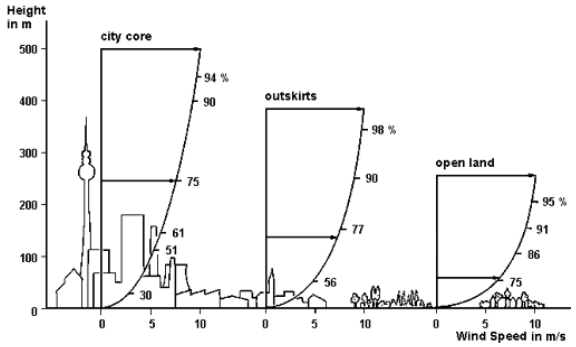

Fig. 9: Decrease in wind speed as influenced by different value of terrain roughness

In the Italian code (CNR, 2008) the value of the mean wind velocity is defined as:

$$U(z) = v_r k_r \ln \frac{z-d}{z_0} \tag{3.4}$$

where v_r is the reference velocity and k_r is a parameter called terrain factor, function of the roughness.

Historically the first representation of the mean wind profile has been the power law:

$$U(z) = U(z_{ref}) \left(\frac{z}{z_{ref}} \right)^{\alpha} \tag{3.5}$$

where α is an exponent dependent upon the roughness of terrain with constant value upon up to the gradient height.

Currently the logarithmic law is regarded by meteorologists as superior representation of strong wind profiles in the lower atmosphere.

Return period

As previously mentioned, the mean wind velocity usually reported in codes and standards is referred to a return period of 50 years. The Italian code (CNR, 2008) provide the possibility to evaluate the mean wind velocity value respect to a different return period, introducing a parameter called the return coefficient c_r plotted in Fig. 10:

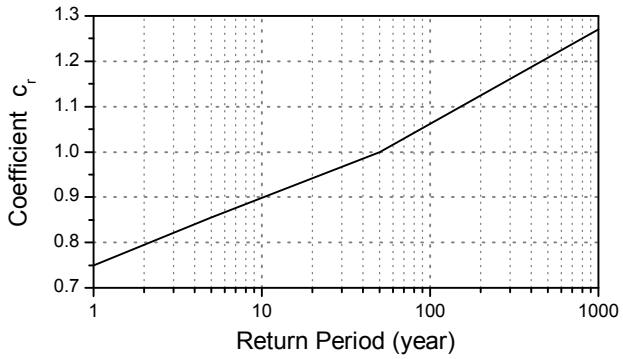

Fig. 10: Return coefficient vs. Return period

In particular, for return period over 50 years it is possible to use the following equation:

$$\mathrm{c_r} = 0{,}65 \left\{ 1 - 0{,}138 \ln \left[-\ln \left[1 - \frac{1}{\mathrm{T_R}} \right] \right] \right\} \tag{3.6}$$

where T_R is the return period value of interest expressed in [years].

3.2.2 Turbulent wind component

The turbulent component of a wind flow can be described by means of several parameters: the standard deviation and the turbulence intensity, the time scales and integral length scales, the power-spectral density function, that define the frequency distribution, and the coherence function, that specify the spatial correlation.

Standard deviation and turbulence intensity

Assuming homogeneous terrain the statistical characteristics of the flow can be considered as they do not change in a horizontal plane, so the standard deviation of the turbulence component σ_u, σ_v and σ_w only depend on the height z above ground. The standard deviations are close to zero at the top of the boundary layer where the flow is not disturbed by the interaction with terrain roughness, and they increase toward the ground. Experimental results show that the three standard deviations usually decrease with height very slowly up to the heights of ordinary structures, and that they are almost constant up to a height of about 100-200 m above homogeneous terrain. Their value can be approximated as:

$$\sigma_u = A\, u_* \qquad \sigma_v = 0.75\, \sigma_u \qquad \sigma_w = 0.50\, \sigma_u \tag{3.7}$$

where A is a parameter that does not vary with height z, but depend only on the roughness of the ground. In (Simiu & Scanlan, 1996) it is reported that:

$$A = \sqrt{\beta} \qquad \sigma_u^2 = \beta u_*^2 \tag{3.8}$$

and the β parameter depends only on the roughness, as reported in Table 2:

z_0 [m]	0.005	0.07	0.30	1.00	2.50
β	6.5	6.0	5.25	4.85	4.00

Table 2: Values of β reported in (Simiu & Scanlan, 1996).

In the Italian code (CNR, 2008) the value of the standard deviation is defined as:

$$\sigma_u = v_r\, k_r \tag{3.9}$$

The turbulence intensity is the dimensionless ratio between the standard deviation and the mean wind velocity at the measurement height z:

$$I_u = \frac{\sigma_u}{U(z)} \qquad I_v = \frac{\sigma_v}{U(z)} \qquad I_w = \frac{\sigma_w}{U(z)} \tag{3.10}$$

From (3.3), (3.9) and (3.10), it follows that:

$$I_u = \frac{1}{\ln \frac{z}{z_0}} \qquad I_v = 0.75\, I_u \qquad I_w = 0.50\, I_u \tag{3.11}$$

Time scale and integral length scale

The fluctuating wind components, u, v and w, may be said having a characteristic memory time, the so-called time scale $T(z)$. Measurements of the turbulence component taken at time t give a great deal of information about itself at a time τ later if $\tau \ll T(z)$ but only little information

if $\tau \gg T(z)$. So, the integral time scale is a common quantitative characterization of the time needed for a signal to decorrelate. The formal definition of time scale $T(z)$ is:

$$T(z) = \int_0^\infty R_u^T(z,\tau)d\tau \tag{3.12}$$

where $R_u^T(z,\tau)$ is the auto-correlation function (or auto-covariance) of the turbulence component u, at time t and $t+\tau$ normalized:

$$R_u^T(z,\tau) = \frac{1}{\sigma_u^2(z)}\, E\{u(x,y,z,t)u(x,y,z,t+\tau)\} \tag{3.13}$$

The autocorrelation function indicates how much information a measurement of the turbulence component $u(x,y,z,t)$ in the mean wind direction will provide about the value of $u(x,y,z,t+\tau)$ measured time τ later, at the same place. The auto-correlation function depends only on height z above ground and on time difference τ due to the assumption of a horizontally homogeneous flow.

If it is considered that the fluctuations in the wind velocity can be assumed to be a superposition of eddies with different size and frequency, then the integral length scale is an estimation of the size of the largest eddies, and it varies with height and depends on the roughness of the upwind terrain. In the real non periodic flow the integral length scale can be computed starting from the space–time correlation function as follows:

$$L_u^x = \int_0^\infty \rho_u(z,r_x)dr_x \tag{3.14}$$

where $\rho_u(z,r_x)$ is the correlation function of the turbulence component u in two different points longitudinally separated by a distance r_x and measured simultaneously:

$$\rho_u(z,r_x) = \frac{1}{\sigma_u^2(z)}\, E\{u(x_1,y_1,z_1)u(x_1+x,y_1+y,z_1+z)\} \tag{3.15}$$

Many measurement points are needed to obtain an acceptable accuracy value. The integral length scales depend on the height z above ground and on the roughness of the terrain z_0, in particular the integral length scale decrease with increasing surface roughness. The wind velocity may also influence the integral length scales at a site.

In the same way, a total of nine integral length scale, and corresponding nine time scale, can be evaluated, corresponding with the u, v and w component of the flow evaluated in the along-wind, cross-wind and vertical direction (x, y and z).

For low turbulence intensity ($I_u < 10\%$) it is assumed that the fluctuations travel with the mean wind velocity. The structure of the eddies does not change in the travel period and the turbulence is called “frozen”. This assumption is known with the name of Taylor’s hypothesis, and it is normally considered to be an accurate approximation in natural wind. The Taylor’s hypothesis

implies that can be assumed $\rho_u(z, r_x) = R_u^T(z, \tau)$, when $r_x = U(z)\tau$, indicating that the longitudinal integral length scale is equal to the time scale multiplied by the mean wind velocity:

$$L_u^x(z) = U(z)T(z) = U(z)\frac{1}{\sigma_u^2}\int_0^\infty R_u^T(z,\tau)d\tau \tag{3.16}$$

In the Italian code (CNR, 2008) the value of the integral length scale is defined as:

$$L_u(z) = 300\left(\frac{z}{200}\right)^\lambda \qquad L_v(z) = 0.25\,L_u(z) \qquad L_w(z) = 0.10 L_u(z) \tag{3.17}$$

where λ is a coefficient whose value depend on the roughness of the terrain. This mathematical expression is close to the empirical one suggested in (Counihan, 1975).

Power-spectral density function

In order to describe the distribution of turbulence with frequency, a function called the *spectral density,* usually abbreviated to "spectrum", is used. Spectral density function are calculated from time series of fluctuating signals by using Fourier techniques. It is defined that the contribution to the variance, σ_u^2, in the range of frequencies from n to $n + dn$, is given by $S_u(n)dn$, where $S_u(n)$ is the spectral density function for $u(t)$. To allow easily spectrum comparison between experiments under different conditions, usually the turbulence is described by the nondimentional power spectral density function $S_N(z, n)$ defined as:

$$S_N(z,n) = \frac{nS_u(z,n)}{\sigma_u^2} \tag{3.18}$$

where n is the frequency in Hz, and $S_u(z, n)$ is the power spectrum for the along-wind turbulence component (similar expression can be write for the other turbulent component).
Then integrating over all frequencies the spectrum, it is obtained:

$$\sigma_u^2 = \int_0^\infty S_u(n)dn \tag{3.19}$$

The Wiener–Khinchin theorem (Ricker, 2003) states that the power spectral density of a wide-sense-stationary random process is the Fourier transform of the corresponding autocorrelation function:

$$\begin{aligned} S_u(n) &= \frac{1}{2\pi}\int_{-\infty}^{+\infty} R_u(\tau)e^{-i\omega\tau}d\tau = \frac{1}{2\pi}\int_{-\infty}^{+\infty} R_u(\tau)\cos(\omega\tau)d\tau \\ R_u(\tau) &= \int_{-\infty}^{\infty} S_u(\omega)e^{i\omega\tau}d\omega = \int_{-\infty}^{\infty} S_u(\omega)\cos(\omega\tau)d\omega \end{aligned} \tag{3.20}$$

In Fig. 11 a schematic view of a spectrum in the neutral atmospheric boundary layer as function of frequency n is given.

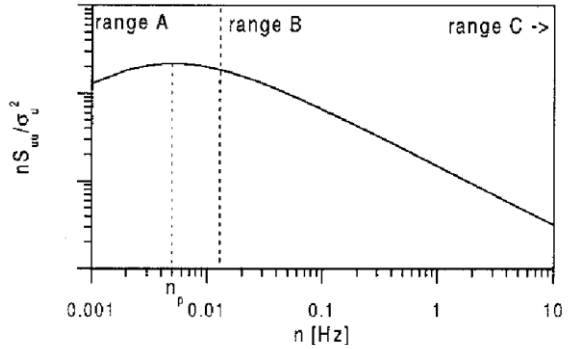

Fig. 11: Schematic view of a wind velocity spectrum in the atmospheric boundary layer.

In neutral condition, energy is produced at low frequency (range A) by shear. In range B, which is called the inertial sub range, energy is passed down to smaller scales (high frequencies), this means that there is a transfer of energy from larger eddies to smaller ones, and that there is little production or dissipation of energy in this range. The slope of the spectrum in the inertial sub range usually is of -5/3, and the normalized spectrum has a slope of -2/3. Finally in range C, kinetic energy is dissipated into internal energy (heat). The frequencies of interest for the determination of dynamic response of buildings are in the order of 0.1 to 10 Hz, that is in the inertial sub range. Detailed descriptions of the spectral properties in the atmospheric boundary layer are contained in references like (Panofsky & Dutton, 1984) and (Kaimal & Finnigan, 1995).

Theoretically, the spectra in the atmospheric boundary layer fit into the following general expression, in (Olesen, Larsen, & Hojstrup, 1984):

$$\frac{nS_{ii}(z,n)}{\sigma_i^2} = \frac{Af^{\gamma}}{(C+Bf^{\alpha})^{\beta}} \qquad i = u,v,w \tag{3.21}$$

where f is a nondimensional parameter called reduced frequency, defined as:

$$f = \frac{nz}{U(z)} \tag{3.22}$$

The shape and position of the spectra are determined by the coefficient $\alpha, \beta, \gamma, A, B \; and \; C$. These coefficients can be calculated for equilibrium flow from theoretical considerations, in particular the values of $A, B \; and \; C$ depend on the ratios σ_i/u^*.

The most common spectra that have been used for $S_u(n)$ in meteorology and wind engineering for the longitudinal velocity component is the von Karman/Harris form (developed for laboratory turbulence by (von Karman, 1948), and adapted for wind engineering by (Harris, 1968)).

$$\frac{nS_u(z,n)}{\sigma_u^2} = \frac{4\left(\frac{nl_u}{U(z)}\right)}{\left[1+70.8\left(\frac{nl_u}{U(z)}\right)^2\right]^{5/6}} \tag{3.23}$$

where l_u is a turbulence length scale that varies with both terrain roughness and height.

In the Italian code (CNR, 2008) the expressions of the normalized spectra are defined as:

$$\frac{n\,S_u(z,n)}{\sigma_u^2} = \frac{n\,S_u(z,n)}{I_u^2(z)\,U^2(z)} = \frac{6{,}868\,n\,L_u(z)/U(z)}{\left[1+10.302\,n\frac{L_u(z)}{U(z)}\right]^{5/3}}$$

$$\frac{n\,S_v(z,n)}{\sigma_v^2} = \frac{n\,S_v(z,n)}{I_v^2(z)\,U^2(z)} = \frac{9.434\,n\,L_v(z)/U(z)}{\left[1+14.151\,n\frac{L_v(z)}{U(z)}\right]^{5/3}} \tag{3.24}$$

$$\frac{n\,S_w(z,n)}{\sigma_w^2} = \frac{n\,S_w(z,n)}{I_w^2(z)\,U^2(z)} = \frac{6.103\,n\,L_w(z)/U(z)}{1+63.181\left[n\frac{L_w(z)}{U(z)}\right]^{5/3}}$$

Coherence function

The wind velocity fluctuations do not vary only in time but also in space. In the frequency domain, the relation between the wind velocity fluctuations at two separated points is given by the cross spectra:

$$S_{cross} = \sqrt{S_u(x,y,z)S_u(x',y',z')}\;coh(x,y,z,x',y',z',n) \tag{3.25}$$

where coh is the coherence function (Davenport, 1961).

A widely accepted formula for the coherence of the longitudinal wind velocity for lateral and vertical separation is the exponential one:

$$coh(y,z,y',z',n) = e^{-n\frac{2\sqrt{(y-y')^2C_y^2+(z-z')^2C_z^2}}{U(z)+U(z')}} \tag{3.26}$$

where C_y and C_z are called decay factors and are experimentally derived. The decay factors depend on the wind velocity and height. A wide range of values for the decay factors from several experiments are reported in (Solari, 1987). The coherence relation in the along-wind direction is taken into account by means of the Taylor hypotesis. From a mathematical point of view this implies a modification of the cross correlation function:

$$R(\tau) = \frac{1}{2\pi}\int_0^{+\infty} S_{cross}\cos\big(w(t+\tau)\big)\,dt$$

$$\tau = \frac{x_1}{U_1} + \frac{x_2}{U_2} \tag{3.27}$$

where τ represents the time the signal takes on average to go from point 1 to point 2.

In the Italian code (CNR, 2008) the expressions of the coherence function is defined as:

$$Coh_{jj}(x,y,z,x',y',z',n) = e^{-n\frac{2\sqrt{(x-x')^2C_{jx}^2+(y-y')^2C_{jy}^2+(z-z')^2C_{jz}^2}}{U(z)+U(z')}} \tag{3.28}$$

where C_{jr} are the decaying factors of the j-th turbulent component in the r direction, that are reported in Table 3:

C_{1x}	C_{1y}	C_{1z}	C_{2x}	C_{2y}	C_{2z}	C_{3x}	C_{3y}	C_{3z}
3.0	10.p	10.0	3.0	6.5	6.5	0.5	6.5	3.0

Table 3: Decaying factors (CNR, 2008).

3.3 Numerical wind generation

Several approaches for the numerical simulation of multivariate and multidimensional processes with a specific cross-spectral density function are available in literature. They can be mainly subdivide in two categories: those performed in the frequency domain, which are based on the superposition principle, and those performed in time domain that are founded on the weighted sum on previous observations of white-noise. In particular, the most famous and renowned work about the numerical simulation in the frequency domain is that proposed in (Shinozuka, 1970) which simulate the random processes by means of the sum of cosine functions with random frequencies and random phase angles (wave superimposition technique). Instead, for what concern the second approach, the most popular algorithms are the AR (auto regressive) and the ARMA (auto regressive moving average). Both of them are founded on purely statistic considerations where the generation of the signal at a given time is performed through a linear combination of the previous events plus a stochastic component. In particular the AR method can be seen as a particular case of the most general ARMA model. Details about these models can be found in (Samaras, Shinozuka, & Tsurui, 1983) and (Li & Kareem, 1990) among the others.

The main difference between these two models stands in the way they describe the purely stochastic contribution. Moreover, ARMA models usually allow a faster generation. A description and comparison of these models can be found in (Samaras, Shinozuka, & Tsurui, 1983) as well as in (Rossi, Lazzari, & Vitaliani, 2004).

In this section the model proposed by Shinozuka is presented, and it will be used to generate the wind field on structures that are going to be analysed.

Shinozuka – Deodatis model

The basic method for analyzing multidimensional, multivariate non-Gaussian process is introduced by (Shinozuka & Jan, 1972). In (Shinozuka, 1974) the fast Fourier transform (FFT) technique is introduced into the algorithm of simulation, improving the computational efficiency. A further development of the spectral representation method to simulate an ergodic stochastic wind velocity field is reported in (Deodatis, 1996).

If a one-dimensional, multivariate stochastic process $\{u(t)\}$,which has n components $u_1(t), u_2(t), \dots, u_n(t)$, with zero as mean value is considered, its cross-spectral density matrix can be write as:

$$S(\omega) = \begin{bmatrix} S_{11}(\omega) & S_{12}(\omega) & \dots & S_{1n}(\omega) \\ S_{21}(\omega) & S_{22}(\omega) & \dots & S_{2n}(\omega) \\ \dots & \dots & \dots & \dots \\ S_{n1}(\omega) & S_{n2}(\omega) & \dots & S_{nn}(\omega) \end{bmatrix} \tag{3.29}$$

$S(\omega)$ is usually a complex matrix, because the generic element $S_{ij}(\omega)$ is formed by the cospectrum (the real part of the cross-spectrum) and the quadrature spectrum (imaginary part of the cross-spectrum). Usually the orthogonal spectrum of wind velocity is very small in atmosphere, so it can be neglected. Hence $S(\omega)$ is a real matrix, whose general element can be expressed as:

$$S_{ij}(\omega) = \sqrt{S_{ii}(\omega)\, S_{jj}(\omega)}\, Coh(\Delta_{ij}, \omega) \tag{3.30}$$

where $Coh(\Delta_{\mathrm{ij}}, \omega)$ is the coherence between the two points, and Δ_{ij} represents their distance.

In the algorithm proposed by Shinozuka the first step is to rewrite the cross-spectral density matrix as the product of a matrix and its transpose:

$$S(\omega) = H(\omega) H^T(\omega) \tag{3.31}$$

where $H(\omega)$ is a lower triangular matrix obtained by the decomposition of $S(\omega)$using Cholesky's method:

$$H(\omega) = \begin{bmatrix} H_{11}(\omega) & 0 & \dots & 0 \\ H_{21}(\omega) & H_{22}(\omega) & \dots & 0 \\ \dots & \dots & \dots & \dots \\ H_{n1}(\omega) & H_{n2}(\omega) & \dots & H_{nn}(\omega) \end{bmatrix} \tag{3.32}$$

Once $S(\omega)$ is decomposed, according to the work of Shinozuka, the typical component $u_j(t)$ of the process can be simulated by the following series:

$$u_j(t) = \sqrt{2\Delta\omega} \sum_{m=1}^{j} \sum_{l=1}^{N} (H_{jm}(\omega_{ml})) \cos(\omega_{ml} t + \phi_{\mathrm{ml}}) \tag{3.33}$$

where N is the number of subdivision of the frequency domain, $\Delta\omega$ is the frequency increment, ϕ_{ml} are random numbers from the uniform distribution in the range $[0 - 2\pi]$, $\omega_{ml} = (l-1)\Delta\omega + (m/N_P)\Delta\omega$, N_P is the number of points, and $\omega_{up} = N\Delta\omega$ is the upper cut-off frequency (so the highest frequency over which the value of $S(\omega)$ is ignored). A criterion to estimate the value of ω_{up} can be found in (Shinozuka & Deodatis, 1991).

If a sufficiently high number of N is used, the simulated functions quite approximate the target process. The use of ω_{ml} guarantee that the simulated stochastic vector is ergodic in the mean value and in correlation, only when the length of the generated sample function is equal to one period. In fact, the simulated signal is periodic, and its period can be evaluated by the formula:

$$T_0 = \frac{2\pi N}{\omega_{up}} N_P \tag{3.34}$$

The ergodicity of the sample function is in the sense that the temporally-averaged mean value and autocorrelation function are identical with the corresponding targets.

Eq.(3.34) indicates that the smaller the $\Delta\omega$, or equivalently the larger the N under a specified upper cut-off frequency ω_{up}, the longer the period of the simulated stochastic process.

The efficiency of the algorithm of simulation can be enhanced greatly by utilizing the FFT technique. Introducing Euler's formula in Eq.(3.33), the generated signal can be expressed by:

$$u_j(t) = \sqrt{2\Delta\omega}\, Re\left\{\sum_{l=1}^{N}\left(\left(\sum_{m=1}^{j} H_{jm}(\omega_{ml})\right) \mathrm{e}^{\mathrm{i}(\omega_{ml}t+\phi_{\mathrm{ml}})}\right)\right\} \tag{3.35}$$

That can be rewritten as:

$$\begin{aligned} u_j(t) &= \sqrt{2\Delta\omega}\, Re\left\{\sum_{m=1}^{j}\left[\sum_{l=1}^{N} H_{jm}(\omega_{ml})\, \mathrm{e}^{\mathrm{i}(lt\Delta\omega+\phi_{\mathrm{ml}})}\right] \mathrm{e}^{\mathrm{i}\left(\frac{m}{N_P}t\Delta\omega\right)}\right\} \\ &= \sqrt{2\Delta\omega}\, Re\left\{\sum_{m=1}^{j}\left[\sum_{l=1}^{N}\left(H_{jm}(\omega_{ml})\, \mathrm{e}^{\mathrm{i}\phi_{\mathrm{ml}}}\right) \mathrm{e}^{\mathrm{i}lt\Delta\omega}\right] \mathrm{e}^{\mathrm{i}\left(\frac{m}{N_P}t\Delta\omega\right)}\right\} \end{aligned} \tag{3.36}$$

The series on brackets (sum on l), is a periodic function with period $T_1 = 2\pi/\Delta\omega$, and can be generated efficiently using the FFT techniques. It is worth noting that the following relation between T_1 and T_0 stands:

$$T_0 = T_1\, N_P \tag{3.37}$$

Simultaneous simulation of horizontal and vertical turbulence.

A generic wind velocity field is composed by three varying components that varies along the deck of the bridge. Hence, the complete wind velocity field should be treated as a multidimensional, multivariate, homogeneous Gaussian stochastic process. In order to properly evaluate the structural response a bridge deck, there are two wind components that have to be taken into account: the longitudinal and the vertical ones. The simultaneous simulation of both the turbulence component can be performed by means of the algorithm presented before, just extending the cross-spectral density matrix in the following way:

$$S(\omega) = \begin{bmatrix} S_u(\omega) & S_{uv}(\omega) \\ S_{uv}^T(\omega) & S_v(\omega) \end{bmatrix} \tag{3.38}$$

where $S_{uv}(\omega)$ is the cross-spectrum between the two turbulent component.

If no experimental data are available, it is possible to use a cross-spectrum derived from literature. One of these was proposed by Kaimal (Kaimal, Wyngaard, Izumi, & Coté, 1972):

$$\frac{n\,S_{uv}(n)}{u_*^2} = \frac{-14\frac{nz}{U}}{\left(1+9.6\left(\frac{nz}{U}\right)\right)^{2.4}} \tag{3.39}$$

Wind generation for bridge decks

The wind velocity field for a long span bridge can be computed as a combination of three independent one-dimensional multivariate stochastic processes with the coherence between different dimensions ignored. Thus, the errors included are usually small (Cao, Xiang, & Zhou, 2000). Moreover it is possible to approximately take the spectra of wind velocity as not varying along the length of the bridge, thus the spectra at each point on the bridge deck is the same:

$$\begin{aligned} S_{11}(\omega) = S_{22}(\omega) = \cdots = S_{nn}(\omega) \\ S_{ij}(\omega) = \sqrt{S_{ii}(\omega)S_{jj}(\omega)}\;Coh(\Delta_{ij}\omega) \end{aligned} \tag{3.40}$$

The model usually adopted for the coherence function is an exponential one:

$$Coh\left(\Delta_{ij}\omega\right) = e^{A(\omega)\Delta_{ij}} \tag{3.41}$$

If a uniformly distribution of n points on the bridge deck is considered, with a distance interval Δ between successive points the coherence function can be rewritten as:

$$Coh\left(\Delta_{ij}\omega\right) = e^{A(\omega)\Delta\,|\mathrm{i-j}|} = C^{|\mathrm{i-j}|} \tag{3.42}$$

The cross spectrum density matrix becomes:

$$S(\omega) = \begin{bmatrix} 1 & C & C^2 & \dots & C^{n-1} \\ C & 1 & C & \dots & C^{n-2} \\ C^2 & C & 1 & \dots & C^{n-3} \\ \vdots & \vdots & \vdots & \ddots & \vdots \\ C^{n-1} & C^{n-2} & C^{n-3} & \dots & 1 \end{bmatrix} \tag{3.43}$$

In this case the Cholesky's decomposition $H(\omega)$ of the cross-spectrum matrix, can be expressed in explicit form:

$$H(\omega) = \sqrt{S(\omega)}G(\omega) \tag{3.44}$$

where:

$$G(\omega) = \begin{bmatrix} 1 & 0 & 0 & \dots & 0 \\ C & \sqrt{1-C^2} & 0 & \dots & 0 \\ C^2 & C\sqrt{1-C^2} & \sqrt{1-C^2} & \dots & 0 \\ \vdots & \vdots & \vdots & \ddots & \vdots \\ C^{n-1} & C^{n-2}\sqrt{1-C^2} & C^{n-3}\sqrt{1-C^2} & \dots & \sqrt{1-C^2} \end{bmatrix} \tag{3.45}$$

Using these expression in Eq.(3.33), the general component $u_j(t)$ can be rewritten as follows:

$$u_j(t) = \sqrt{2\Delta\omega} \sum_{m=1}^{j} \sum_{l=1}^{N} \sqrt{S_{jm}(\omega_{ml})} G_{jm}(\omega_{ml}) \cos(\omega_{ml} t + \phi_{\mathrm{ml}}) \tag{3.46}$$

This is the simplified formula that can be used to simulate one of the three independent dimensional multivariate stochastic processes.

Chapter 4

Wind load models

4.1 Fluid-structure interaction

The main target of Aerodynamic and Aeroelastic disciplines is the analysis of wind loads acting on a structure when affected by a flow.

The main assumption considered in the Aerodynamic field is that the body subjected to the wind action experiments small displacements. Such hypothesis allows to consider the undeformed configuration as the reference one; in this case the structural response (R) does not depend on fluid-structure interaction effects. In such situation the mechanism of the structural response generation is schematically represented by the chain in Fig. 12 where the aerodynamic forces are indicated by the symbol F_a.

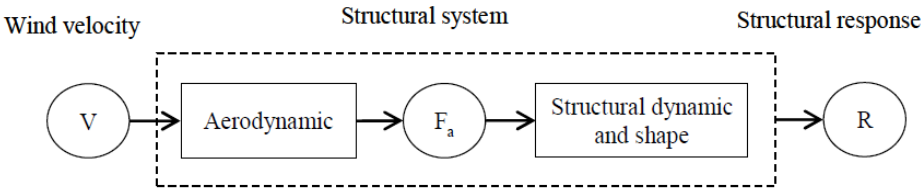

Fig. 12: Aerodynamic "chain" (Petrini, 2009)

In the Aeroelasticity field, instead, the interaction between the flow field and the structural motion is the crucial point for the proper evaluation of the wind load. This interaction is a typical phenomenon that occurs when elastic structures are analyzed. In fact, if the body significantly moves under the wind induced forces, these deflections change the boundary conditions in the surrounding flow, affecting the fluid forces which in turn will influence the deflections. In other word, aerodynamic forces are function of structural displacements, and structural displacements are function of the aerodynamic forces. Such forces are usually referred as "self-excited" and all the structural instability phenomena that could arise are due to self-excited forces that act upon the body as a consequence of its motion.

The chain shown in Fig. 13 represents the mechanism of the structural response generation, where the self-excited forces generated from the fluid-structure interaction mechanism are indicated by the symbol F_{se}.

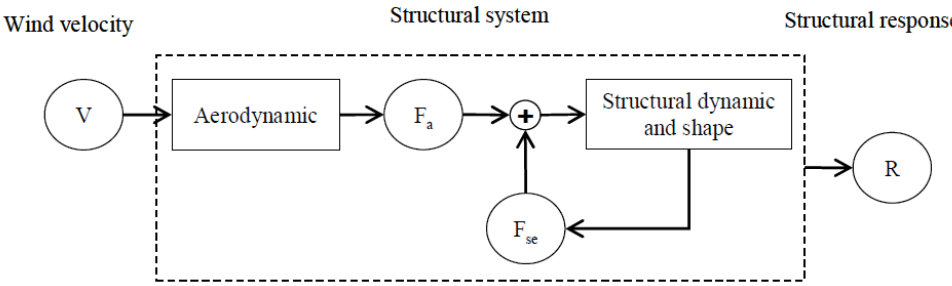

Fig. 13: Aeroelastic "chain" (Petrini, 2009)

Another definition of aeroelasticity has been provided by Arthur Collar in 1947. He defined the concept of aeroelasticity as *"the study of the mutual interaction that takes place within the triangle of the inertial, elastic and aerodynamic forces acting on structural members exposed to an airstream, and the influence of this study on design".* This concept is graphically represented in Fig. 14 where A, E and I are respectively the aerodynamic, elastic and inertial forces.

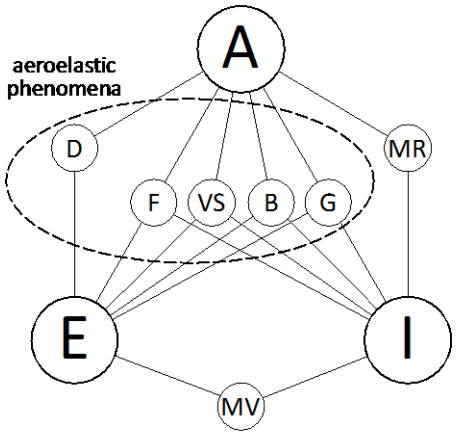

Aeroelastic Phenomena	
Tors. Divergence	D
Vortex Shedding	VS
Galloping	G
Flutter	F
Buffeting	B

Non Aeroelastic Phenomena	
Mechanics of Vibrations	MV
Mechanics of rigid body	MR

Fig. 14: Collar's triangle

In the reported diagram it is possible to identify three different types of phenomena depending on the force component involved. Only a brief description of aeroelastic phenomena, which involve both elastic and aerodynamic forces, is reported hereafter, while a thorough study about flutter instability and buffeting load will be later provided.

Hereafter, the term "aeroelastic force" will be used to mark all the wind loads components that give rise to aeroelastic phenomena.

Torsional divergence

Torsional divergence is the first type of aeroelastic instability recognized and understood. It is a static instability phenomenon in which torsional moment due to aeroelastic forces overcomes the elastic resistant moment of the body.

Divergence speed is evaluated considering the equation of motions for one single degree of freedom, ignoring inertial effects. Since the static nature of this phenomenon, it can be studied representing the wind forces by means of a steady load model. So, the critical divergent wind speed is evaluated through the simplified equilibrium equation obtained by linearizing the aerodynamic moment coefficient around the deformed position ($\alpha = \alpha_0$), as reported in section 4.3. The divergence wind speed is obtained when vanishing value of the total stiffness is reached:

$$\mathrm{U_{div}} = \sqrt{\frac{2\mathrm{K_\alpha}}{\rho B^2 C'_M(\alpha_0)}} \tag{4.1}$$

where K_α is the torsional stiffness, ρ is the air density, B the deck width and $C'_M(\alpha_0)$ is the derivative of the moment aerodynamic coefficient evaluated in correspondence of α_0.

Torsional divergence is usually not a very relating problem to bridge structures, as it tends to appear with wind speed sensibly higher than the flutter one.

Galloping

Galloping refers to structural vibrations in a direction almost perpendicular to the wind one, mainly because of negative aerodynamic damping. An asymmetry in the flow starts a vertical oscillation that leads to fluctuating aerodynamic forces. Their intensity depend on both body velocity oscillations and aerodynamic damping value. The motion becomes unstable if the aerodynamic damping is opposite and greater than the structural one.

Also in this case, galloping wind speed is calculated considering the equation of vertical motions, which describes the wind forces by means of the steady load equations linearized around the deformed position ($\alpha = \alpha_0$), as reported in section 4.3. Galloping critical wind speed is reached when the total damping value vanishes:

$$\mathrm{U_g} = -\frac{2\mathrm{C_h}}{\rho \mathrm{B}\left(\mathrm{C_D}(\alpha_0) + \mathrm{C'_L}(\alpha_0)\right)} \tag{4.2}$$

where C_h is the structural damping of the vertical motion. Looking at (4.2) it is remarkable that a negative aerodynamic damping is the necessary condition for galloping occurrence:

$$\mathrm{C_D}(\alpha_0) + \mathrm{C'_L}(\alpha_0) < 0 \tag{4.3}$$

This is a typical type of instability of non-circular slender structures like iced cables; however, it doesn't usually affect bridges deck.

Vortex shedding

When a body is invested by a wind, the separation of flow occurs around the body and produces forces on it: a pressure force on the windward side and a suction force on the leeward side. Both these forces result in the generation of vortices in the wake region, causing structural deflections. The shedding of vortices balances the change of fluid momentum along the whole body surface. The structural response depends on the vortices shed frequency. In particular, when the natural frequency of the structure and the wake ones are not close each others, the structural response is the same as that of a rigid and fixed body. On the other hand, when the vortex-induced and the structural frequencies are the same, the amplitude of oscillation of the structural elements increases, even if it rarely exceeds half of the across wind dimension of the body (Simiu & Scanlan, 1996). In this condition, the so called lock-in phenomena occurs. In Fig. 15 a graphical representation of this phenomenon is reported. It is possible to observe that the wake frequency remains the same as the structural one in a defined range of wind velocities. This is because the structural motion interacts with the wind field in such a way that the dominating vortex shedding frequency synchronizes with the structure natural frequency. When the wind velocity increases over this range, the wake frequency breaks away from the natural one.

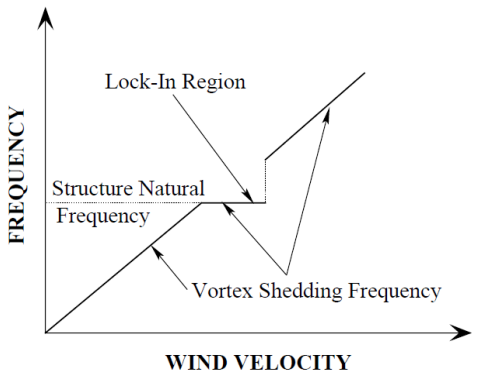

Fig. 15: Qualitative trend of vortex shedding frequency with wind velocity during lock-in

The nature and extent of the vortex shedding phenomenon depends on two dimensionless parameters: the Reynolds and Strouhal numbers.

Reynolds number represents the ratio between inertial and viscous forces: $Re = \rho UD/\mu$. It has been seen that, for a very low Reynolds number, the flow remains almost undisturbed, just circumventing the obstruction on its way. While for higher Reynolds numbers the flow starts to separate around the edges of the body and in its wake vortices start to be generated. Thereafter, when the Reynolds number increases over again, it causes the creation of cyclically alternating vortices which are carried downstream with the flow. In such a condition, the inertial effects becomes dominant over the viscous effects.

The Strouhal number describes the oscillating flow mechanisms. It is given as: $St = N_s D/U$ where N_s is the frequency of full cycles of vortex shedding. It is usually depending on the cross section shape and dimension, on the surface roughness and on the wind turbulence. When the value of N_s is close to the structural frequency, large structural vibrations can occur.

The occurrence of vortex shedding phenomenon should be always checked, since it usually affects the structural serviceability and may lead to fatigue problems.

Flutter

The load acting on a flexible body immersed in a flow is determined by the flow configuration in the surface proximity zone; thus it is function of the body motion. The coupling between the flow and the structural motion represents an auto-excited dynamic system. This type of aeroelastic load generates self-sustained oscillations that may lead to a dynamic instability called “flutter”. A better understanding of flutter phenomenon can be achieved by appealing to energy concepts. Some structural movements can extract work from the airstream. When lift force (L) and vertical motion (h) have the same sign, work is produced on the structure increasing the total energy of the system; instead, when lift force is opposite to the motion, energy is extracted. The same phenomena can occur when moment force (M) and torsional degree of freedom (α) are considered. Therefore, classical flutter occurs when the timing of the structural motion, over one cycle, is such that the force is on average in phase with the deck motion, rather than opposing it (in other words $\int L(t)h(t)dt > 0$ and $\int M(t)\alpha(t)dt > 0$). On the other hand, classical flutter with growing amplitude can therefore occur with the proper timing of aerodynamic forces with structural motion. Such a condition is represented in Fig. 16.

When the velocity of the wind flow is equal to the flutter one, then a critical phasing between the motion and the load occurs. This leads to the extraction from the airstream of an amount of energy equal to that dissipated by the internal structural damping during each cycle. In such a condition, any disturbance introduced in the system leads the body to sustain a neutrally stable periodic motion. At lower speeds any disturbance will be damped, while at higher speeds, or at least in a range of higher speeds, the motion will be amplified.

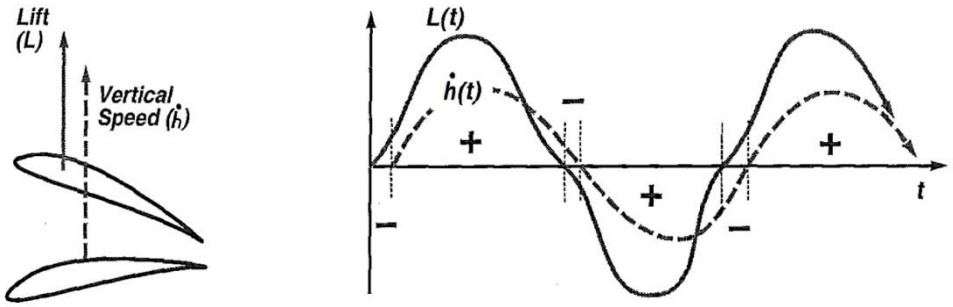

Fig. 16: Timing of vertical motion and aerodynamic lift force

Mainly, two different types of flutter can be detected: single degree of freedom flutter and coupled flutter. The first is a case of negative aerodynamic damping: a single structural motion induces an aeroelastic force whose component is in the direction of the motion and always in phase with the velocity. The second one is more complex because of the coupling of the two degrees of freedom. In this case, the vanishing of the total damping of the system doesn’t necessary imply a negative aerodynamic damping.

Buffeting

Buffeting loads are due to the action of time random forces variable both in intensity and direction. They are generated by the intrinsic turbulence within the atmospheric boundary layer. Since this gustiness has vertical as well as horizontal variations of the wind velocity values, the analysis of structures immersed in a turbulent flow should take into account also the effects of the random variation of the angle of attack. The magnitude of the structural response due to buffeting loads generally increases monotonically as the average wind velocity rises, reaching the highest value in correspondence of maximum winds. Motion induced forces have to be considered for a proper evaluation of the structural response, especially for those values of the wind speed where the mode coupling is no more negligible.

The relationship between the fluctuating wind velocity and the resulting wind load acting on the structure is commonly mentioned as “aerodynamic admittance”. This function is usually defined by means of wind tunnel experiments and its value depends on the reduced frequency parameter (see section 4.2). Different experimental procedures can be used to determine the aerodynamic admittance function, some of them are described in (Larose, 1999) and in (Cigada, Diana, & Zappa, 2002).

When the structure under analysis has great dimensions, the correlation between values of forces acting on different location of the structure has to be considered. In case of rigid structure the force correlation can be assumed the same of that in the wind velocity field, but when elastic structures are under analysis this assumption may be no longer valid, and specific relations must be considered.

4.2 Wind loads on bridge decks

As the trend of bridge decks is to become more lightweight and flexible, flow-structure interaction plays a crucial role in their design.

The first analytical models to simulate wind forces acting on bridge decks were based on wing theories already available in the aeronautic field. These studies were mainly focused on the analyses of the aeroelastic behaviour of airplanes wings. A thin boundary layer completely attached over the body surface, with a small and thin wake behind, is the main features of these type of sections. All the cross-sections with these characteristics are classified as “a*erodynamic bodies”,* or *“streamlined bodies”*. Subsequently, these force models have been extended and adapted to *“bluff bodies”*. The wind velocity field around these cross-sections have an unsteady nature since their boundary layer usually separates from their surface giving rise to a wake with significant depth and great lateral dimensions.

For streamline bodies the assessment of aeroelastic forces can be performed by means of analytical relations, while in case of bluff bodies wind tunnel tests must be conducted in order to predict the amount of aeroelastic loads acting on them. Even if several wind tunnel test have been carried out on different cross sections geometry over the years, aeroelastic forces are still not predictable without experimental campaigns. An attempt in this direction is provided in (Mannini,

2006), where the flutter behavior of several types of bridges is compared and organised according to the definition of a few classes of deck cross-sectional geometry.

The investigation of the aeroelastic behaviour of models subjected to wind induced vibration can be conducted by means of three different types of wind tunnel tests: full bridge models, taut-strip models and sectional models. Full bridge models are not always the most sensitive instruments to study aeroelastic phenomena. In fact, it is well known that full aeroelastic models for long span bridges are generally quite scaled down, and some undesired Reynolds number effects (due to air viscosity and inertia scaling problems) can take place. Furthermore, they are economically very expensive. Taut-strip models, which are much simpler than full models, are intended to form the prototype mode shapes of the deck alone. It is an aeroelastic model which can be regarded as in-between the sectional model and the full aeroelastic bridge ones. Generally, taut strip models are rarely used for the determination of flutter derivatives. Instead, the experimental modelling of a short rigid section of the deck free or forced to oscillate when impacted by the wind flow is the most used approach to assess the structural response. This is due to the fact that the cross-sectional deck shape is the most challenging and crucial feature in the evaluation of the wind load, while the structural response can be adequately simulated by means of numerical methods. The most appealing characteristics of sectional models is the extendibility of experimental results to any other structure with a deck of the same geometry, but different mass, mass moment of inertia, torsional and heaving frequencies (Bartoli & Righi, 2006). Experimental campaigns conducted on sectional models are usually performed to extract both aerodynamic coefficients and flutter derivatives. These parameters are used to define aerodynamic forces, as well as aeroelastic loads, as function of structural motions.

As already mentioned, wind loads can be associated with different types of wind-structure interactions. For this reason different aeroelastic problems can be identified. In particular they can be classified in three different categories:

- **Response problems:** in which there is a dynamic equilibrium between the body and the wind forces; the expression of the forces does not depend on the structural motions;
- **Stability problems:** in which the interchanging energy between the body motion and the aeroelastic forces produces a gradual and unlimited increment of the motion energy, leading to the dynamic equilibrium instability at a ‘‘critical velocity’’; in these problems the loads expression depends on the structural motions;
- **Mixed (stability and response) problems:** in which both motion-induced force and buffeting load are considered for the investigation of both structural serviceability and fatigue. They are used also for the analysis of the amplitude of oscillation when the ultimate limit state is reached.

This thesis deals with the effects of turbulent wind field on bridges regarding at both stability and mixed problems. Its main contribution is about how the presence of turbulence affects the flutter threshold. Furthermore, the structural response at high wind velocity (that means in presence of mode coupling) is deeply investigated.

4.2.1 Structural dynamic in presence of self-excited forces

The structural analysis of bridges can be carried out by means of different approaches. The starting point of all of them is the differential equations of the dynamic equilibrium. Representing the bridge deck as a discrete multi degree of freedom mechanical system, when both aeroelastic and aerodynamic loads are considered, the differential equations are:

$$[M]\{\ddot{x}\} + ([C] + [\mathrm{C_{ae}}])\{\dot{x}\} + ([K] + [\mathrm{K_{ae}}])\{x\} = \{\mathrm{F_{est}}\} \tag{4.4}$$

Where $\{x\}$ is the generalized displacement vector; $[M], [C], [K]$ are the mass, damping and stiffness structural matrices, $[C_{ae}]$ and $[K_{ae}]$ are the matrices representing the aeroelastic wind load due to self excited forces, while $\{\mathrm{F_{est}}\}$ is the vector that represents the other external forces (including the aerodynamic ones). In the evaluation of aeroelastic and aerodynamic loads, it is quite common not to consider the mutual interaction between self-excited and buffeting forces. In particular, the effects of the turbulent wind component are completely neglect if only the structural stability is under investigation. However, in recent years there are some attempts to consider these effects; they will be presented in future sections, at the moment only the aeroelastic loads due to self excited forces are taken into account.

If the structural response in correspondence of each deck section is of interest, then a three-dimensional analysis has to be performed; on the contrary, the use of a sectional model can be considered as a suitable tool for a good representation of the overall structural response.

The three-dimensional analysis can be performed in two different ways: one is to apply the unsteady aerodynamic forces directly to the three-dimensional finite element model of the structure (known as direct method); another is to decompose the structural response in various vibration modes and then assembling them (known as superposition method).

The direct finite element method for the evaluation of the flutter threshold has been adopted in (Dung, Miyata, & Yamada, 1998), (Ge & Tanaka, 2000) and (Chen, Matsumoto, & Kareem, 2000b). The main advantage of this method is that the involvement of the full natural modes of vibration is considered. Moreover within this approach it is possible to take into account any types of nonlinearities. Instead, its main drawback is that the calculation is time-consuming.

The superposition method can be considered an accurate and efficient tool when the structural response of linear elastic systems is under analysis. The main assumptions of linear structure experiencing small amplitudes of oscillations are at the basis of this approach. Under these hypothesis, the system can be solved by modal analysis method. All the degrees of freedom are so separated into the spatial and time-dependent component as:

$$\mathrm{x(t)} = \sum_{\mathrm{i=1}}^{\mathrm{N}} \phi_{\mathrm{i}} \mathrm{e}^{\lambda_{\mathrm{i}} \mathrm{t}}\, \mathrm{x_{0,i}} \tag{4.5}$$

where N is the number of degrees of freedom, $\lambda_i$and ϕ_i are respectively the characteristic eigenvalues and eigenvectors of the eigenproblem that controls the dynamic stability.

Once decided the numbers of modal shapes necessary to well reproduced the structural motion, a finite element method can be used to reproduce the structural response by means of the presented modal techniques. This approach has been used in (Agar, 1989) and (Namini, 1992).

If only the critical wind speed is of interest then a second approach can be developed in the frequency domain. In particular the flutter threshold can be obtain by means of the determinant search method. With this aim, the second order equation (4.4) representing the structural dynamic equilibrium can be transformed into a first order equivalent dynamic problem in state space as function of $\{y\} = [x \ \dot{x}]^T$:

$$\{\dot{y}\} = [\mathrm{A}]\{y\} \tag{4.6}$$

the resulting eigenproblem is:

$$([\mathrm{A}] - \lambda_\mathrm{i}[\mathrm{I}])\phi_\mathrm{i} = 0 \tag{4.7}$$

Generally, the eigenvalues that solve the dynamic stability problem, come in complex conjugate pairs:

$$\lambda_\mathrm{i} = \mathbf{Re}(\lambda_\mathrm{i}) + \mathbf{I}(\lambda_\mathrm{i}) = \mathrm{p_i} + \ i\ \mathrm{q_i} \tag{4.8}$$

where λ_i is the exponential term of the motion, which can be represented as:

$$e^{\lambda_i t} = e^{p_i t}(\cos(q_i t) + i\sin(q_i t)) \tag{4.9}$$

Just observing the components of the motion it is possible to identify three different types of response:

- dynamically stable when the real parts of each individual eigenvalue are negative;
- dynamically instable if the real component of at least one of the eigenvalues assumes positive value. An exponentially growing motion is established and divergent oscillations occur.
- harmonically oscillating when two real roots join together on the real axis and “branch out” into a complex plane (i.e., all real parts of the eigenvalues are zero). This is the case of classical, or coupled, flutter.

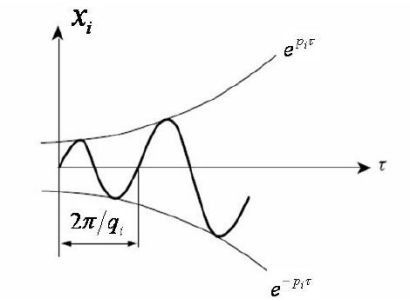

Fig. 17: Exponentially growing motion with nonzero real value.

When the mean wind velocity is equal to the “critical flutter value” the structural response reaches the “flutter condition”, that is the transitional point between damped and growing oscillations. In other word, in correspondence of the flutter point, due to aeroelastic force component, the total damping of the system becomes equal to zero and the structural motion becomes oscillatory with constant amplitude.

The prediction of the critical flutter velocity by means of the solution of the complex eigenvalue problem has been adopted in (Scanlan & Jones, 1990), (Tanaka, Yamamura, & Tatsumi, 1992) and (Chen, Matzumoto, & Kareem, 2000a). In the particular case in which the multi-modal approach is simplified by restricting the analysis to only two principal structural modes, then the solution of the resulting eigenproblem can be achieved only by solving a couple of complex equations. All the details for the evaluation of the critical flutter velocity in this specific case are reported in (Dyrbye & Hansen, 1997).

From the analysis of the behaviour of lots of bridge cross-sections gained over the years, it is possible to drawn some general conclusions about their aeroelastic stability condition. According to (Diana, Cheli, Zasso, Collina, & Bruni, 1998), bridge deck stability is mainly controlled by the following three parameters:

- the frequency ratio between torsional and vertical motion: $r_f = \frac{f_h}{f_\alpha}$;
- the ratio between the structural stiffness and the equivalent stiffness due to aeroelastic effects: $r_{k,h} = \frac{k_h}{k_h^{ae}}$ and $r_{k,\alpha} = \frac{k_\alpha}{k_\alpha^{ae}}$;
- the total amount of damping, evaluated considering both structural and aeroelastic contributions $C_h^{tot} = C_h^s + C_h^{ae}$ and $C_\alpha^{tot} = C_\alpha^s + C_\alpha^{ae}$.

Higher are the values of these parameters, greater is the stability of the structure. In particular, some strategies can be adopted in order to assure the feasibility of the structure. These are:

- optimization of the bridge cross-section structural design with the aim to increase the value of the r_f parameter;
- optimization of the aerodynamic deck design, modifying the deck shape in order to reduced the aerodynamic forces without reducing the structural stiffness;
- improvement of the total structural damping by means of the adoptions of damping device or active control devices.

Until now, a global review about how flutter condition arises has been reported. Now the focus is moved towards the analytical force formulations in order to evaluate the element of the aeroelastic matrices introduced in (4.4). Mainly, two different force models are available in literature: the quasi steady approach and the Scanlan one. These two force models are presented in the following paragraphs, underlining the hypotheses on which they are based.

4.2.2 Quasi steady force model

In the quasi steady theory the aerodynamic loads acting on the bridge deck at a certain time are evaluated considering that the body is motionless. In other words, the structural motion is

described as a succession of steps in which the configuration is considered steady. The wind induced forces acting on the structure at a certain instant are so equal to those obtained when the body moves with constant translational and rotational velocities, whose value is equal to the real instantaneous ones. Since in this approach the flow field around the structure is considered to be steady, then the aerodynamic load is evaluated only as function of the instantaneous angle of attack, rather than the history of the angles due to the structural motion. That is, the quasi-steady theory does not consider the aerodynamic delay, utilizing static aerodynamic coefficients evaluated by means of wind tunnel experiments, in which the tested sectional model is kept in a fixed position, or it is moved at a very low frequency.

Taking the reference axis to be the one identified by wind-structure relative velocity U_r, see Fig. 18, the equations of the wind forces are:

$$\begin{aligned} \mathrm{L(t)} &= \frac{1}{2}\rho\, U_r^2(t)\, B\, C_L(\alpha_e) \\ \mathrm{D(t)} &= \frac{1}{2}\rho\, U_r^2(t)\, B\, C_D(\alpha_e) \\ \mathrm{M(t)} &= \frac{1}{2}\rho\, U_r^2(\mathrm{t})\, B^2\, C_M(\alpha_e) \end{aligned} \tag{4.10}$$

where ρ is the air density, B the deck width, C_L, C_D and C_M are the aerodynamics coefficients for lift, drag and torsional forces, U_r is the relative velocity due to the incoming wind and structural motion, and α_e is the actual angle of incidence.

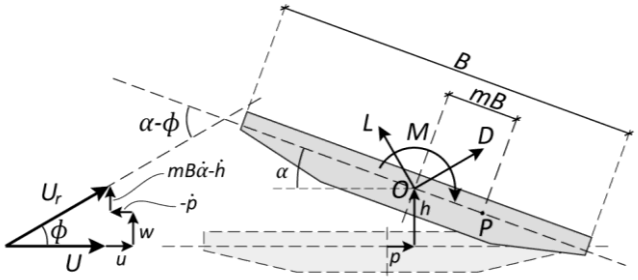

Fig. 18: Quasi steady convection

The relative velocity and the angle of incidence are mathematically defined as:

$$\mathrm{U_r(t)} = \sqrt{\left(\mathrm{U + u(t) - \dot{p}(t)}\right)^2 + \left(\mathrm{w(t) - \dot{h}(t) + mB\dot{\alpha}(t)}\right)^2} \tag{4.11}$$

$$\begin{aligned} \alpha_\mathrm{e}(\mathrm{t}) &= \alpha_\mathrm{s} + \alpha(\mathrm{t}) + \phi(\mathrm{t}) \\ \phi(\mathrm{t}) &= \tan^{-1}\left(\frac{w(t) - \dot{h}(t) + mB\dot{\alpha}(t)}{U + u(t) - \dot{p}(t)}\right) \end{aligned} \tag{4.12}$$

In (4.12) the effective angle of incidence between the wind flow and deck position is defined as the sum of three components: α_s that is the angle due to aerostatic forces, $\alpha(t)$ due to the

instantaneous torsional displacement, and ϕ that represents the angle formed by the wind relative velocity respect to the reference system. Both the values U_r and ϕ are expressed as function of the dimensionless parameter m. It represents the distance between the elastic centre of the girder section and the point at the aerodynamic centre, which is the point of intersection of the drag and lift force directions. This parameter is generally difficult to measure, and its value should be dynamically assessed. It is not correct to use the same value of the parameter m for all the three components of the wind forces, but three different values should be determined by considering the asymptotic behaviour for vanishing oscillation frequency of the aeroelastic derivatives P_2, H_2 and A_2, respectively (Salvatori, 2007). In literature different procedures for the evaluation of this parameter are proposed. Originally, the parameter m was introduced in (Irwin, 1978). It was considered as a floating coefficient used for the proper evaluation of the torsional aerodynamic damping contribution in the equation of motion. Some specific experimental procedures to determine the value of this parameter have been proposed, i.e. (Falco, Gasparetto, & Scaramelli, 1978).

The evaluation of the parameter m can be performed also by means of analytical relation. When the ratio between the thickness D and the length chord B of the cross-section is sufficiently small, the deck profile can be considered sufficiently ''aerodynamic''. Under this condition, the flow separation does not dramatically affect the sectional aerodynamics and the global structural behaviour can be considered close to that of the thin flat plate. In this case, it is possible to evaluate the parameter m considering the analogy with the theoretical solution proposed by (Theodorsen, 1935). It is so obtained: $m_L = 1/2$ and $m_M = 0$ (the along wind component is identically zero for the thin airfoil, therefore no analogy can be established for the coefficient related to the drag force). In other works it is suggested to use the same value for all three components of m, i.e. in (Stoyanoff, 2001) it is assumed that $m_L = m_D = m_M = 0$, while in (Borri & Costa, 2004) and also in (Miyata, Yamada, Boonyapinyo, & Santos, 1995) it is considered that the motion of the section is driven by the phenomena occurring at the leading edge, obtaining $m_L = m_D = m_M = -0.25$. In (Salvatori & Borri, 2007) has been proposed to determine the value of m_h, m_p and m_α considering the asymptotic behaviour for vanishing oscillation frequency of the aeroelastic derivatives H_2, P_2 and A_2. In this case, the obtained values of the parameter m intrinsically considers that the quasi steady conditions are reached.

The evaluation of the wind induced loads by means of the quasi-steady approach can be considered correct when the reduced frequency $K = \omega B/U$ is small enough, or the reduced velocity $U_{red} = 2\pi/K$ is sufficiently great. This assumption implies that the time taken by the flow to traverse the bridge deck is short in respect to the structural oscillation time or, equivalently, the effects of the motion of the deck are communicated rapidly to the flow region surrounding it. In other words, the quasi-steady force model can be adopted when the dimensions of the disturbances in the approaching flow are bigger than the deck width.

The main attractive feature of this force formulation is its ability to evaluate the wind load as function of the effective angle of incidence between the flow and the structure. This means that using this approach it is possible to take into account load nonlinearities due to the time

dependence angle value. Starting from the wind force equations (4.10), several mathematical models can be developed basing on different approximation hypothesis. The most wildly used method is the one founded on the linearization of the force equations around the original undeformed position (usually around $\alpha = 0°$). A different approximation of the aerodynamics coefficients has been used in (Borri & Costa, 2004) where a cubic function has been assumed to develop the expressions of the aerodynamic forces. The comparison between this two different solutions has underlined that the critical wind speed obtained using linear steady model with nonlinear one has nearly the same value; in particular the adoption of the cubic nonlinearities modifies just the post critical behaviour. This insensitivity of the flutter limit has been also pointed out in (Shahrzad & Mahzoon, 2002) by means of a different model. More details about the linearization of the force equations will be provided in section 4.3.

Even if this force model has the interesting quality to describe the phenomena in a physical way, its major drawback is that the unsteady fluid memory effect, due to the frequency dependence of the aerodynamic forces, is completely neglected. This can leads toward a wrong evaluation of the flutter threshold. For example, the analysis of the aerodynamic behaviour of an airfoil section, reported in (Shahrzad & Mahzoon, 2002), has highlighted that, between the steady and unsteady model, there is some difference of critical wind velocity values.

4.2.3 Scanlan force model

Because of the crucial role of bridge structures, the design of every deck cross-section is performed so that instability conditions could arise only at high values of the mean wind velocity. Under this condition the flow separates from the sectional surface over a significant amount of its boundary, as in the case of the rectangular cross section where several shear layers separate from the leading and trailing edges. This remarks that the quasi-steady model cannot represent in a proper way the phenomena occurring in this wind velocity range, and that a different mathematical formulation has to be used to the right evaluation of aeroelastic loads.

In (Theodorsen, 1935) the first analytical force model for the definition of non-stationary loads has been presented. It has been developed to study the behaviour of a wing profile oscillating in a smooth flow. This force model is usually adopted for all the cross-section with a streamlined profile. However, the assumption of fully attached flow must be rejected for the most common bridge sections usually adopted. For this reason the previous model has been subsequently extended and adapted to bluff sections.

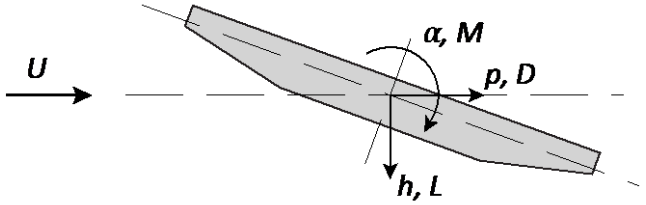

Fig. 19: Scanlan convection

Considering the sign conventions of forces and displacements reported in Fig. 19, assuming a small amplitude isofrequent harmonic motion, the current unsteady load model describing self-excited forces for bridge decks was first introduced in (Scanlan & Tomoko, 1971). In this force formulation self-excited forces are divided into in-phase and out-of-phase components with respect to the structural motion. The frequency dependent aerodynamic characteristics of the wind load are described by means of flutter derivatives coefficients extracted by means of dynamic experimental test campaign. In particular, the time-varying self-excited force components are expressed as the sum of terms associated with each structural motion, as reported as follows:

$$\begin{aligned} F_L &= \frac{1}{2}\rho U^2 B \left(KH_1 \frac{\dot{h}}{U} + KH_2 \frac{B\dot{\alpha}}{U} + K^2 H_3 \alpha + K^2 H_4 \frac{h}{B} + KH_5 \frac{\dot{p}}{U} + K^2 H_6 \frac{p}{B} \right) \\ F_D &= \frac{1}{2}\rho U^2 B \left(KP_1 \frac{\dot{h}}{U} + KP_2 \frac{B\dot{\alpha}}{U} + K^2 P_3 \alpha + K^2 P_4 \frac{h}{B} + KP_5 \frac{\dot{p}}{U} + K^2 P_6 \frac{p}{B} \right) \\ F_M &= \frac{1}{2}\rho U^2 B^2 \left(KA_1 \frac{\dot{h}}{U} + KA_2 \frac{B\dot{\alpha}}{U} + K^2 A_3 \alpha + K^2 A_4 \frac{h}{B} + KA_5 \frac{\dot{p}}{U} + K^2 A_6 \frac{p}{B} \right) \end{aligned} \tag{4.13}$$

where $H_i, P_i, and\ A_i\ (i = 1-6)$ are the aeroelastic derivatives functions of the reduced frequency. Usually, the last two components, those with indices 5 and 6, can be neglected since the force contribution due to the sway motion is generally less relevant than those in the others two directions.

In the presented force model the effects of the wind loads are “experienced” at the level of the flexible structure as a change in both natural frequencies and damping values of the structural response. It is important to remark that the fluid flow does not change the frequency or the damping of the structure. What is meant is that the effects of the fluid can be commonly visualized in terms of equivalent changes in frequency and damping values.

The wind force expression in (4.13) is formulated in the mixed frequency-time domain. Numerical simulation performed using this force expression usually evaluate aeroelastic derivatives at a single frequency that is often obtained through a trial procedure and is valid only at the critical flutter condition. As already discussed in previous section, two different strategies can be adopted to overcome this problem. One is to accept the hypothesis of small-amplitude motions and superposition of effects, allowing the development of the dynamic system completely in the frequency domain. The other approach is the extension of the wind force equation completely in the time domain. This allows to consider both structural and load nonlinearities. This method is based on convolution techniques and the final wind force expression in the time domain is obtained by means of the introduction of indicial or impulse response function. In (Scanlan, Béliveau, & Budlong, 1974), (Chen, Matsumoto, & Kareem, 2000b) and (Caracoglia & Jones, 2003a), the effectiveness of this method is highlighted. An extensive description of the analytical force model developed in time domain using the impulse response function is reported in section 4.4. Time domain models also offer other advantages. For example, the combination of self excited and buffeting forces is straightforward and the along-span wind coherence can be easily considered.

The evaluation of the aeroelastic load by means of the aforementioned models allows to consider the influence of the reduced frequency, but It is well known that self-excited forces are also functions of both the geometric configurations of bridge sections and the incoming wind fluctuations. For this reason, the choice of the load model and of the assumptions that must be adopted to perform the analyses of a structure should be carefully considered because final results are strongly affected by them. This has been also pointed out in (Petrini, Giuliani, & Bontempi, 2007), where it is shown that, increasing the complexity of the force formulations, the amplitude response of the structure usually decreases and the frequency probability density functions assume a narrower shape.

Although the use of flutter derivatives for the aerodynamic analysis of bridge decks have been adopted for long time, their representation can be performed referring to different conventions. An overview of the most used conventions is here proposed highlighting each one advantages and limitations.

The first and the most commonly adopted convention is the *Scanlan* one. Writing the velocity terms in the frequency domain as $\dot{h} = i\omega h$, $\dot{\alpha} = i\omega\alpha$, the force equations (4.13) can be rewritten in the form:

$$\begin{aligned} \mathrm{L} &= \frac{1}{2}\rho \mathrm{U}^2 B \frac{1}{\mathrm{U}_{\mathrm{red}}^{*\,2}}\left\{(\mathrm{H}_4 + \mathrm{iH}_1)\frac{\mathrm{h}}{\mathrm{B}} + (\mathrm{H}_3 + \mathrm{iH}_2)\alpha\right\} \\ \mathrm{M} &= \frac{1}{2}\rho \mathrm{U}^2 B^2 \frac{1}{\mathrm{U}_{\mathrm{red}}^{*\,2}}\left\{(\mathrm{A}_4 + \mathrm{iA}_1)\frac{\mathrm{h}}{\mathrm{B}} + (\mathrm{A}_3 + \mathrm{iA}_2)\alpha\right\} \end{aligned} \tag{4.14}$$

where $\mathrm{U}_{\mathrm{red}}^{*} = \frac{1}{K} = \frac{U}{\omega B}$ is the reduced velocity in term of circular frequency. The force expression in (4.14) highlight the advantages of this flutter convention, that are:

- direct interpretation of the flutter derivatives in terms of transfer functions;
- possibility of quantitative comparison of the aerodynamic forces on different sections (the ratio of coefficients of different sections is equal to the ratio of the corresponding non-dimensional forces);
- wide use of the convention.

However the following disadvantages can be detected:

- at low reduced velocity values the resolution is lost as the coefficients have necessarily zero values, so that diagrams are useless in this range;
- the analytical model is far from a physical interpretation of the non stationary aerodynamic forces; in fact, all the coefficients show a prevailing linear and quadratic trends with $\mathrm{U}_{\mathrm{red}}^{*}$, even if representative of very different sections.

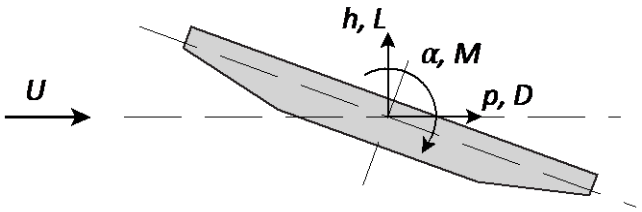

Fig. 20: Quasi-steady modified convection

Another flutter sign convention with a definition quite close to the previous one is the *Kussner* convention, in which the forces are divided by U^2 and scaled by the constant $2\pi, \pi$ or $\pi/2$. Since its similarity to the Scanlan convention, also this one presents the same type of advantages and limitations above underlined.

Referring to the sign convention reported in Fig. 20, a different expression of the unsteady wind force component is here reported, according to the *quasi-steady modified* convention:

$$F_L = \frac{1}{2}\rho \mathrm{U}^2 B \left\{ -\mathrm{h}_1^*(\mathrm{C_{D0}} + \mathrm{C'_{L0}})\frac{\mathrm{i}\omega \mathrm{h}}{\mathrm{U}} + \mathrm{h}_4^* \frac{\pi}{2\mathrm{U}_{\mathrm{red}}^{*\,2}}\frac{\mathrm{h}}{\mathrm{B}} - \mathrm{h}_2^*(\mathrm{C_{D0}} + \mathrm{C'_{L0}})\frac{\mathrm{i}\omega \mathrm{B}\alpha}{\mathrm{U}} + \mathrm{h}_3^* \mathrm{C'_{L0}}\alpha \right\}$$
$$F_M = \frac{1}{2}\rho \mathrm{U}^2 B^2 \left\{ -\mathrm{a}_1^* \mathrm{C_{M0}}\frac{\mathrm{i}\omega \mathrm{h}}{\mathrm{U}} + \mathrm{a}_4^* \frac{\pi}{2\mathrm{U}_{\mathrm{red}}^{*\,2}}\frac{\mathrm{h}}{\mathrm{B}} - \mathrm{a}_2^* \mathrm{C'_{M0}}\frac{\mathrm{i}\omega \mathrm{B}\alpha}{\mathrm{U}} + \mathrm{a}_3^* \mathrm{C'_{M0}}\alpha \right\} \quad (4.15)$$

The main advantages derived from the adoption of this convention are:

- the analytical model relies on a physical interpretation of the aerodynamic forces in terms of a quasi-steady approach, especially at high reduced velocities $\mathrm{U}_{\mathrm{red}}^*$;
- the chosen normalisation factors give numerical value of the coefficients that are generally asymptotic to 1 at high $\mathrm{U}_{\mathrm{red}}^*$ (steady conditions) for streamlined sections; as the data are independent from the specific aerodynamic characteristics of the sections, the difference from unity has always the meaning of distance from a quasi-steady aeroelastic behaviour;
- optimal resolution is allowed in any $\mathrm{U}_{\mathrm{red}}^*$ range;

At the same time, its limitations are:

- direct comparison of the aerodynamic forces on different sections is not allowed because of their different normalisation factors;
- $h_i^* \; and \; a_i^*$ coefficients allow to calculate the aerodynamic forces only if the normalisation factors $C_{D0}, C'_{L0} \; and \; C'_{M0}$ are known, so that their values have always to be associated with the flutter derivatives diagrams.

Finally, in (Zasso, 1996) a new force expression has been introduced, always referred to the sign convention in Fig. 20. The main attempt of this flutter convention is to mix the advantages of the previously described notations, without any normalization factors.

$$F_L = \frac{1}{2}\rho \mathrm{U}^2 B \left\{ -\mathrm{h}_1 \frac{\mathrm{i}\omega \mathrm{h}}{\mathrm{U}} + \mathrm{h}_4 \frac{\pi}{2\mathrm{U}_{\mathrm{red}}^{*\,2}} \frac{\mathrm{h}}{\mathrm{B}} - \mathrm{h}_2 \frac{\mathrm{i}\omega \mathrm{B}\alpha}{\mathrm{U}} + \mathrm{h}_3 \alpha \right\}$$
$$F_D = \frac{1}{2}\rho \mathrm{U}^2 B \left\{ -\mathrm{p}_1 \frac{\mathrm{i}\omega \mathrm{h}}{\mathrm{U}} + \mathrm{p}_4 \frac{\pi}{2\mathrm{U}_{\mathrm{red}}^{*\,2}} \frac{\mathrm{h}}{\mathrm{B}} - \mathrm{p}_2 \frac{\mathrm{i}\omega \mathrm{B}\alpha}{\mathrm{U}} + \mathrm{p}_3 \alpha \right\} \qquad (4.16)$$
$$F_M = \frac{1}{2}\rho \mathrm{U}^2 B^2 \left\{ -\mathrm{a}_1 \frac{\mathrm{i}\omega \mathrm{h}}{\mathrm{U}} + \mathrm{a}_4 \frac{\pi}{2\mathrm{U}_{\mathrm{red}}^{*\,2}} \frac{\mathrm{h}}{\mathrm{B}} - \mathrm{a}_2 \frac{\mathrm{i}\omega \mathrm{B}\alpha}{\mathrm{U}} + \mathrm{a}_3 \alpha \right\}$$

In particular, thanks to this convention an optimal resolution of the flutter derivatives representation is obtained in any $\mathrm{U}_{\mathrm{red}}^{*}$ range. Furthermore, a quantitative comparison of the forces on different sections is allowed, with no reference to specific normalisation factors. In other words, the advantages of both Scanlan and quasi-steady-modified convention are combined. Again, since the use of normalisation factors has been abandoned, the asymptotic trend to 1 for high value of $\mathrm{U}_{\mathrm{red}}^{*}$ is lost. However, the identification of the achievement of the quasi-steady behaviour may be performed just looking at the asymptotic trend of the coefficients.

The relation between the wind forces describing parameters that have been adopted in this last representation (that are $h_i, p_i,\ and\ \alpha_i$), and the corresponding ones in the Scanlan convention, ($H_i, P_i, and\ A_i$), is reported as follows :

$h_1 = -H_1 K = -\frac{H_1}{U_{red}^*}$	$p_1 = P_1 K = \frac{P_1}{U_{red}^*}$	$a_1 = A_1 K = \frac{A_1}{U_{red}^*}$
$h_2 = H_2 K = \frac{H_2}{U_{red}^*}$	$p_2 = -P_2 K = -\frac{P_2}{U_{red}^*}$	$a_2 = -A_2 K = -\frac{A_2}{U_{red}^*}$
$h_3 = -H_3 K^2 = -\frac{H_3}{U_{red}^{*2}}$	$p_3 = P_3 K^2 = \frac{P_3}{U_{red}^{*2}}$	$a_3 = A_3 K^2 = \frac{A_3}{U_{red}^{*\,2}}$
$h_4 = H_4 \frac{2}{\pi}$	$p_4 = -P_4 \frac{2}{\pi}$	$a_4 = -A_4 \frac{2}{\pi}$

Table 4: Relation between Zasso and Scanlan cofficients.

Later in this chapter a literature review of the principal model for the evaluation of the self excited forces by means of flutter derivative parameters in time domain is addressed, highlighting strengths and weakness of each of them. Moreover a new wind load model able to take into account both frequency and angle nonlinearities will be presented.

Single degree dynamic instability: vertical motion

The dynamic equation of motion in presence of aeroelastic load is expressed by (4.4) where the aerodynamic matrices are defined by terms reported in (4.13). If coupling force terms are neglected (that means to impose $H_2 = H_3 = A_1 = A_4 = 0$) then also the equation of motion becomes uncoupled. If only the vertical degree of freedom is considered it becomes:

$$\mathrm{M}\,\ddot{\mathrm{h}}(\mathrm{t}) + \mathrm{C}_{\mathrm{h}}\,\dot{\mathrm{h}}(\mathrm{t}) + \mathrm{K}_{\mathrm{h}}\,\mathrm{h}(\mathrm{t}) = \frac{1}{2}\rho \mathrm{U}^2 \mathrm{B} \left(\mathrm{K}\mathrm{H}_1(\mathrm{K}) \frac{\dot{\mathrm{h}}(\mathrm{t})}{\mathrm{U}} + \mathrm{K}^2 \mathrm{H}_4(\mathrm{K}) \frac{\mathrm{h}(\mathrm{t})}{\mathrm{B}} \right) \qquad (4.17)$$

The total damping of the system, given by the sum of both the structural and the aeroelastic ones, is:

$$C_h^{tot} = C_h - \frac{1}{2}\rho B^2 \omega_h^{ae} H_1(K) \tag{4.18}$$

where ω_h^{ae} is the vertical frequency of vibration that differ from the structural one due to the presence of aeroelastic forces (the term that depends on $H_4(K)$ in (4.18)) When the total damping vanishes, then the instability of the vertical degree of freedom arises. The value of the mean wind velocity in correspondence of which this phenomena occur can be evaluated starting from the knowledge of the reduced frequency value that verify the following relation:

$$H_1(K) = \frac{2C_h}{\rho B^2 \omega_h^{ae}} \tag{4.19}$$

It is evident that $H_1(K)$ should be calculated iteratively since ω_h^{ae} depends on the amount of aerodynamic forces, that means on the value of the reduced frequency. Anyway, iteration can be avoided if the approximation $\omega_h^{ae} = \omega_h$ is accepted.

Considering decks normally used for long span bridges, aerodynamic damping in pure vertical bending vibrations is positive when the values of $H_1(K)$ are negative.

This type of instability is the same previously presented as galloping, but in this case the evaluation of the mean wind velocity at which galloping phenomenon arise is evaluated considering also the unsteadiness characteristics on the incoming flow.

Single degree dynamic instability: torsional motion

As for the analysis of pure vertical motion, also in this case the dynamic equilibrium equation of pure torsional motion have been obtained neglecting the coupling force terms.

$$I_P\,\ddot{\alpha}(t) + C_\alpha\,\dot{\alpha}(t) + K_\alpha\,\alpha(t) = \frac{1}{2}\rho U^2 B^2 \left(KA_2(K)\frac{B\,\dot{\alpha}(t)}{U} + K^2 A_3(K)\,\alpha(t)\right) \tag{4.20}$$

Also in this case the total damping of the system is given by the sum of both the structural and the aeroelastic ones as follows:

$$C_\alpha^{tot} = C_\alpha - \frac{1}{2}\rho B^4 \omega_\alpha^{ae} A_2(K) \tag{4.21}$$

where ω_α^{ae} is the vibration torsional frequency corrected by the presence of aeroelastic forces (the term that depends on $A_3(K)$ in (4.20)) When the total damping vanishes, then the instability of the torsional degree of freedom arises. The mean wind velocity in correspondence of which this phenomena occur can be evaluated solving the following relation as function of the reduced frequency value:

$$A_2(K) = \frac{2C_\alpha}{\rho B^4 \omega_\alpha^{ae}} \tag{4.22}$$

Also in this case iterative procedure should be performed since ω_α^{ae} depends on the amount of aerodynamic forces. If the approximation $\omega_\alpha^{ae} = \omega_\alpha$ is adopted, a direct evaluation of the wind velocity can be performed.

Pure torsional instability can be detected for all those cross-sections whose derivative $A_2(K)$ assumes positive values. This may happen especially for non-streamlined bridge decks.

4.3 Linearized quasi-steady theory

As already mentioned in section 4.2.2, quasi-steady force model can take into account nonlinearities in aerodynamic forces through the static force coefficients, which are nonlinear functions of the angle of incidence. However, it is possible to simplify the forces equations developing a linearized expression of the forces by means of a linear approximation of the aerodynamic coefficients around the static deformed structural configurations.

The linearization procedure starts rewriting the force equations referring to a fixed Cartesian system (X Y Z) and not to the one based on wind direction:

$$\begin{aligned} F_L &= \left(\frac{1}{2}\rho\, U_r^2(t)\, B\, C_L(\alpha_e)\right)\cos\phi + \left(\frac{1}{2}\rho\, U_r^2(t)\, B\, C_D(\alpha_e)\right)\sin\phi \\ F_D &= \left(\frac{1}{2}\rho\, U_r^2(t)\, B\, C_L(\alpha_e)\right)\sin\phi + \left(\frac{1}{2}\rho\, U_r^2(t)\, B\, C_D(\alpha_e)\right)\cos\phi \\ F_M &= \frac{1}{2}\rho\, U_r^2(\mathrm{t})\, B^2\, C_M(\alpha_e) \end{aligned} \tag{4.23}$$

Simplifying the expression of the relative velocity and of the ϕ angle:

$$\mathrm{U_r^2} \cong (\mathrm{U} + \mathrm{u} - \dot{\mathrm{p}})^2 \cong \mathrm{U}^2 + 2\mathrm{Uu} - 2\mathrm{U}\dot{\mathrm{p}} = \mathrm{U}^2\left(1 + 2\frac{\mathrm{u}}{\mathrm{U}} - 2\frac{\dot{\mathrm{p}}}{\mathrm{U}}\right) \tag{4.24}$$

$$\phi \cong \frac{\mathrm{w} - \dot{\mathrm{h}} + \mathrm{mB}\dot{\alpha}}{\mathrm{U}} \tag{4.25}$$

and linearizing the expression of coefficients $C_L(\alpha_e), C_D(\alpha_e)$ and $C_M(\alpha_e)$ around the satic configuration described by angle α_s:

$$\begin{aligned} \mathrm{C_L}(\alpha_\mathrm{e}) &\cong \mathrm{C_L}(\alpha_\mathrm{s}) + \mathrm{C_L'}(\alpha_\mathrm{s})(\alpha + \phi) = \mathrm{C_L} + \mathrm{C_L'}(\alpha + \phi) \\ \mathrm{C_D}(\alpha_\mathrm{e}) &\cong \mathrm{C_D}(\alpha_\mathrm{s}) + \mathrm{C_D'}(\alpha_\mathrm{s})(\alpha + \phi) = \mathrm{C_D} + \mathrm{C_D'}(\alpha + \phi) \\ \mathrm{C_M}(\alpha_\mathrm{e}) &\cong \mathrm{C_M}(\alpha_\mathrm{s}) + \mathrm{C_M'}(\alpha_\mathrm{s})(\alpha + \phi) = \mathrm{C_M} + \mathrm{C_M'}(\alpha + \phi) \end{aligned} \tag{4.26}$$

considering that $sin\phi \cong \phi$ and $cos\phi \cong 1$, Eq.(4.23) becomes:

$$F_L = \frac{1}{2}\rho \mathrm{U}^2 B\left(1 + 2\frac{\mathrm{u}}{\mathrm{U}} - 2\frac{\dot{\mathrm{p}}}{\mathrm{U}}\right)\left\{\left(\mathrm{C_L} + \mathrm{C'_L}(\alpha + \phi)\right) + \left(\mathrm{C_D} + \mathrm{C'_D}(\alpha + \phi)\right)\phi\right\}$$
$$F_D = \frac{1}{2}\rho \mathrm{U}^2 B\left(1 + 2\frac{\mathrm{u}}{\mathrm{U}} - 2\frac{\dot{\mathrm{p}}}{\mathrm{U}}\right)\left\{\left(\mathrm{C_L} + \mathrm{C'_L}(\alpha + \phi)\right)\phi + \left(\mathrm{C_D} + \mathrm{C'_D}(\alpha + \phi)\right)\right\} \quad (4.27)$$
$$F_M = \frac{1}{2}\rho\, \mathrm{U}^2 B^2\left(1 + 2\frac{\mathrm{u}}{\mathrm{U}} - 2\frac{\dot{\mathrm{p}}}{\mathrm{U}}\right)\left(\mathrm{C_M} + \mathrm{C'_M}(\alpha + \phi)\right)$$

Finally, neglecting the multiplication of infinitesimals terms, the final quasi-steady linearized force formulation is:

$$F_L = \frac{1}{2}\rho \mathrm{U}^2 B\left\{[\mathrm{C_L}] + \left[(\mathrm{C_D} + \mathrm{C'_L})\frac{-\dot{\mathrm{h}} + \mathrm{m_h B}\dot{\alpha}}{\mathrm{U}} + \mathrm{C'_L}\alpha - 2\mathrm{C_L}\frac{\dot{\mathrm{p}}}{\mathrm{U}}\right] + \left[(\mathrm{C_D} + \mathrm{C'_L})\frac{\mathrm{w}}{\mathrm{U}} + 2\mathrm{C_L}\frac{\mathrm{u}}{\mathrm{U}}\right]\right\}$$
$$F_D = \frac{1}{2}\rho \mathrm{U}^2 B\left\{[\mathrm{C_D}] + \left[(\mathrm{C'_D} - \mathrm{C_L})\frac{-\dot{\mathrm{h}} + \mathrm{m_p B}\dot{\alpha}}{\mathrm{U}} + \mathrm{C'_D}\alpha - 2\mathrm{C_D}\frac{\dot{\mathrm{p}}}{\mathrm{U}}\right] + \left[(\mathrm{C'_D} - \mathrm{C_L})\frac{\mathrm{w}}{\mathrm{U}} + 2\mathrm{C_D}\frac{\mathrm{u}}{\mathrm{U}}\right]\right\} \quad (4.28)$$
$$F_M = \frac{1}{2}\rho\, \mathrm{U}^2 B^2\left\{[\mathrm{C_M}] + \left[\mathrm{C'_M}\frac{-\dot{\mathrm{h}} + \mathrm{m_\alpha B}\dot{\alpha}}{\mathrm{U}} + \mathrm{C'_M}\alpha - 2\mathrm{C_M}\frac{\dot{\mathrm{p}}}{\mathrm{U}}\right] + \left[\mathrm{C'_M}\frac{\mathrm{w}}{\mathrm{U}} + 2\mathrm{C_M}\frac{\mathrm{u}}{\mathrm{U}}\right]\right\}$$

It is worth noting that in the obtained force expression, three different components can be detected. Each of them is grouped inside brackets and is respectively the static, the aeroelastic and the buffeting force component (Lazzari, 2005).

The importance of the steady aerodynamic force coefficients can be depicted as follows:

- C_D and C'_L contribute to the damping in drag and lift respectively by an amount proportional to the mean wind velocity U;
- the vertical aerodynamic damping is proportional to C'_L. If this value is negative the overall vertical damping will be negative for a certain wind speed and galloping instability will occur;
- the pitching moment coefficient C'_M contributes to the torsional stiffness of the system. If it is positive, the torsional stiffness will decrease in proportion to U^2, that means the torsional frequency will decrease and, at some wind velocity, it will approach the vertical frequency creating grounds for development of classical flutter. Moreover, the effective torsional stiffness could become negative, and in this case divergent instability will arise;
- the gust forces depend on the longitudinal and vertical component of the aerodynamic fluctuating velocity u and w, and are function of the aerodynamic coefficients usually evaluated at zero angle of incidence.

The quasi-steady force model is only considered valid at very-high reduced wind velocities since it neglects the unsteady fluid memory effect. Moreover, in (Oudheusden, 2000) it has been pointed out its inaccuracy in the description of self-excited forces even at low wind velocities, in particular it

fails in accurately describing forces induced by torsional motion even at very high reduced velocities, where the fluid memory effect plays an essential role in force generation. On the other hand, it represents a useful tool for a qualitative investigation of the global behaviour of the cross-sections because of its straightforward force model.

4.4 Self excited forces in time domain

In section 4.2.3, the Scanlan force formulation in the mixed frequency-time domain has been introduced. The main issue here addressed is the extension of the self-excited force model in the time domain.

The equivalency between time and frequency domains has been initially studied in the aeronautical field, as firstly pointed out by (Garrick, 1938) and subsequently developed by (Jones, 1940). Starting from their approach, several force formulations for the wing profile have continued to appear in literature. The possibility of extending that approach to bluff bodies, such as bridge deck sections, was widely investigated. In particular a non-linear least-square technique for the definition of a set of indicial functions, starting from the knowledge of the set of flutter derivatives, was firstly pointed out in (Scanlan, Béliveau, & Budlong, 1974). In (Caracoglia & Jones, 2003a) a comprehensive discussion about the validity of this approach is shown. Afterwards, in (Caracoglia & Jones, 2003b) it has been proposed a methodology for the direct extraction of the indicial functions from wind tunnel test, as an alternative to aeroelastic derivatives evaluated in the frequency domain.

A modified version of the original approach based on Dirac's delta functions can be found in (Lin & Yang, 1983) and (Bucher & Lin, 1988). In their works, the expression of the self-excited forces per unit span induced by an arbitrary structural motion are represented in terms of convolution integrals. In (Chen & Kareem, 2002) the comparison of the two force models developed in time domain, one based on indicial function and the other on impulse response function, is reported. In this paper it is pointed out the equivalence of the two mathematical formulations and the relationships among the impulse and indicial response functions is deduced.

This work thesis deals with the representation of self-excited forces by means of impulse response functions, whose evaluation will be derived from the experimentally measured flutter derivatives. In (4.29) the frequency dependent forces represented in terms of convolution integrals are reported:

$$
\begin{aligned}
L_{se}(t) &= \frac{1}{2}\,\rho U^2 \int_{-\infty}^{t} \Big(I_{Lh}(t-\tau)h(\tau) + I_{Lp}(t-\tau)p(\tau) + I_{L\alpha}(t-\tau)\alpha(\tau) \Big)\, d\tau \\
D_{se}(t) &= \frac{1}{2}\,\rho U^2 \int_{-\infty}^{t} \Big(I_{Dh}(t-\tau)h(\tau) + I_{Dp}(t-\tau)p(\tau) + I_{D\alpha}(t-\tau)\alpha(\tau) \Big)\, d\tau \\
M_{se}(t) &= \frac{1}{2}\,\rho U^2 \int_{-\infty}^{t} \Big(I_{Mh}(t-\tau)h(\tau) + I_{Mp}(t-\tau)p(\tau) + I_{M\alpha}(t-\tau)\alpha(\tau) \Big)\, d\tau
\end{aligned}
\tag{4.29}
$$

where $I_{R_i X_j}$ ($R_i = L, D, M$ and $X_j = h, p, \alpha$) indicates the aerodynamic impulse response functions.

The adoption of this force expression implies that the self-excited load evaluated at a certain time t has memory of the structural motion in a certain period of time.

It is worth to remark that with the introduction of (4.29) it is tacitly assumed that the variations of the effective angle of incidence can be considered sufficiently small, so that the corresponding changes in aerodynamic characteristics can be neglected. Generally, it is considered adequate the use of the sectional aerodynamic characteristics obtained at $\alpha = 0°$. However, when very long span bridges are under analysis it is extremely important to estimate the aerodynamic parameters taking into account the torsional displacement suffered by the deck section due to the static wind load component.

The evaluation of the impulse response functions can be performed by means of two different strategies. One consists in the direct determination of these functions by wind tunnel test, as proposed in (Caracoglia & Jones, 2003b). Anyway, this procedure is not commonly adopted because of all the difficulties that have to be overcame during the experimental campaign. Conversely, the identification of flutter derivatives in the frequency domain have been extensively developed over the years. For this reason, the second approach is based on the development of a mathematical relationship between the impulse response functions, that are defined in time domain, and the flutter derivatives, that represent the unsteady force parameters defined in frequency domain.

With this aim, as first step wind forces in (4.13) are translated in the frequency domain through their Fourier transformation:

$$\begin{bmatrix} F[L_{se}(t)] \\ F[D_{se}(t)] \\ F[M_{se}(t)] \end{bmatrix} = \frac{1}{2}\rho U^2 \begin{bmatrix} K^2(H_4 + iH_1) & K^2(H_6 + iH_5) & K^2B(H_3 + iH_2) \\ K^2(P_4 + iP_1) & K^2(P_6 + iP_5) & K^2B(P_3 + iP_2) \\ K^2B(A_4 + iA_1) & K^2B(A_6 + iA_5) & K^2B^2(A_3 + iA_2) \end{bmatrix} \begin{bmatrix} F[h(t)] \\ F[p(t)] \\ F[\alpha(t)] \end{bmatrix} \tag{4.30}$$

In the same way the force expression in (4.26) is translated in the frequency domain:

$$\begin{bmatrix} F[L_{se}(t)] \\ F[D_{se}(t)] \\ F[M_{se}(t)] \end{bmatrix} = \frac{1}{2}\rho U^2 \begin{bmatrix} F[I_{Lh}] & F\left[I_{Lp}\right] & F[I_{L\alpha}] \\ F[I_{Ph}] & F\left[I_{Dp}\right] & F[I_{P\alpha}] \\ F[I_{Mh}] & F\left[I_{Mp}\right] & F[I_{M\alpha}] \end{bmatrix} \begin{bmatrix} F[h(t)] \\ F[p(t)] \\ F[\alpha(t)] \end{bmatrix} \tag{4.31}$$

Comparing the two obtained force expression, it is possible to write the impulse response functions as follows:

$$\begin{aligned} &F[I_{Lh}] = K^2(H_4 + iH_1) && F\left[I_{Lp}\right] = K^2(H_6 + iH_5) && F[I_{L\alpha}] = K^2B(H_3 + iH_2) \\ &F[I_{Lh}] = K^2(P_4 + iP_1) && F\left[I_{Lp}\right] = K^2(P_6 + iP_5) && F[I_{L\alpha}] = K^2B(P_3 + iP_2) \\ &F[I_{Mh}] = K^2B(A_4 + iA_1) && F\left[I_{Mp}\right] = K^2B(A_6 + iA_5) && F[I_{M\alpha}] = K^2B^2(A_3 + iA_2) \end{aligned} \tag{4.32}$$

As the frequency domain force parameters are normally known only at a limited number of discrete values of the reduced frequency, it is not possible to quantify the impulse response functions directly through the inverse Fourier transformation of the above relationship. Therefore,

a continuous function to approximate the aerodynamic force parameters with respect to the reduced frequency have to be introduced. At this purpose, rational functions are the most prevalent analytic transfer function approximations used in bridge engineering. The following expression is so obtained, (Tiffany & Adams, 1988):

$$F\left[I_{R_iX_j}\right] = a_{0,R_iX_j} + a_{1,R_iX_j}\left(\frac{i\omega B}{U}\right) + a_{2,R_iX_j}\left(\frac{i\omega B}{U}\right)^2 + \sum_{i=3}^{m+3}\left(\frac{a_{i,R_iX_j}\,4\pi^2}{d_i^2U_r^2+4\pi^2} + i\frac{a_{i,R_iX_j}2\pi d_iU_r}{d_i^2U_r^2+4\pi^2}\right) \quad (4.33)$$

where a_{0,R_iX_j} are the frequency independent coefficients, R_i represents the force component of Lift, Drag and Moment while X_j is referred to the structural motion h, p, α.

Comparing the real and imaginary parts of the previous rational function with that of the impulse function in (4.32), expressions similar to those reported in (4.34) for the I_{Lh} impulse function are obtained:

$$\begin{aligned} Real\ part \quad & K^2H_4 = a_{0,\mathrm{Lh}} - a_{2,\mathrm{Lh}}\frac{4\pi^2}{U_r^2} + \sum_{i=3}^{m+2} a_{i,\mathrm{Lh}}\,\frac{4\pi^2}{d_i^2U_r^2+4\pi^2} \\ Immaginary\ part \quad & K^2H_1 = a_{1,\mathrm{Lh}}\frac{2\pi}{U_r} + \sum_{i=3}^{m+2} a_{i,\mathrm{Lh}}\,\frac{2\pi d_iU_r}{d_i^2U_r^2+4\pi^2} \end{aligned} \quad (4.34)$$

Once defined the number and the value of the poles d_i, the frequency independent coefficients a_{0,R_iX_j} is determined by fitting the experimentally obtained flutter derivatives at different reduced frequencies in a least square sense. The number of rational terms considered defines the accuracy level of the approximation. More detail about the choice of the poles is reported in (Peil & Kirch, 2008).

Once the rational function coefficients are calculated, then the aerodynamic transfer function can be extended into the Laplace domain introducing the dimensionless parameter $s = Ut/B$. The inverse Laplace transform makes the aerodynamic impulse function as follows:

$$I_{R_iX_j} = a_{0,R_iX_j}\delta(t) + a_{1,R_iX_j}\frac{B}{U}\,\dot{\delta}(t) + a_{2,R_iX_j}\frac{B^2}{U^2}\ddot{\delta}(t) + \sum_{i=3}^{m+2} a_{i,R_iX_j}\left(\delta(t) - \frac{d_iU}{B}e^{-\frac{d_iU}{B}t}\right) \quad (4.35)$$

where $\delta(t)$ is the Dirac delta function.

Finally, introducing (4.35) in (4.29), the self excited lift force induced by an arbitrary vertical motion can be rewritten as follows:

$$L_h(t) = a_{0,R_iX_j}h(t) + a_{1,R_iX_j}\frac{B}{U}\,\dot{h}(t) + a_{2,R_iX_j}\frac{B^2}{U^2}\ddot{h}(t) + \sum_{i=3}^{m+2}\int_{-\infty}^{t} a_{i,R_iX_j}e^{-\frac{d_iU}{B}(t-\tau)}\,\dot{h}(\tau)d\tau \quad (4.36)$$

Similar relationships can be obtained also for Drag and Moment force component. Looking at the obtained expression, it is worth to underline the physical meaning of each term: the first coefficient represents the non-circulatory static-aerodynamics, the second one directly modifies

the structural damping value, the third denotes the additional aerodynamic mass and the final summatory is the so called “memory term”, that considers the influence of structural motion history in the expression of the aeroelastic forces by means of structural velocity terms. Another way to explain the sense of this force component is like an “aerodynamic delay” which represents the transient effect due to the adjustment time of aerodynamic field in consequence of a change in body geometric configuration. Larger value of the “aerodynamic delay” implies larger complexity and rotationally nature of the flow field.

Looking at the force expression in (4.36) it is immediate to note that the calculation of the integral term is the most time consuming component. In order to avoid or at least to reduce the computational burden of these terms, several strategies have been developed. One method consists in considering each integral term as a new variable:

$$\Gamma_{\mathrm{i,R_iX_j}} = \int_{-\infty}^{t} a_{i,R_iX_j} e^{-\frac{d_i U}{B}(t-\tau)}\, \dot{\mathrm{X}}_{\mathrm{j}}(\mathrm{t}) d\tau \qquad i = 3\ to\ (m+2) \tag{4.37}$$

and to introduce the following first order differential equation to solve the global system:

$$\begin{gathered} \dot{\Gamma}_{\mathrm{i,R_iX_j}}(\mathrm{t}) = \int_{-\infty}^{\mathrm{t}} \mathrm{a_{iR_iX_j}} \left(-\frac{\mathrm{d_i U}}{\mathrm{B}}\right) \mathrm{e}^{-\frac{\mathrm{d_i U}}{\mathrm{B}}(\mathrm{t}-\tau)}\, \dot{\mathrm{X}}_{\mathrm{j}}(\tau)\, \mathrm{d}\tau + \mathrm{a_{iR_iX_j}}\, \dot{\mathrm{X}}_{\mathrm{j}}(\mathrm{t}) \\ \dot{\Gamma}_{\mathrm{i,R_iX_j}}(\mathrm{t}) = -\frac{\mathrm{d_i U}}{\mathrm{B}} \Gamma_{\mathrm{i,R_iX_j}} + \mathrm{a_{iR_iX_j}} \dot{\mathrm{X}}_{\mathrm{j}}(\mathrm{t}) \end{gathered} \tag{4.38}$$

Another approach to evaluate the integral term is extensively described in Lazzari (Lazzari, 2005). It is based on the idea to calculate the integral memory terms by means of a recursive expression. In other words, by means of this approach the value of the integral term $\Gamma_{\mathrm{i,R_iX_j}}$ at a general time t can be calculated in an approximate way considering its value obtained at the previous time step and adding a corrective term evaluated as function of the structural velocity. The final expression of the memory term is:

$$\Gamma_{\mathrm{i,R_iX_j}}(t_i) \cong e^{-\frac{d_i U}{B}\Delta t}\, \Gamma_{\mathrm{i,R_iX_j}}(t_{i-1}) + \mathrm{a_{iR_iX_j}}\, e^{-\frac{d_i U}{2B}\Delta t}\, \dot{\mathrm{X}}_{\mathrm{j}}(\mathrm{t_{i-1}})\, \Delta \mathrm{t} \tag{4.39}$$

The value of the memory term calculate by means of this recursive relation can be considered a good approximation of the real one if a small enough time step value is chosen.

More details about the computational implementation of these two methods are furnished in section 5.3.

4.5 Buffeting forces in time domain

Buffeting forces for bridge cross-sections are commonly treated under the quasi-steady theory main assumption, namely that the turbulence load is not depending on the frequency. In order to achieve a more realistic representation of wind-structure interaction, several attempts to remove these hypotheses can be found in literature.

In (Davenport, 1962) the definition of buffeting loads depending on frequency parameters has been proposed through the introduction of aerodynamic admittance functions, so as to describe the relationship between the smooth and turbulent wind response of the deck. Subsequently, the unsteadiness of the buffeting load has been extended also in the time domain, as first suggested in (Scanlan, 1993) which modeled the forces by means of indicial functions. An alternative expression of admittance functions in time domain was proposed in (Chen, Matsumoto, & Kareem, 2000b) using rational function approximation techniques. Since the latter approach is coherent with the one adopted in the previous section to describe self-excited forces, the mathematical formulation to simulate turbulent wind loads using the rational function technique is here reported.

The frequency dependent buffeting forces per unit span are commonly expressed as follows:

$$\begin{aligned} L_b(t) &= \frac{1}{2}\,\rho U^2 B\left(2C_L\,\chi_{\mathrm{L,bu}}\frac{u(\tau)}{U} + (C_L' + C_D)\chi_{L,bw}\frac{w(\tau)}{U}\right) \\ D_b(t) &= \frac{1}{2}\,\rho U^2 B\left(2C_D\chi_{\mathrm{D,bu}}\frac{u(\tau)}{U} + C_D'\chi_{D,bw}\frac{w(\tau)}{U}\right) \\ M_b(t) &= \frac{1}{2}\,\rho U^2 B^2\left(2C_M\chi_{\mathrm{M,bu}}\frac{u(\tau)}{U} + C_M'\chi_{M,bw}\frac{w(\tau)}{U}\right) \end{aligned} \tag{4.40}$$

where $\chi_{F,bq}$ ($F = L, D, M$ and $q = u, w$) represents the aerodynamic transfer functions between fluctuating wind velocities and buffeting forces.

On the other hand, the buffeting forces per unit span can be expressed in terms of the convolution integrals involving the aerodynamic impulse functions and fluctuating wind velocities:

$$\begin{aligned} L_b(t) &= \frac{1}{2}\,\rho U^2\int_{-\infty}^{t}\left(I_{L,bu}(t-\tau)\frac{u(\tau)}{U} + I_{L,bw}(t-\tau)\frac{w(\tau)}{U}\right)d\tau \\ D_b(t) &= \frac{1}{2}\,\rho U^2\int_{-\infty}^{t}\left(I_{D,bu}(t-\tau)\frac{u(\tau)}{U} + I_{D,bw}(t-\tau)\frac{w(\tau)}{U}\right)d\tau \\ M_b(t) &= \frac{1}{2}\,\rho U^2\int_{-\infty}^{t}\left(I_{M,bu}(t-\tau)\frac{u(\tau)}{U} + I_{M,bw}(t-\tau)\frac{w(\tau)}{U}\right)d\tau \end{aligned} \tag{4.41}$$

where $I_{F,bq}$ ($F = L, D, M$ and $q = u, w$) indicates the aerodynamic impulse functions of buffeting forces. This expression for the buffeting force component implies that the deck at a certain time t is excited not only by the turbulence component incoming at time t, but also by what has happened between the eddies in the flow and the deck at previous time $(t - \tau)$. In other words, there are a phase lag and a time lag between the source of the excitations and the aerodynamic forces themselves.

Following the same procedure as for the self excited forces, the frequency dependent buffeting forces can be extended in the time domain comparing the Fourier transform of aerodynamic impulse function of buffeting forces with those obtained for the aerodynamic transfer functions as follows:

$$F\left[I_{\mathrm{L,bu}}\right] = 2\mathrm{B}\,\chi_{\mathrm{L,bu}}\,\mathrm{C_L} \qquad F\left[I_{\mathrm{L,bw}}\right] = \mathrm{B}\,\chi_{\mathrm{L,bw}}(\mathrm{C_D} + \mathrm{C'_L})$$
$$F\left[I_{\mathrm{D,bu}}\right] = 2\mathrm{B}\,\chi_{\mathrm{D,bu}}\,\mathrm{C_D} \qquad F\left[I_{\mathrm{D,bw}}\right] = \mathrm{B}\,\chi_{\mathrm{D,bw}}(\mathrm{C'_D} - \mathrm{C_L}) \tag{4.42}$$
$$F\left[I_{\mathrm{M,bu}}\right] = 2\mathrm{B}^2\,\chi_{\mathrm{M,bu}}\,\mathrm{C_M} \qquad F\left[I_{\mathrm{M,bw}}\right] = \mathrm{B}\,\chi_{\mathrm{M,bw}}\,\mathrm{C'_M}$$

Also in this case, because the aerodynamic admittance function is extracted from wind tunnel test performed at discrete value of the reduced frequency, their expression have to be approximate in terms of rational functions:

$$\chi_{\mathrm{L,bu}} = a_{0,L,bu} + \sum_{\mathrm{j}=1}^{\mathrm{m}} \left(a_{\mathrm{j},L,bu} - a_{\mathrm{j},L,bu} \frac{\mathrm{d_j U}}{\mathrm{i\omega B} + \mathrm{d_j U}} \right) \tag{4.43}$$

Accordingly, the impulse function of buffeting forces can be extended into the Laplace domain introducing the dimensionless parameter s:

$$\mathrm{I_{L,bu}} = 2\mathrm{BC_L} \left(\left(a_{0,L,bu} + \sum_{\mathrm{j}=1}^{\mathrm{m}} a_{\mathrm{j},L,bu} \right) \delta(\mathrm{s}) - \sum_{\mathrm{j}=1}^{\mathrm{m}} a_{\mathrm{j},L,bu} \mathrm{d_j e^{-d_j s}} \right) \tag{4.44}$$

The resulting expression of wind turbulent loads in the time domain results as follows:

$$L_{bu}(t) = \frac{1}{2}\rho \mathrm{BU^2(2C_L)} \left(\left(\sum_{\mathrm{j}=0}^{\mathrm{m}} a_{\mathrm{j},L,bu} \right) \frac{u(t)}{U} - \sum_{j=1}^{m} \frac{\mathrm{d_j U}}{\mathrm{B}}\, \Phi_{\mathrm{j,L,bu}}(\mathrm{t}) \right)$$
$$\dot{\Phi}_{\mathrm{j,L,bu}}(\mathrm{t}) = -\frac{d_j U}{B} \Phi_{L,bu}(t) + a_{j,L,bu} \frac{u(t)}{U} \tag{4.45}$$

where $\Phi_{L,bu}(t)$ is the augmented aerodynamic state vector. Similar expression for other buffeting force components can be obtained in analogous way.

Usually wind tunnel tests adopt passive turbulence generation methods to define the aerodynamic admittance function. In (Diana, Bruni, Cigada, & Zappa, 2002) a new experimental technique, based on the use of an active turbulence generator is adopted. This particular experimental rig allows to separate and investigate in details the effect of parameters like the reduced velocity and the gust wavelength. A new expression of the buffeting forces has been proposed introducing a complex aerodynamic admittance function. The use of this new force expression allows to check the hypothesis of linearity and to account for both amplitude and phase of the turbulent wind response. The effectiveness of the proposed method is shown by means of the comparison between spring-supported sectional model response in wind tunnel and numerical simulations. It has been also pointed out that the phase of the aerodynamic admittance function plays a role in the definition of the total force due to the different attack angle harmonic components, which could lead to ambiguous results if ignored.

The bridge design process is generally focused on the evaluation of the critical wind velocity, and usually the definition of the aerodynamic admittance function is not performed during the wind tunnel campaign. For this reason, in literature several analytical investigation on the possible existence of phenomenological relationships between buffeting and self-excited parameters are available. Although in principle they are different, under the hypothesis that vertical gust and vertical bridge velocity give similar aerodynamic loads a relationships between these functions may exist. (Hatanaka & Tanaka, 2002), (Tubino, 2005) and (Costa, Borri, Flamand, & Grillaud, 2007) follow this path defining admittance functions from all eight flutter derivatives.

Finally, another aspect that affects the structural response in presence of turbulence, is the effective correlation among aerodynamic forces along the deck span. In fact, several wind tunnel tests have shown that force correlation is stronger than the one due to the turbulence fluctuations in the incoming air flow, (Larose & Mann, 1998). In particular, experimental measurements performed on a rectangular section have indicated that, for self-excited forces, the values remains quite close to unity, while turbulence results in a slight loss of the span wise correlation (Hann, 2000).

4.6 Other wind force models

In the wind load models presented until now the interaction between self-excited and aeroelastic wind forces is neglected and superposition of effects is adopted. In particular, two different linear models have been presented: the quasi-steady one that consider the load nonlinearities due to the effective angle of incidence, and those based on Scanlan force expressions, in which the unsteadiness of the flow is considered so that the self-excited load results function of frequency coefficients. These force models are commonly used to evaluate the bridge deck stability considering the aeroelastic characteristics of the cross-section evaluated in correspondence of the undeformed deck configuration, $\alpha = 0°$. However, when the design of long-span bridges is under investigation, particular care has to be given to the static wind action which could lead to large structural deformation because of its low stiffness. On the one hand, the large deformation will influence the structural stiffness and the dynamic characteristics. Moreover, the aerodynamic shape remarkably changed because of the static torsional displacement, leading to significant variation and non uniform distribution of the wind force acting on the bridge (Zhang, Xiang, & Sun, 2002). For all these reason, the effects due to structural deflections have to be considered for a proper evaluation of the aerodynamic behavior of long-span bridges.

Some advanced models for the evaluation of wind loads have been developed in last decades. Particular attention has been paid to the investigation of the effects of turbulence on the structural stability. A first improvement to the classical models have been performed treating the presence of turbulence as a stochastic process (Caracoglia, 2008). In (Bartoli, Borri, & Gusella, 1997) both stabilizing and destabilizing effects due to turbulence have been observed on different sectional bridge models, which suggest that extracting flutter derivatives from wind tunnel tests in smooth flow may be no longer valid, since the aeroelastic load can be influenced by the properties of the turbulence. Furthermore, another important effects that has to be carefully considered is the

change of the effective angle of incidence due to the turbulent wind flow presence. In fact, from several wind tunnel test campaigns it has observed that the aeroelastic behavior of deck sections is generally strongly affected by this type of load nonlinearities. Several authors have investigated this problem. A comprehensively review of their works is hereafter reported. Finally, an extensively description of a new and effective aeroelastic nonlinear force model is provided and widely commented.

Corrected quasi-steady theory

In relation to the studies done for the bridge over Stetto di Messina in Italy, in (Diana, Cheli, Zasso, Collina, & Brownjohn, 1992), (Diana, Cheli, Bruni, Collina, & Larose, 1993) and (Diana, Falco, Bruni, Cigada, & Collina, 1994) the development of a new aeroelastic force model close to the quasi steady one is proposed, where some limitation have been lifted by the development of a "corrected" theory. In particular, the motion-induced forces for the vertical and torsional degrees of freedom are included in this formulation considering also the unsteadiness of the flow. Furthermore, the location of the centre of the aerodynamic forces is defined by means of the analysis of the aerodynamic derivatives behaviour.

An equivalent linearization at each reduced velocity is proposed to include the motion-induced forces:

$$\begin{aligned} \mathrm{C_L^*}(\alpha) &= \mathrm{C_L}(\alpha_0) + \int_{\alpha_0}^{\alpha} \mathrm{K_L^*}\, \mathrm{d}\overline{\alpha} \\ \mathrm{C_M^*}(\alpha) &= \mathrm{C_M}(\alpha_0) + \int_{\alpha_0}^{\alpha} \mathrm{K_M^*}\, \mathrm{d}\overline{\alpha} \end{aligned} \tag{4.46}$$

where $C_L^*(\alpha)$ and $C_M^*(\alpha)$ are the corrected aerodynamic coefficients, $C_L(\alpha_0)$ $\mathrm{C_M}(\alpha_0)$ are the static coefficient at angle of attack α_0 of the equilibrium position, K_L^* and $\mathrm{K_M^*}$ are the aerodynamic derivatives (lift slope varying with reduced velocity) computed as reported in Eq.(4.47) and α is the apparent angle of attack based on Eq.(4.25).

$$\begin{aligned} \mathrm{K_L^*} &= \mathrm{h_3} \cdot \left(\frac{\partial \mathrm{C_L}}{\partial \alpha}\right)_{\alpha=\overline{\alpha}} \\ \mathrm{K_M^*} &= \mathrm{a_3} \cdot \left(\frac{\partial \mathrm{C_M}}{\partial \alpha}\right)_{\alpha=\overline{\alpha}} \end{aligned} \tag{4.47}$$

For multi degree of freedom structures, the motion frequency is seen as a combination of overall mode shape frequencies. When nonlinear structure are under analysis, these vary at every instant, depending on the state of the structure. For this reason, the computation of (4.47) is not easily practicable. To overcame this problem, it is propose to evaluate the aerodynamic coefficients considering the reduced velocity value evaluated in reference to the fundamental structural frequency. In the same work it is shown that this force formulation can be considered adequate in many ways, excepting when it deals with the response of higher modes.

In this force formulation the load nonlinearities due to the effective angle of incidence are taken into account, however this force model does not consider in a exhaustive way the effects due to the aerodynamic delay. In particular, the dependence of forces from the oscillation motion frequency and the span wise coherence of forces are not dealt with. Anyway, in (Zasso, 1996) it is outlined that for streamlined sections the quasi-steady-modified approach gives a good estimation of the aeroelastic behaviour of the bridge deck. Moreover, the proposed analytical model scheme is close to a physical interpretation of the phenomenon; for this reason the quasi-steady approach is considered to be a powerful tool in the prediction of the sectional aeroelastic behaviour.

Another method based on the quasi-steady theory developed in the time domain has been proposed in (Su, Fan, & He, 2007). Also in this case, the main issue pursued is about the simulation of frequency domain characteristics of both the wind loads and the bridge deck motion. After the assumption of some hypothesis and the introduction of some approximations, the obtained final force formulation appears as follows:

$$\begin{aligned} L_{se}(t) &= \frac{1}{2}\rho U^2 B\left[-h_1(C'_L + C_D)\frac{\dot{h}}{U} + h_2(C'_L + C_D)\frac{r}{B}\frac{B\dot{\alpha}}{U} - h_3 C'_L \alpha\right] \\ M_{se}(t) &= \frac{1}{2}\rho U^2 B^2\left[a_1 C'_M \frac{\dot{h}}{U} - a_2 \frac{C'_M}{B}\frac{r}{U} + a_3 C'_M \alpha\right] \end{aligned} \tag{4.48}$$

where:

$$\begin{aligned} h_1 &= -\frac{1}{(C'_L + C_D)} K H_1(K) \qquad h_2 = \frac{B1}{(C'_L + C_D)} K H_2(K) \qquad h_3 = -\frac{B1}{C'_L} K^2 H_3(K) \\ a_1 &= \frac{1}{C'_M} K A_1(K) \qquad a_2 = -\frac{1}{r\, C'_M} K A_2(K) \qquad a_3 = \frac{1}{C'_M} K^2 A_3(K) \end{aligned} \tag{4.49}$$

The authors have observed that generally both mode shapes and frequencies of the structural response are little modified by the influence of the aerodynamic forces. Furthermore, from the analysis of a bridge deck, they observed that the above introduced corrected coefficients do not change significantly with respect to different vertical or torsional frequencies values. For all these reasons, the reduced frequency values used to evaluate all the aerodynamic parameters are assumed to be equal to the first vertical and torsional natural frequencies.

It is worth pointing out that this force formulation is really close to the one proposed by the research group of "Politecnico di Milano Mechanical Department", so that the same advantages and limitations can be detected in both the models.

Nonlinear unsteady aerodynamic forces developed by Chen and Kareem

In (Chen, Kareem, & Haan, 2000) a new nonlinear force formulation developed in the time domain is proposed and subsequently developed in (Chen & Kareem, 2001), (Chen & Kareem, 2003). In this approach the nonlinear unsteady aerodynamic forces are modelled based on static coefficients, flutter derivatives, and admittance functions along with the span wise correlations at

varying angles of incidence. In particular, it is proposed to separate the effective angle of incidence in two component, one in low and the other in high frequency, considering the lowest natural frequency of the bridge as cut-off frequency value:

$$\alpha_{eff}(t) = \alpha_{eff}^{l}(t) + \alpha_{eff}^{h}(t) \tag{4.50}$$

It is assumed that the both the structural and the wind turbulent low frequency components contribute to change the global aerodynamic behaviour of the deck section, while the corresponding high frequency components alter the flow condition around the cross-section. Accordingly to the angle decomposition, also the nonlinear aerodynamic forces are approximately expressed as the sum of low and high frequency components:

$$F = F\left(\alpha_{eff}\right) \approx F\left(\alpha_{eff}^{l}\right) + \left.\frac{dF}{d\alpha}\right|_{\alpha_{eff}^{l}} \alpha_{eff}^{h} = F^{l} + F_{se}^{h} + F_{b}^{h} \tag{4.51}$$

In the last equation, the low frequency force is expressed as a nonlinear function of the angle of attack in light of the quasi-steady theory as reported in (4.10), (4.11) and (4.12) where only the low frequency part of wind fluctuation and structural motion are considered. In the authors opinion, the choice of the quasi-steady approach to model the low frequency force component is considered appropriate because of its validity at high reduced velocities. Conversely, the high frequency components of the aerodynamic forces are expressed by a linearization around the low-frequency effective angle of attack $\alpha_{eff}^{l}(t)$ and further separated into self-excited and buffeting force components. In particular, the self-excited forces are considered spatially fully correlated and their evaluations is performed by means of the convolution integral technique, as reported in section 4.4. For the lift force it is:

$$\begin{aligned} L_{se}^{h}(t) = \frac{1}{2}\rho U^{2} \int_{-\infty}^{t} \Big(& I_{Lh}\left(\alpha_{eff}^{l}, t-\tau\right) h^{h}(\tau) + I_{Lp}\left(\alpha_{eff}^{l}, t-\tau\right) p^{h}(\tau) \\ & + I_{L\alpha}\left(\alpha_{eff}^{l}, t-\tau\right) \alpha^{h}(\tau) \Big) \, d\tau \end{aligned} \tag{4.52}$$

where h^h, p^h and α^h are the high frequency components of the dynamic displacements in vertical, lateral and torsional directions, and I_{Lh}, I_{Lp} and $I_{L\alpha}$ are the correspondingly aerodynamic impulse response functions. Similar expression can be obtained also for the other two force components of drag and moment.

In a similar way, the high frequency buffeting force components are evaluated in terms of the following convolution integral:

$$\begin{aligned} L_{b}^{h}(t) = -\frac{1}{2}\rho U^{2} \int_{-\infty}^{t} \int_{-\infty}^{\tau_2} \Bigg(& J_{Lu}\left(\alpha_{eff}^{l}, t-\tau_2\right) \times I_{Lu}\left(\alpha_{eff}^{l}, \tau_2-\tau_1\right) \frac{u^{h}(\tau_1)}{U} + J_{Lw}\left(\alpha_{eff}^{l}, t-\tau_2\right) \\ & \times I_{Lw}\left(\alpha_{eff}^{l}, \tau_2-\tau_1\right) \frac{w^{h}(\tau_1)}{U} \Bigg) d\tau_1 d\tau_2 \end{aligned} \tag{4.53}$$

where u^h and w^h are the high frequency component of turbulence, I_{Lu} and I_{Lw} are the aerodynamic impulse functions of unsteady characteristics of buffeting forces and J_{Lu} and J_{Lw} indicate the impulse response function of the spatial correlation.

In Fig. 21 the analysis framework of the proposed nonlinear approach is reported.

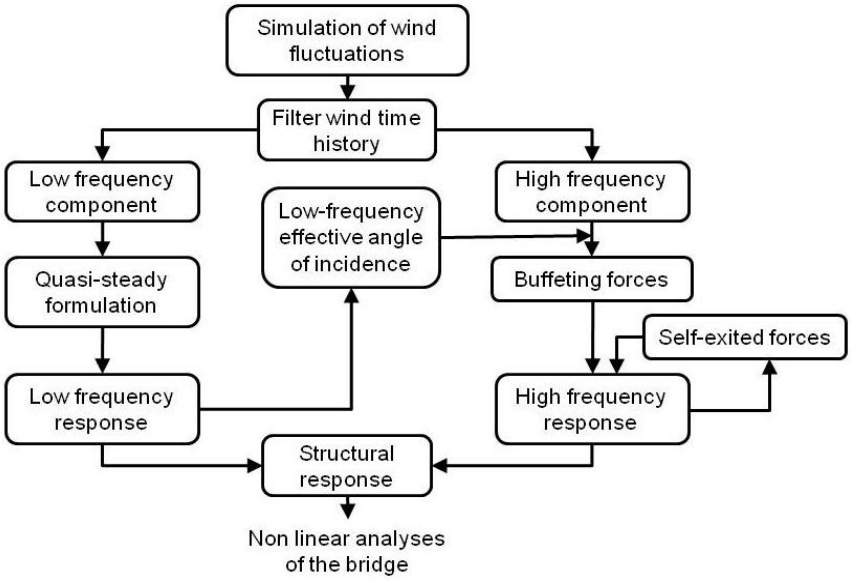

Fig. 21: Nonlinear analysis framework developed by Chen and Kareem

More details about this approach can be find in their papers where several long-span bridges are investigated using this nonlinear analysis framework. From the results reported it is possible to observed that aerodynamic nonlinearities may influence the buffeting response as well as the flutter threshold presenting both stabilizing or destabilizing effects. However, the comparison of results computed by means of the nonlinear model with those obtained using the classical linear approach does not show significant differences between each other.

Nonlinear unsteady aerodynamic forces developed by Diana

In (Diana, Cheli, Zasso, Collina, & Bruni, 1998), (Diana, Bruni, Cigada, & Zappa, 2002) and (Diana, Bruni, & Rocchi, 2005) a new framework to evaluate the aerodynamic forces considering the effects due to the presence of the turbulent wind is proposed. The main idea at the base of this approach is the decomposition of the structural response into components referred to different frequencies. Accordingly, the wind spectrum is divided into several bands, which corresponds to one low frequency range, identified as “0 band”, and several high frequency sub-ranges as reported in Fig. 22.

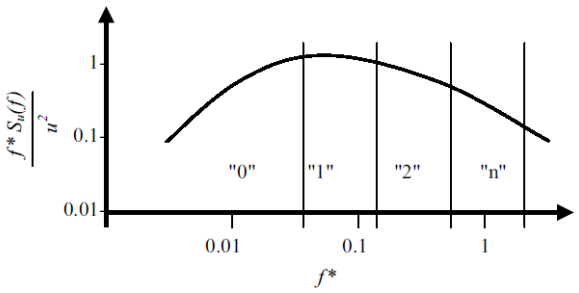

Fig. 22: Wind bands (Diana, Bruni, Cigada, & Zappa, 2002)

In this force model, the upper value of the low-frequency range is the one related to the lowest reduced velocity value in correspondence of which the quasi steady assumption is still valid. In other words, the “0 band” represents the slowly varying components of the wind where the quasi-steady theory is adopted to calculate the structural response. In this way, in the low-frequency range, nonlinearities due to angle of incidence variation are accounted for, while the aerodynamic coefficients are considered frequency independent. The response induced by the high frequency range is reproduced by means of the “corrected quasi-steady theory” linearizing the solution around the results obtained by the low frequency response; in this way the slow angle of attack are considered in the definition of aeroelastic characteristics. It is worth to remark that the choice of the frequency band boundaries is performed in order to follow the aerodynamic coefficients variability with the reduced frequency, and not depending on the values of the structure natural frequencies.

In all the numerical model presented until now, an attempt to include both frequency and angle nonlinearities effects have been pursued. However, another particular type of load nonlinearities has been recently pointed out by means of wind tunnel investigation; it is the one related to the amplitude of oscillation of the structural motion. With this aim, a new fully nonlinear numerical model for the simulation of aeroelastic loads has been recently presented in (Diana, Resta, & Rocchi, 2008) and (Diana, Rocchi, Argentini, & Muggiasca, 2010). A rheological mechanical model stands at the basis of this new approach. The fundamental idea is based on the comparison between the aerodynamic forces measured on deck sections with the hysteretic effects measured on the mechanical systems as function of the instantaneous angle of attack. The crucial point of this approach is the identification of the aerodynamic force characteristic loop by means of wind tunnel tests, which have to be measured under low turbulence wind condition while the model is driven to oscillate in torsional motion at high amplitudes of the angle of incidence. An application in the time domain of this new approach is reported in the second reference cited, and the aerodynamic instability of a deck section model is extensively investigated. The comparison between linear and nonlinear models highlights again the importance to consider the effects due to the variations of the instantaneous angle of incidence.

4.7 Proposal of a new wind load model

The analysis of the structural response of a bridge deck is usually investigated by means of a linear aerodynamic force model. Until now, this approach has proven its utility for many applications. However, linear models are not suited to completely address the challenges posed by the design of innovative bridges that generally show high sensitivity to the effective angle of incidence. In classical linear approach the flutter threshold is determined referring only to the mean wind velocity since structural response due to buffeting load is considered as uncoupled with respect to the aeroelastic one. As a matter of fact, turbulence plays an important role in flutter instability, as (Scanlan & Lin, 1978) has firstly pointed out.

In recent papers, like (Matsumoto, Yagu, Ishizaki, Shitato, & Chen, 1998) and (Zhang, Xiang, & Sun, 2002), the results of wind tunnel test, carried out on several cross section characterized by different shapes in correspondence of different angles of incidence, have been reported. All these experimental campaigns have highlighted that aerodynamic forces are highly sensitive to the angle of attack value. Moreover, experimental evidences in (Bocciolone, Cheli, Curami, & Zasso, 1992) have outlined that even with small levels of turbulence the effective angle of incidence may vary to such a degree that analysis results may not be realistic without accounting for aerodynamic nonlinearities.

In (Ricciardelli & Marra, 2008), (Haan, Kareem, & Szewczyk, 1998) and (Haan & Kareem, 2009) another interesting aspect of the aerodynamic behaviour of cross-sections has been pointed out. These papers report the results of wind tunnel experimental campaign performed on sectional models instrumented with multiple pressure transducers under both laminar and turbulent wind conditions. It has been observed that the pressure field around the cross sections changes topology depending on the flow acting on them, also affecting the flutter derivatives values.

In other works, the focus has been posed on the turbulence influence on the aeroelastic stability. Particular attention has been paid on the effects due to the lack of correlation of the incoming wind flow along the bridge deck. Several experimental campaigns, like those reported in (Bartoli & Righi, 2006) and (Ehsan & Bosch, 1989), have shown the sectional models tendency to reduce the amplitude response when immersed in a turbulent field. It has been mainly attributed to the reduction of the span-wise correlation of aerodynamic forces in turbulent flow compared to those obtained in smooth flow, as it has been observed also in (Sarpkaya, 1979) and (Ehsan & Scanlan, 1990).

For all these reasons, in recent years great interest has been devoted to the development of numerical techniques allowing to correctly simulate the turbulence effects on bridge stability as well as the nonlinear effects associated with high angle of incidence. For example, in (Nakamura, 1993) some experimental wind tunnel studies have pointed out that the presence of turbulence can both stabilize or destabilize the flutter instability depending on the geometric configuration of bridge sections and on the characteristics of wind fluctuations.

When the influence of turbulence on flutter analysis is considered, the problem becomes extremely intricate, even more when nonlinear terms are taken into account.

In this section a new wind load model based on flutter derivatives used in time domain by means of impulse response function is proposed. The influence of nonlinearities due to both effective angle of incidence and reduced wind velocity are taken into account. In particular, the turbulence effects on self-excited forces are modelled through the changes of the effective angle of incidence caused by the turbulence, so that its influence on flutter instability can be investigated.

The new force formulation is based on the idea to enhance the classical linear approach in time domain presented in Section 4.4, where the frequency dependent parameters of unsteady aerodynamic forces are considered using a rational function approximation technique. In the linear model wind forces are linearized around the static deformed deck configuration; in other words, the aeroelastic load is evaluated by means of the set of flutter derivatives obtained from wind tunnel test performed at just one fixed angle. The most relevant aspect of the nonlinear framework here proposed is that the aerodynamic characteristics are modulated by the spatiotemporally varying low-frequency effective angle of incidence. This means that, at each time step, the set of flutter derivatives used to evaluate the aeroelastic forces are updated as function of the angle of incidence. The crucial point of this nonlinear model is the proper evaluation of the angle that have to be used to choose the set of flutter derivatives. The global effective angle of incidence due to structural motion and wind turbulence is defined as:

$$\alpha_{eff}(t) = \alpha_s + \frac{w(t)}{U + u(t)} + \alpha(t) \tag{4.54}$$

As already pointed out by several authors, whose works have been reported in previous sections, it is not correct using the total angle of incidence reported in (4.54) to change the set of flutter derivatives at each time step. In particular, only the low frequency component should be considered since the change of the angle must be slow enough to influence the aeroelastic behaviour of the whole section. A cut-off frequency value has to be defined in order to split the effective angle of incidence in both high and low frequency components. Again, when the quasi-steady condition is reached, unsteadiness effects can be neglected and aeroelastic forces can be described just as function of the angle of incidence. For these reasons, the identification of the cut-off frequency value is performed as follows. First, according to the flutter derivatives representation of Zasso convention, when the reduced velocity grows the trend of aeroelastic derivatives tends to be constant since the quasi-steady behaviour is approached. The cut-off frequency value is calculated choosing the reduced velocity value over which the quasi-steady behaviour is reached. Reminding that $U_{red} = \frac{2\pi}{K} = \frac{1}{f}\frac{U}{B}$, the cut-off frequency is defined as:

$$f_{cut-off} = \frac{U}{U_{red}^{cut-off} \cdot B} \tag{4.55}$$

where U is the mean wind velocity at which the analysis will be performed.

The calculated cut-off frequency represents the limit value under which the angle of incidence variation is considered slow enough not to affect the unsteadiness characteristics of the flow field

around the body. Anyway, because of the varying angle of incidence, the global aerodynamic behaviour of the cross section changes too, quite like in a quasi-steady condition.

Under these assumption, it is correct to calculate the aerodynamic forces, that change the set of aeroelastic derivatives at each time step, according to the low frequency component of the angle of attack:

$$\alpha_{f.d.}(\mathrm{t}) = \alpha_s + \frac{w^{LF}(\mathrm{t})}{U + u^{LF}(\mathrm{t})} + \alpha^{LF}(\mathrm{t}) \tag{4.56}$$

The parameter $\alpha_{f.d.}(\mathrm{t})$ is the sum of three terms: the static angle that is the mean deformed configuration of the deck under the static wind forces, the fluctuating angle due to the low frequency turbulence component and the low frequency component of structural torsional displacement. Since the evaluation of aerodynamic forces depends on $\alpha_{f.d.}(\mathrm{t})$ and this one depends on the unknown structural response, an iterative procedure should be performed to solve the problem. However, it is possible to introduce some simplifications, as follows.

Let's consider the action of a wind turbulence characterized by a spectrum $S(n)$. In the frequency domain, the structural response is represented by the transfer function $|H(n)|^2$, also called mechanical admittance function. The deck response to wind turbulence is evaluated, as in (Holmes, 2001), using the following equation:

$$\mathrm{S_x(n)} = \frac{1}{\mathrm{k}^2}|H(n)|^2\mathrm{S(n)} \tag{4.57}$$

In Fig. 23 a qualitative representation of these functions is reported. When both buffeting and aeroelastic loads are considered, the structural response in the low frequency range is negligible comparing to the resonant component. It is also confirmed looking at all the graphs about the structural spectral response reported in Chapter 6.

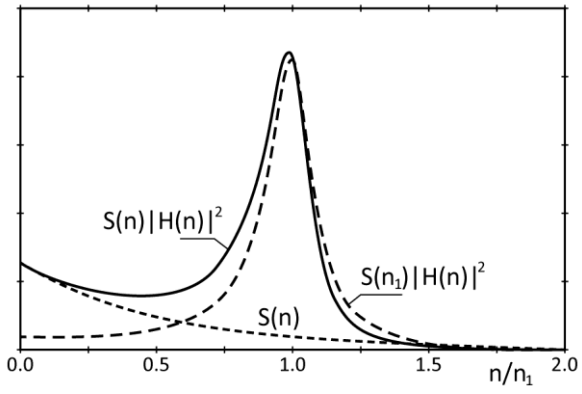

Fig. 23: Structural response in frequency domain

So, it is possible to neglect the contribution of $\alpha^{LF}(\mathrm{t})$ in the evaluation of the angle $\alpha_{f.d.}(\mathrm{t})$, and its value can be simply calculated as:

$$\alpha_{f.d.}(\mathrm{t}) = \alpha_s + \frac{w^{LF}(\mathrm{t})}{U + u^{LF}(\mathrm{t})} \tag{4.58}$$

This direct evaluation of $\alpha_{f.d.}(\mathrm{t})$ lets to avoid the iterative procedure of which before.

The parameter $\alpha_{f.d.}(\mathrm{t})$ values depend on the choice of both the turbulent wind field characteristics and of the cut-off frequency value. Anyway, its value can range in an interval of several degrees. As flutter derivatives are extracted by means of wind tunnel campaign, their values are known only at few angle of incidence. Therefore, an extrapolation of these coefficients to the whole domain of interest should be performed. To this issue, a fitting procedure of the known values must be adopted. As a first step, for every chosen angle of incidence, all the flutter derivatives sets we obtained by the wind tunnel tests are approximated with rational functions. Then, throughout a polynomial interpolation, the function describing the variation of the flutter derivatives is obtained with respect to the angle of incidence.

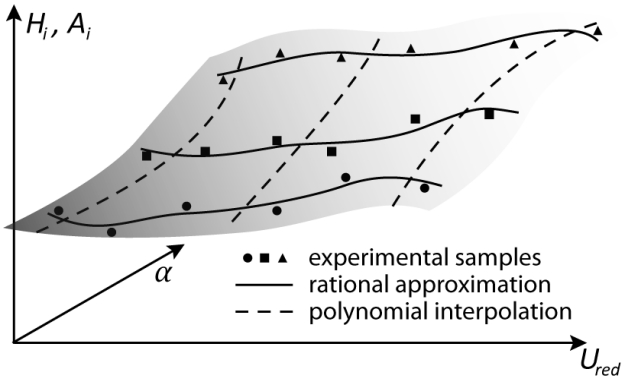

Fig. 24: Flutter derivatives approximation

Once the value of $\alpha_{f.d.}(t)$ is defined in this way, the expression of self-excited forces in the proposed nonlinear force model is similar to those reported in (4.13), where flutter derivatives values depend not only on the reduced frequency parameter but also on the value of the low frequency component of the angle of incidence. If only two degrees of freedom are considered, then the equations of aeroelastic forces become:

$$\begin{aligned} L_{se}(t) = \frac{1}{2}\rho U^2 B \Bigg(& KH_1(K,\alpha_{f.d.})\frac{\dot{h}}{U} + KH_2(K,\alpha_{f.d.})\frac{B\dot{\alpha}}{U} + K^2H_3(K,\alpha_{f.d.})\alpha \\ & + K^2H_4(K,\alpha_{f.d.})\frac{h}{B}\Bigg) \end{aligned} \tag{4.59}$$

$$\begin{aligned} M_{se}(t) = \frac{1}{2}\rho U^2 B \Bigg(& KA_1(K,\alpha_{f.d.})\frac{\dot{h}}{U} + KA_2(K,\alpha_{f.d.})\frac{B\dot{\alpha}}{U} + K^2A_3(K,\alpha_{f.d.})\alpha \\ & + K^2A_4(K,\alpha_{f.d.})\frac{h}{B}\Bigg) \end{aligned}$$

Like in the linear approach case, the aerodynamic forces are expressed by a linearization, but now around the angle $\alpha_{f.d.}(t)$. So, their expression in time domain is given in terms of a convolution integral, that for the lift component is:

$$L(t) = \frac{1}{2}\rho U^2 \int_{-\infty}^{t} \Big(I_{Lh}(\alpha_{f.d.}(t), t-\tau)h(\tau) + I_{Lp}(\alpha_{f.d.}(t), t-\tau)p(\tau) + I_{L\alpha}(\alpha_{f.d.}(t), t-\tau)\alpha(\tau) \Big) d\tau \quad (4.60)$$

Where, like in the linear approach, the impulse response functions are evaluated, by means of their relationship with flutter derivatives, that will change at each time step since their dependence on the value of $\alpha_{f.d.}(t)$.

The most important feature of the proposed nonlinear analysis framework are reported in the flow chart of Fig. 25.

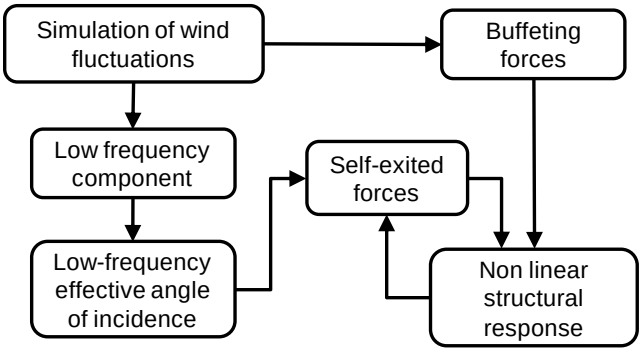

Fig. 25: Flow chart of the nonlinear force model

Summarizing, the structural static deformed configuration at a given mean wind velocity must be first calculated. Then, time histories turbulent wind components at the center of each bridge elements must be numerically simulated once the cross power spectral density matrix is known. By means of a digital filter, the low-frequency components of the simulated wind fluctuations are calculated, so that the value of the angle $\alpha_{f.d.}(t)$ and the associated aerodynamic parameters, could be defined in correspondence of each time step. Finally, the aeroelastic forces can be computed.

This unique analysis framework allows to numerically investigate the effects of wind turbulence on flutter and buffeting responses.

It is worth to stress that the proposed approach differs from the classical one because of the aerodynamic force parameters modulation by the instantaneous angle of incidence $\alpha_{f.d.}(t)$, while in the traditional linear analysis the force parameters take their values at the statically deformed position of bridge sections. For all those deck sections whose aerodynamic characteristics are highly sensitive to the changes of the mean angle, the nonlinearities in the aerodynamic forces should not be neglected.

Chapter 5

Numerical procedures

5.1 Introduction

In this section a complete description of the computational procedures that have been implemented to analyse the effects of wind load on bridges is addressed.

The first step is the schematization of the real bridge by means of a three dimensional finite element model. With this aim, starting from the fully developed 3D FE model of the bridge as it was produced by the design team, a strong simplification of the numerical model is done neglecting all the special features for the details design, necessary for the constructors, but maintaining or better highlighting the global behaviour of the structure under the effects of a overall excitation. This step allows to draw attention to the dynamic performance of the whole bridge subjected to the wind loads underlining the natural frequencies and the modal shapes with a simple FE model which can be easily checked during any step of the procedure. Moreover a simplified model with clean natural frequencies and modal shapes lets the designer to include different damping ratios in relation to the different modes in agreement with the results of full scale tests. Obviously the last remark is applicable only for existing bridges subjected to deeply investigations.

A further simplification is usually adopted in literature in order to reduced the whole system to an equivalent sectional model characterized just by three degrees of freedom. This simple mechanical model, that perfectly reproduces the physical model that is tested in wind tunnel, allow to investigate the bridge deck aerodynamic behaviour by means of easier and faster calculations. It represents a 2D rigid cross section whose having pitching and sway motions are restricted by linear springs. In this way the complete structure is reduced to an equivalent bimodal system that, if properly calibrated, can leads almost to the same results of the three dimensional model when the flutter instability is investigated. The equivalence between full and sectional model results is mainly due to the fact that flutter phenomena generally arise from the coupling of only a heaving and a torsional mode, or more rarely of a sway and a torsional ones.

In the present work the following assumptions have been considered:

- the contribution of lateral displacement and drag forces are negligible;
- the sectional model is characterized by modes that are a pure vertical bending and a pure torsional ones. This assumption is generally verified for all cross sections that presents a vertical symmetry (Bartoli & Mannini, 2005);
- the values of mass and mass moment of inertia of the deck are constant along the span. This implies that in the sectional model these parameters assume the same values as those detected per unit span of the deck (Bartoli & Mannini, 2005).

Once the mass and the mass moment of inertia are defined, the stiffness of springs are calculated imposing that the frequencies of selected modes of the complete structure are perfectly reproduced.

Although the use of two-dimensional models implies a simplified point of view about the complete structure, when suitably calibrated, they are able to accurately predict the critical wind speed and to give qualitative information about the structural motion. In any case, if the overall behaviour of the bridge is of interest more refined analysis should be performed considering also the nonlinearities due to structural geometry, dynamic characteristics and aeroelastic forces. All these different aspects can be considered using the three dimensional finite element model.

In Chapter 6 the analysis of a cable-stayed bridge is performed. Several aspects have been investigated by means of both sectional and 3D models. In particular the 3D model has been used to compute the static deformed configuration under the static wind load, in order to evaluate the critical flutter velocity and to reproduced the structural response due to buffeting load. The obtained results are used as a benchmark for testing the accuracy of the analysis performed by means of the cross-sectional model. In this way all the hypotheses assumed to define the parameters of the sectional model can be verified. Due to the computational cost problems, the sectional model has been used also to evaluate the aeroelastic forces by means of the proposed nonlinear approach. The obtained results are representative of the wholly structural behaviour since the reliability of the sectional models has been tested.

5.2 Wind field generation procedure

When buffeting loads is considered, longitudinal and vertical turbulent wind time histories must be simulated once for each nodes of the model.

The simulation procedure is performed by means of a program developed in Fortran language that implements the spectral model proposed by (Cao, Xiang, & Zhou, 2000) and reported in section 3.3. In particular the cross-spectrum between along-wind and vertical turbulent components is considered negligible, while the exponentially decaying coherence function (3.46) is used.

Considering equations (3.36) and (3.44) the wind turbulent component can be written as:

$$u_j(t) = \sqrt{2\Delta\omega}\, Re\left\{\sum_{m=1}^{j}\left[\sum_{l=1}^{N}\left(\sqrt{\mathrm{S_{ij}(\omega_{ml})}}\mathrm{G_{ij}(\omega_{ml})}\ \mathrm{e}^{\mathrm{i}\phi_{ml}}\right)\ \mathrm{e}^{\mathrm{i}lt\Delta\omega}\right]\ \mathrm{e}^{\mathrm{i}\left(\frac{m}{N_P}t\Delta\omega\right)}\right\} \tag{5.1}$$

where the meaning of each symbol is described in section 3.3.

Looking at the term under parenthesis it is evident that it is possible to use FFT techniques to improve the efficiency of the generation. This term can be rewritten in the following form:

$$\mathrm{A_{jm}(k\Delta t)} = \sum_{l=1}^{N}\mathrm{Bl_{jm}}\ \mathrm{e}^{\mathrm{i}(l\mathrm{k}\Delta\mathrm{t}\Delta\omega)} \tag{5.2}$$

where $\mathrm{Bl_{jm}} = \sqrt{\mathrm{S_{ij}(\omega_{ml})}}\mathrm{G_{ij}(\omega_{ml})}\ \mathrm{e}^{\mathrm{i}\phi_{ml}}$ and $k = 1, \dots, N_{fr}$.

It is worth noting that function $A_{jm}(k\Delta t)$ is periodic with period $T_1 = 2\pi/\Delta\omega$ and it can be generated using inverse FFT technique. Reminding (3.34) it is evident that the period of the signal generated is N_P times T_1. For this reason it is possible to introduce the following function:

$$\mathrm{h_{jm}(p\Delta t)} = \begin{cases}\mathrm{A_{jm}(\Delta t)} & \mathrm{p} = 0 \dots \mathrm{N}-1\\ \mathrm{A_{jm}((p-N)\Delta t)} & \mathrm{p} = \mathrm{N} \dots 2\mathrm{N}-1\\ \mathrm{A_{jm}((p-N_pN)\Delta t)} & \mathrm{p} = (\mathrm{N_P}-1)\mathrm{N} \dots \mathrm{N_pN}-1\end{cases} \tag{5.3}$$

It is so possible to rewrite (5.1) in a more efficiently way as:

$$u_j(p\Delta t) = \sqrt{2\Delta\omega}\, Re\left\{\sum_{m=1}^{j}\mathrm{h_{jm}(p\Delta t)}\ \mathrm{e}^{\mathrm{i}\left[\left(\frac{m}{N_P}\Delta\omega\right)\mathrm{p}\Delta\mathrm{t}\right]}\right\} \tag{5.4}$$

that can be also written as:

$$u_j\big((k+sN)\Delta t\big) = \sqrt{2\Delta\omega}\, Re\left\{\sum_{m=1}^{j}\mathrm{A_{jm}(k\Delta t)}\ \mathrm{e}^{-\left[\left(\frac{m}{N_P}\right)(\mathrm{k+sN})\Delta\mathrm{t}\Delta\omega\right]}\right\} \tag{5.5}$$

where $s = 0,1,2 \dots \big(N_p - 1\big)$.

Looking at the final equation it is possible to see that all the modifications introduced lead to a formula whose implementation is not so evident. For this reason is here reported a pseudo-code to describe how the generation has been implemented.

The parameters that have to be defined before starting the generation procedure are: the cut-off frequency ω_u, the Number of division of the frequency range considered N, the time step Δt the number of time step of the generated sample N_{step}, and finally the number of division of the minimum period considered N_{div} (typically 2).

The matrices used by the code are: $\Phi(N_P x N_{fr})$ that contains values uniform distribuited in the range $(0,2\pi)$, $H(N_P x N_P)$ and $Hl(N_P x N_{fr})$ lower and upper triangular real matrix, $A_j(N_{fr})$ complex vector, and finally $u(N_P x N_{step})$ that is the output vector.

The generation algorithm is described here in the following:

Φ =Random Number Generator $(0,2\pi)$
$\Delta\omega = \omega_u / N$
$N_{fr} = N * N_{div}$
Do $m = 1, N_P$
  Do $l = 0, N_{fr} - 1$
    Calculate $\omega_{ml}(l)$
    Calculate $\mathrm{H}(:,:) = \sqrt{\mathrm{S}(\omega_{ml}(l))}\,\mathrm{G}(\omega_{ml}(l))$
    $Hl(:,l) = H(:,m)$
  End do
  Do $j = m, N_P$
    Do $k = 0, N_\omega$
      $Coef(k+1) = Hl(j,k)\ \mathrm{e}^{\mathrm{i}\phi(\mathrm{m,k})}$
    End do
    $A_j = InverseFFT(Coef)$
    Do $ii = 0, N_{fr}$
      $k = 0$
      Do while $(ii + k \le N_{step})$

$$u(j,(ii+k)) = u(j,(ii+k)) + \sqrt{2\Delta\omega}\ Re(A_j(ii)e^{Im\left(\frac{m}{N_P}\Delta\omega(ii+k)\Delta t\right)})$$

        $k = k + N_{fr}$
      End do
    End do
  End do
End do

As already stated, this generation procedure is applied twice as the two turbulent component are generated in a separated way, because the cross-spectrum between longitudinal and vertical wind is considered negligible.

5.3 Computational framework

In present work two approaches for the analysis of bridges under wind load have been developed: the full-order flutter analysis approach where the aeroelastic loadings are applied directly to the physical coordinate of the 3D structure and the bimodal flutter analysis approach where only the two coupling modes that lead to instability condition of the bridge are considered.

For both these models the equations of motion can be written as function of the three components of the displacement, which define the vibration of the structure:

$$[\mathrm{M}]\{\ddot{\mathrm{x}}\} + [\mathrm{C}]\{\dot{\mathrm{x}}\} + [\mathrm{K}]\{\mathrm{x}\} = \{\mathrm{F}^{\mathrm{est}}\} \tag{5.6}$$

where $\{x\}$ is the vector of nodal degrees of freedom, [M] is the mass matrix, [C] is the damping matrix, $[K]$ is the stiffness matrix and $\{\mathrm{F}^{\mathrm{est}}\}$ is the vector of external forces that are the dead load, the pretension of the cables and the aerodynamic load both self-excited and the buffeting component.

When the aeroelastic forces are expressed as function of flutter derivatives, see (4.36), the dynamic equation of motion becomes:

$$([\mathrm{M}] - [\mathrm{M}_{\mathrm{ae}}])\{\ddot{\mathrm{x}}\} + ([\mathrm{C}] - [\mathrm{C}_{\mathrm{ae}}])\{\dot{\mathrm{x}}\} + ([\mathrm{K}] - [\mathrm{K}_{\mathrm{ae}}])\{\mathrm{x}\} = \{\mathrm{P}_{\mathrm{dead}}\} + \{\Gamma_{\mathrm{mem}}\} + \{F_{buff}\} \tag{5.7}$$

where $[M_{ae}]$, $[C_{ae}]$ and $[K_{ae}]$ include the contribution of each modelled cross section, $\{\Gamma_{\mathrm{mem}}\}$ is the so called "memory term" and $\{F_{buff}\}$ is the vector of buffeting load. The system (5.7) corresponds to the vibration of a forced system where mass, damping and stiffness matrices are modified by aeroelastic components.

In order to create a three dimensional FE model of the cable-stayed bridge, it has been necessary the implementation of special conditions for the modification of the mass stiffness and damping matrices as required for the aerodynamic instabilities. Thanking to the cooperation with the University of Padua and the International Centre for Numerical Methods in Engineering (CIMNE), all the necessary elements and conditions have been implemented into the open-source code named Kratos (KRATOS-Wiki).

Kratos is a framework for building multi-disciplinary finite element codes. It provides several tools for an easy implementation of finite element applications and a common platform for the natural interaction of the same in different ways. Kratos is a variable base interface designed and implemented to be used at different levels of abstraction. A flexible data structure can be used to store any type of data in a type-safe manner. An extendible IO is also present to overcome a bottleneck in dealing with multi-disciplinary problems and the major interpreting tasks are given to the Python interface. Further details about Kratos are reported in (Dadvand, 2007). The pre and post processing are committed to the commercial code GiD (GID), also developed at CIMNE, in order to define the domain geometries, applying the boundary conditions, the element properties and to generate the meshes.

Fig. 26 shows the strategy used to run the analyses for the evaluation of aerodynamic and aeroelastic parameters.

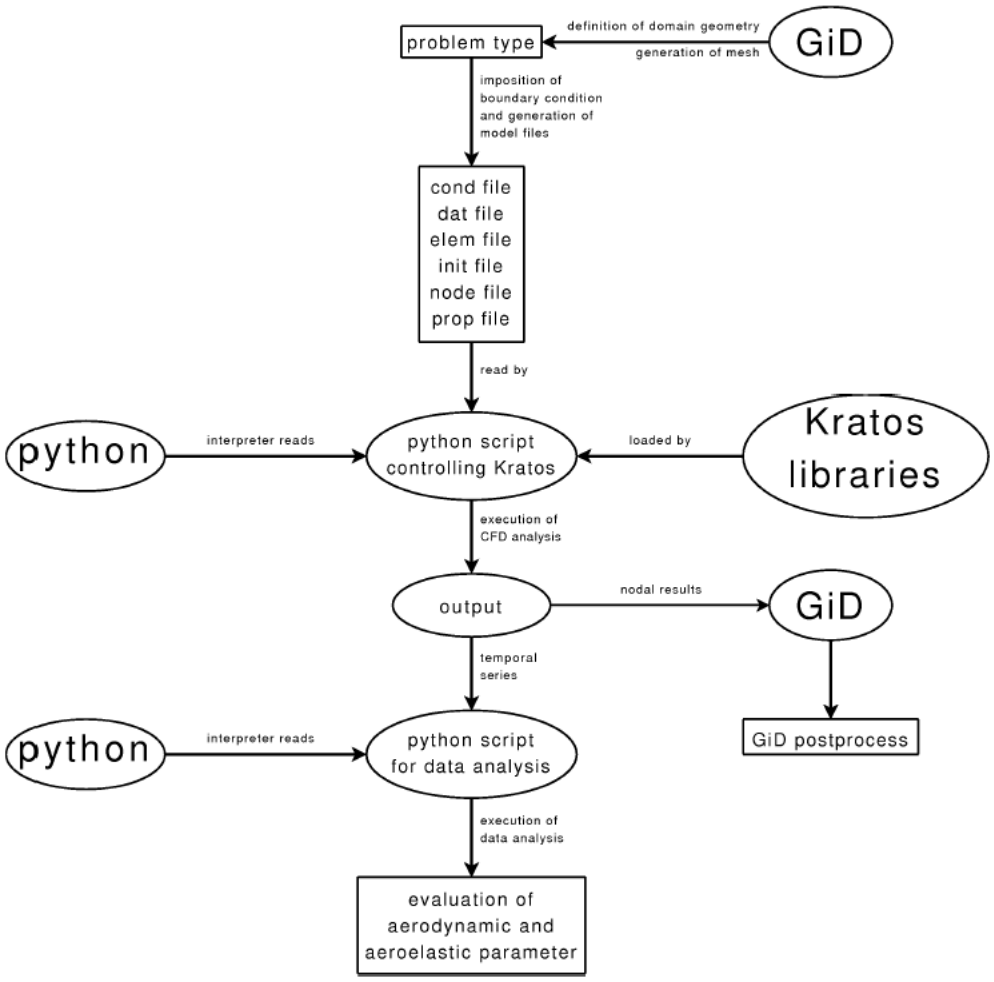

Fig. 26: Diagram of analysis strategy (Stecca, 2008)

As reported in the flow chart above, the framework starts with the creation of a mesh through GiD. The modelling of bridge structures can be performed by means of just a pair of finite element as follows: pylons and deck are meshed by means of beam elements, while the stays are meshed with geometrically non-linear truss elements. The initial condition of prestress assigned to stay elements guarantees that they remain always in a tension state of stress, making unnecessary the implementation of material nonlinearities.

An ad-hoc *problem type* for this application created in GiD specifies all the variables and the parameters that can be set into the model for each kind of analysis. For the sake of simplicity, translational and rotational masses are punctually included into the 3D model instead of assigning density to the elements. In this way the total mass and inertia can be easily controlled and modified in the calibration process without losing accuracy in the results.

The structural damping is modelled in terms of modal damping ratios by means of Rayleigh coefficients:

$$[\mathrm{C}] = \alpha[\mathrm{M}] + \beta[\mathrm{K}] \tag{5.8}$$

When the modal damping ratios for the ith and jth modes are measured or assumed, the proportionality coefficients can be obtain by (Clough & Penzien, 1993):

$$\begin{aligned} \alpha &= 2\frac{\omega_i\omega_j}{\omega_j^2 - \omega_i^2}(\omega_j\xi_i - \omega_i\xi_j) \\ \beta &= 2\frac{\omega_i\omega_j}{\omega_j^2 - \omega_i^2}\left(-\frac{\xi_i}{\omega_j} + \frac{\xi_j}{\omega_i}\right) \end{aligned} \tag{5.9}$$

where ω_i and ξ_i are the circular frequency and damping ratio for the ith mode and ω_j and ξ_j are the circular frequency and damping ratio for the jth mode.

In addition to standard elements, two special features have been added to Kratos in order to include the aerodynamic forces according to the *quasi-steady* and *flutter derivatives* theories. The latter are called "conditions" which are treated like the finite elements allowing to modify both the local system and the residual term.

In (5.10) and (5.11) the modification of stiffness and damping matrices following the quasi-steady assumptions are reported:

$$\left[\mathrm{K_{QS}}\right] = -\frac{1}{2}\rho\mathrm{U}^2\mathrm{BL}\begin{bmatrix} 0 & 0 & \mathrm{C'_L} \\ 0 & 0 & \mathrm{C'_D} \\ 0 & 0 & \mathrm{BC'_M} \end{bmatrix} \tag{5.10}$$

$$\left[\mathrm{C_{QS}}\right] = -\frac{1}{2}\rho\mathrm{U}^2\mathrm{BL}\begin{bmatrix} -\dfrac{\mathrm{C_D} + \mathrm{C'_L}}{\mathrm{U}} & -\dfrac{2\mathrm{C_L}}{\mathrm{U}} & (\mathrm{C_D} + \mathrm{C'_L})\dfrac{\mathrm{m_h B}}{\mathrm{U}} \\ -\dfrac{\mathrm{C'_D} - \mathrm{C_L}}{\mathrm{U}} & -\dfrac{2\mathrm{C_D}}{\mathrm{U}} & (\mathrm{C'_D} - \mathrm{C_L})\dfrac{\mathrm{m_p B}}{\mathrm{U}} \\ -\dfrac{\mathrm{C'_M B}}{\mathrm{U}} & -\dfrac{2\mathrm{C_M B}}{\mathrm{U}} & \mathrm{C'_M}\dfrac{\mathrm{m_\alpha B^2}}{\mathrm{U}} \end{bmatrix} \tag{5.11}$$

Where L is the along-span influence length calculated as half of the distance between the two nodes close to the one in which the aeroelastic forces are under evaluation.

In (5.12), (5.13) and (5.14) the same modification derived from the flutter derivatives theory are reported, with the addition of the aerodynamic mass:

$$[\mathrm{K_{FD}}] = \frac{1}{2}\rho\mathrm{U}^2\mathrm{L}\begin{bmatrix} \mathrm{a_{0,Lh}} & \mathrm{a_{0,Lp}} & \mathrm{a_{0,L\alpha}} \\ \mathrm{a_{0,Dh}} & \mathrm{a_{0,Dp}} & \mathrm{a_{0,D\alpha}} \\ \mathrm{a_{0,Mh}} & \mathrm{a_{0,Mp}} & \mathrm{a_{0,M\alpha}} \end{bmatrix} \tag{5.12}$$

$$[\mathrm{C_{FD}}] = \frac{1}{2}\rho\mathrm{U}^2\left(\frac{\mathrm{B}}{\mathrm{U}}\right)\mathrm{L}\begin{bmatrix} \mathrm{a_{1,Lh}} & \mathrm{a_{1,Lp}} & \mathrm{a_{1,L\alpha}} \\ \mathrm{a_{1,Dh}} & \mathrm{a_{1,Dp}} & \mathrm{a_{1,D\alpha}} \\ \mathrm{a_{1,Mh}} & \mathrm{a_{1,Mp}} & \mathrm{a_{1,M\alpha}} \end{bmatrix} \tag{5.13}$$

$$[\mathrm{M_{FD}}] = \frac{1}{2}\rho\mathrm{U}^2\left(\frac{\mathrm{B}}{\mathrm{U}}\right)^2\mathrm{L}\begin{bmatrix} \mathrm{a_{2,Lh}} & \mathrm{a_{2,Lp}} & \mathrm{a_{2,L\alpha}} \\ \mathrm{a_{2,Dh}} & \mathrm{a_{2,Dp}} & \mathrm{a_{2,D\alpha}} \\ \mathrm{a_{2,Mh}} & \mathrm{a_{2,Mp}} & \mathrm{a_{2,M\alpha}} \end{bmatrix} \tag{5.14}$$

where the aeroelastic matrices are expressed as a function of the coefficients obtained from the rational function approximation of the flutter derivatives, as reported in (4.34).

Both conditions modify the three degrees of freedom correlated to the lift h, drag p and moment α motion. Considering the 6 dofs for each node of a standard structural finite element code, the conversion has been simplified imposing that the bridge axis is always directed along the global X axis, the gravity operates in the negative of the Z axis and the wind blows always in the positive direction of the Y axis. This care permits the biunique relation between the degrees of freedom.

When aeroelastic forces are evaluated by means of the formulation based on flutter derivatives, the memory term vector must be computed as following:

$$\{\Gamma_{\mathrm{mem}}\} = \frac{1}{2}\rho \mathrm{U}^2 \mathrm{L} \begin{bmatrix} \Gamma_{Lh} + \Gamma_{Lp} + \Gamma_{L\alpha} \\ \Gamma_{Dh} + \Gamma_{Dp} + \Gamma_{D\alpha} \\ \Gamma_{Mh} + \Gamma_{Mp} + \Gamma_{M\alpha} \end{bmatrix} \tag{5.15}$$

In the developed 3D finite element model, wind loads are applied through a special one-node "condition" characterized by an along-span influence length. The aerodynamic forces described in latter equations are proportional to this length. To convert these uniformly distributed forces into member and effects, a simple lumping procedure is adopted whereby one-half of the force is assumed to act at each member node.

In order to evaluate the "memory term" a numerical integration should be performed. Since the evaluation of the integral term could be extremely time consuming, two different strategies to calculate it are here reported, following the theory reported in section 4.4.

One of these methods is based on the idea to treat the "memory term" as an unknown quantity and introduce some new equations to solve the system. These equations can be obtained considering that the following relation for "memory term" stands:

$$\dot{\Gamma}_{\mathrm{i,Lh}}(\mathrm{t}) = -\frac{\mathrm{d_i U}}{\mathrm{B}}\Gamma_{\mathrm{i,Lh}}(\mathrm{t}) + \mathrm{a}_{(\mathrm{i+3}),\mathrm{Lh}}\dot{\mathrm{h}}(\mathrm{t}) \qquad (\mathrm{i}=1,\ldots,\mathrm{m}) \tag{5.16}$$

Similar expression can be obtained for the other terms.

The total system obtained introducing these equations become:

$$\begin{cases} ([\mathrm{M}] - [\mathrm{M_{ae}}])\{\ddot{\mathrm{x}}\} + ([\mathrm{C}] - [\mathrm{C_{ae}}])\{\dot{\mathrm{x}}\} + ([\mathrm{K}] - [\mathrm{K_{ae}}])\{\mathrm{x}\} = \{\mathrm{P_{dead}}\} + \{\Gamma_{\mathrm{mem}}\} + \{F_{buff}\} \\ \{\dot{\Gamma}\} + [D]\{\Gamma\} - [\Lambda]\{\dot{\mathrm{x}}\} = [0] \end{cases} \tag{5.17}$$

Considering just one cross section, the vector that contain the memory term is:

$\{\Gamma\}_{(9\cdot m)\times 1} = \{\Gamma_{Lh,1} \ldots \Gamma_{Lh,m}\ \Gamma_{Lp,1} \ldots \Gamma_{Lp,m}\ \Gamma_{L\alpha,1} \ldots \Gamma_{L\alpha,m} \ldots\ldots \Gamma_{Mh,1} \ldots\ldots \Gamma_{M\alpha,m}\}^T$

and matrix $[D]_{(9\cdot m)\times(9\cdot m)}$ is a diagonal matrix composed by terms $-\frac{\mathrm{d_i U}}{\mathrm{B}}$ and matrix $[\Lambda]_{(9\cdot m)\times(9\cdot m)}$ contains the coefficients $\mathrm{a}_{(\mathrm{i+3})}$.

The evaluation of the "memory term" performed using this technique allow to calculate the integral term without introducing any type of approximation on its evaluation. However, as more

than one cross section is considered, the number of augmented equations starts rapidly to increase.

The second method that has been implemented to evaluate the “memory term” is reported in (4.40). In this case the memory term is evaluated at each time step without computing the numerical evaluation of all the integral terms, but just modifying the values obtained at the previous step with a correction factor. This procedure leads to an approximate evaluation of the “memory term” that can be considered good enough if a sufficiently small time step is chosen to perform the analysis.

Finally, buffeting forces are implemented as external loads by using the linearized quasi-steady model:

$$\{\mathrm{F_{buff}}\} = \frac{1}{2}\rho \mathrm{U}^2 \mathrm{BL}\left(\begin{bmatrix} 2\mathrm{C_L} \\ 2\mathrm{C_D} \\ 2\mathrm{C'_M} \end{bmatrix}\frac{\mathrm{u(t)}}{\mathrm{U}} + \begin{bmatrix} \mathrm{C_D} + \mathrm{C'_L} \\ \mathrm{C'_D} - \mathrm{C_L} \\ \mathrm{B\ C'_M} \end{bmatrix}\frac{\mathrm{w(t)}}{\mathrm{U}}\right) \tag{5.18}$$

where $u(t)$ and $w(t)$ are respectively the along and vertical wind turbulent component.

Concluding, starting from the knowledge of both structural and aerodynamic characteristics, two numerical models for the evaluation of the structural response under wind load have been developed. One of them is a 3D finite element model obtained by means of subsequently simplifications of the complete 3D model. The aerodynamic wind loads are directly applied to the physical coordinate of the 3D structure by means of special point conditions for the modifications of mass, damping and stiffness structural matrices and the evaluation of the integral memory term. Since the evaluation of the integral terms is very time consuming the evaluation of these terms has been implemented by means of a recursive expression. The second model adopted is the bimodal one where only the first bending and the first torsional mode are considered. In this case the contribution of the integral memory terms have been implemented in two different way, one is by means of the same recursive expression adopted for the 3D model, and the other is by means of additional equations representing the aerodynamic states. In both 2D and 3D models, the buffeting load has been implemented by means if the quasi-steady theory.

Chapter 6

The cable-stayed bridge over the Adige river

6.1 Structural description

In order to improve the road system in the Veneto region, a new highway called "Valdastico A31" is under construction and will link directly the cities of Vicenza and Rovigo. Along this highway a cable-stayed bridge has been designed and built in order to cross the Adige river. It has a main span of 310m while its total length is 590m. In Fig. 27 the road layout is depicted.

The plan of the cable-stayed bridge is mainly straight, except in the Badia Polesine side, however the steel deck is built completely straight. The two towers are located outside the river banks, in order to avoid the usage of piers in the river bed.

Fig. 27: Road layout of "Valdastico A31"

The deck is rigidly connected to both pylons and to four trusses which connect the external spans to the ground. The latter have been designed with special devices which allow the longitudinal rotations.

The access ramps are connected to the bridge deck by means of Gerber saddles.

The bridge deck is placed at an average height of 15 meters above the ground level.

Fig. 28: Bridge over the Adige river

Eight symmetrically arranged stays are adopted for each tower as a support for the three spans; the deck results therefore subdivided into 17 segments of 34 m each, excepting for the central one which presents a length of 38 m. The stays are connected to the tower at a height of about 80 m above the deck.

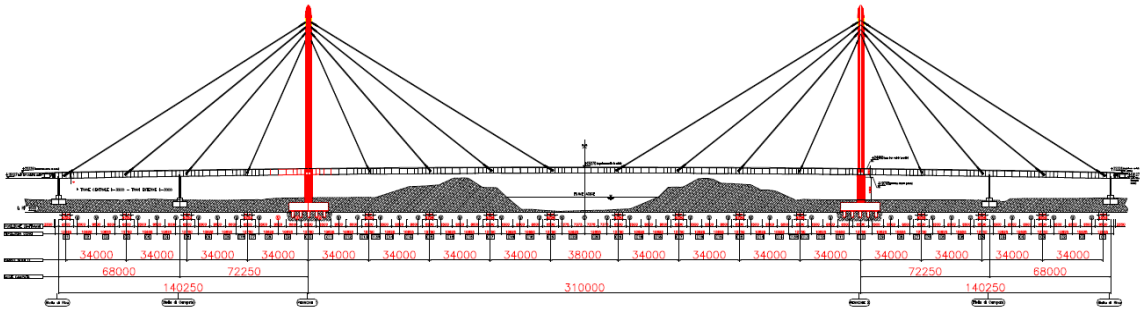

Fig. 29: Elevation of the bridge over the Adige river.

The bridge cross section is made up of three main girders, with double-T shape, and a concrete slab thickness of 0.26 m. The two lateral girders are 3.0 m high while the central one is 3.2 m. All the girders are made through welded plates of different thickness, for a total of twenty different segments. The whole cross-section have a trapezoidal shape, with a length of about 30 m on the upper edge and 17 m on the bottom one (which is the total distance between the two lateral girders). In the area between the two stays closer to the pylons, the lower part of the cross section is closed by means of a metal plate, while in the rest of the deck, the girders are inferiorly connected to each other by a bracing system.

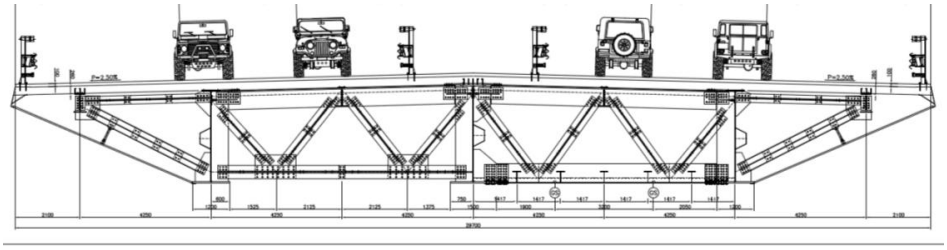

Fig. 30: Bridge deck cross section – girder section on the left, box section on the right

The whole structure is a complex system. Therefore, in order to assess the global response of the bridge and evaluate the parameters the sectional program needs, four different models have been developed each of them with a given level of accuracy. In this way the complexity of the system has been step by step reduced. The four developed models are here depicted:

- MODEL 1: The first and most accurate model is here presented. All the peculiarities of the structure are modelled in order to reproduce natural frequencies and displacements as close as possible to the real bridge. The deck is modelled considering 20 different types of cross-section geometries. Secondary elements such as stringers and bracings, are also taken into account. A detailed representation of the head of pylons and of the way the stays are connected to it is reproduced. Particular attention is finally paid to perform a correct mass distribution. The main target of this model is to define the natural frequencies of the structure and to estimate the deck's movements in correspondence of the deck central point. Such information is used as benchmarks to evaluate the behaviour of simplified models subsequently developed.

Modal shape	Eigen frequency value
Vertical symmetric VS1	$f_1 = 0{,}415\text{Hz}$
Torsional symmetric TS1	$f_2 = 0{,}588\text{Hz}$
Vertical Skew-symmetric VSS2	$\text{f}_3 = 0{,}593\text{Hz}$
Lateral symmetric LS1	$f_4 = 0{,}792\text{Hz}$
Vertical symmetric VS3	$f_5 = 0{,}877\text{Hz}$

Table 5: Main equivalent section characteristics

- MODEL 2: As first step towards the realisation of a simplified model, all the secondary structural elements are neglected, and a new model, consisting only of the main elements, has been created. In particular, beam elements are used to model the three main beams of the girder deck and the pylons; truss elements are used to represent the stays and plate elements for the slab. In order to simplify the deck complexity only two different types of cross sections has been considered: one in the area close to the pylons where a box section is adopted, while the other is a girder deck consisting of three main beams. In Fig. 31 the created model is illustrated. As previously mentioned, the model has been compared with the initial one in order to verify the simplifying assumptions introduced. The natural frequencies of this model are: $f_{VS1} = 0{,}405\text{Hz}$ and $f_{TS1} = 0{,}583\text{Hz}$.

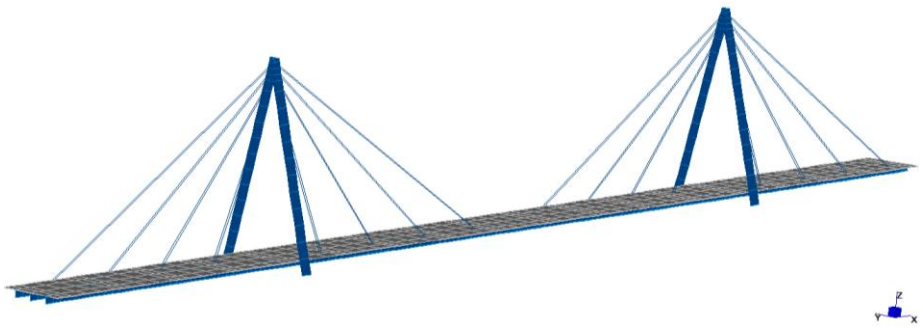

Fig. 31: Bridge MODEL 2

- MODEL 3: At this stage of the simplifying process the deck section is represented by using only one beam element.

Modal shape	Eigen frequency value
Vertical symmetric VS1	$f_1 = 0{,}420\text{Hz}$
Torsional symmetric TS1	$f_2 = 0{,}605\text{Hz}$

- Table 6 summarizes the main properties of the cross sections. The mass distribution is performed considering two different values with respect to the two sections. All the stays are connected to the pylons in one point placed at their top. The obtained model is reported in Fig. 32. Comparisons with MODEL 1 have also been carried out to check the introduced assumptions.

	Box section	**Girder deck**
Mass	$m = 44300\ kg/m$	$m = 40750\ kg/m$
Polar mass	$J_p = 3005900\ kgm^2/m$	$J_p = 2823500 kgm^2/m$
Area	$A = 218\ m^2$	$A = 179\ m^2$
Bending moment of inertia	$I_x = 2.7\ m^4$	$I_x = 2.0\ m^4$
Torsional moment of inertia	$I_t = 8\ m^4$	$I_t = 4\ m^4$
Modal shape	Eigen frequency value	
Vertical symmetric VS1	$f_1 = 0{,}420\text{Hz}$	
Torsional symmetric TS1	$f_2 = 0{,}605\text{Hz}$	

Table 6: Main cross-sections proprieties

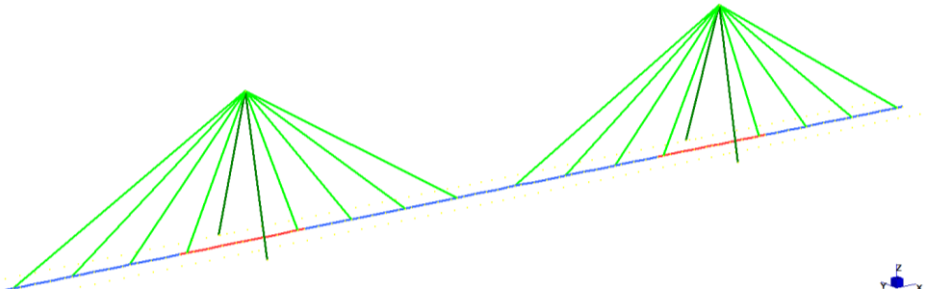

Fig. 32: Bridge MODEL 3

- MODEL 4: As final step, the most simplified 3D model of the structure is here presented. The deck is represented by means of a single beam element, whose mechanical properties, reported in Table 7, are assumed to be constant along the entire span length. The parameters about the mass distribution, translational mass and polar mass, are also considered constant along the deck; their values are assigned throughout the model as concentrated masses (one for each node). Finally, the model has been compared with the first one to evaluate the adopted simplifications. In Fig. 33 the model used in this last analysis is reported.

Mass	$m = 41700\ kg/m$
Polar mass	$J_p = 2900000\ kg\ m^2/m$
Area	$A = 200\ m^2$
Bending moment of inertia	$I_x = 1.9\ m^4$
Torsional moment of inertia	$I_t = 4.9\ m^4$
Modal shape	**Eigen frequency value**
Vertical symmetric VS1	$f_1 = 0{,}415\text{Hz}$
Torsional symmetric TS1	$f_2 = 0{,}590\text{Hz}$

Table 7: Main cross section proprieties

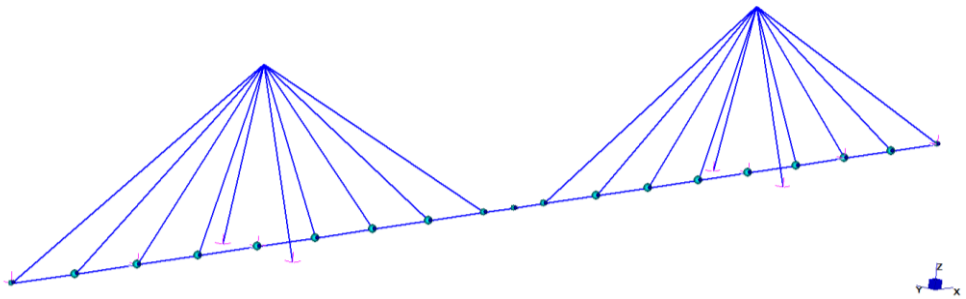

Fig. 33: Bridge MODEL 4

- SECTIONAL MODEL: As final step, the whole behaviour of MODEL 4 can be represented by means of a sectional model, whose characteristics are calculated as explained in section 5.1. The parameters thus obtained are resumed in Table 8.

Mass	$m = 41700\ kg/m$
Mass moment of inertia	$J_p = 2900000\ kg\ m^2/m$
Circular frequency (1° vertical mode)	$\omega_F = 2.61\ rad/s\ (f_1 = 0{,}415Hz)$
Circular frequency (1° torsional mode)	$\omega_T = 3.71\ rad/s\ \ (f_2 = 0{,}590Hz)$
Structural damping	$\xi_{st} = 0.5\%$
Section width	$B = 29.7\ m$

Table 8: Main geometric and dynamic bridge properties of cross-sectional model

Since the knowledge of the amount of structural damping is not available during the design stage, the choice of its value is here performed in an arbitrary way using the most common accepted value for these type of structures. The influence of this parameter in the analysis will be investigated in the following sections.

6.1.1 In-situ experimental test campaign

As previously mentioned, the bridge under analysis has been recently built. The construction of the main structures have been completed at the end of 2010. Accordingly, a first experimental test campaign has been organized to define the effective structural characteristics of the bridge, as natural frequency and damping values. With this aim, the following experimental set has been realized. In order to excite the deck, a truck with a weight of about 41 tons has been transited with constant velocity along one lane on which were been fixed several wooden planks 3 cm high, placed at a distance of 15 m from each other. The structural response has been recorded by means of six accelerometers placed respectively at both the side of the cross-section in the middle, in the quarter and third of the main span deck. The truck has made several crossing with the following transit velocities: from 18 up to 23 Km/h with an incremental step at each passage of 1Km/h and in the range from 25 to 31 Km/h with a step of 2Km/h. In this way the bridge has been excited with a cyclic load with frequency ranging from 0,33 Hz to 0,57 Hz.

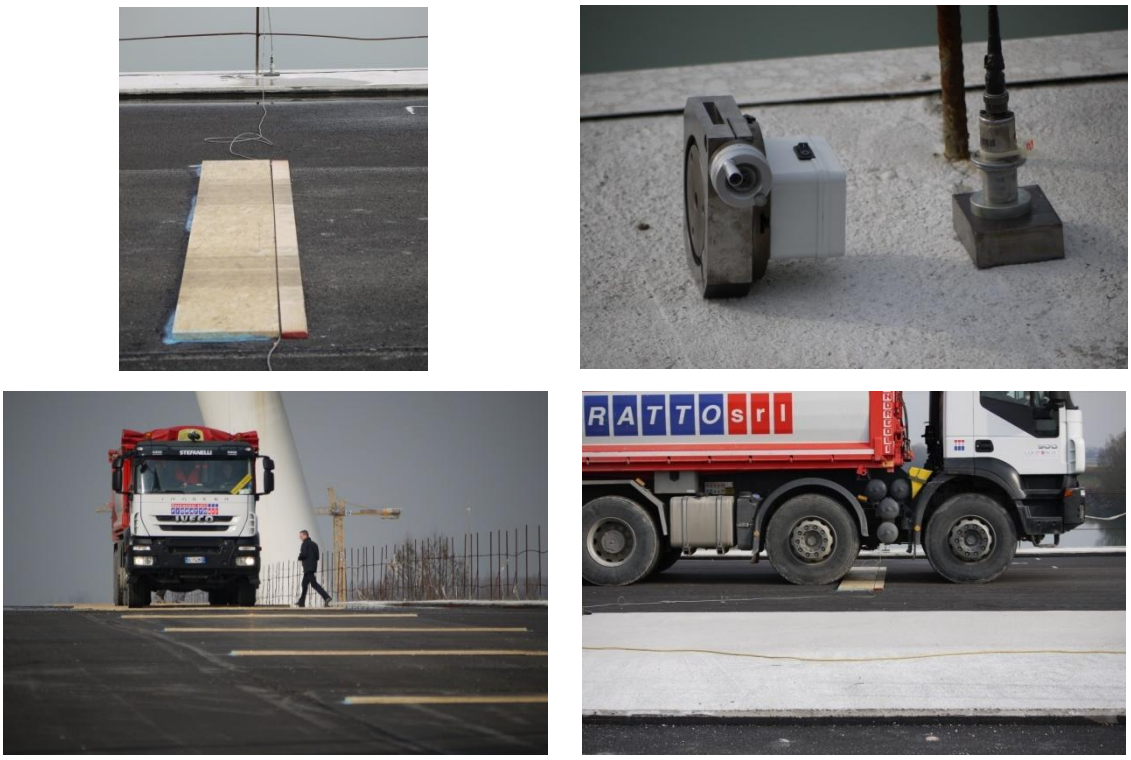

Fig. 34: In-situ experimental set campaign

From a preliminary analysis of the obtained data it has been observed that:

- the natural frequency values of the structure are in good agreement with those obtained by means of the numerical model previously presented. In particular torsional modes result to be the most excited and easily to identify from the recorded response, while the vertical skew-symmetric outcome to be the most difficult to detect;
- a roughly evaluation of the damping coefficient have highlighted a value of about $\xi_{cr} = 0{,}3\%$

Since at the current state of the art the bridge is lacking for all the ancillary works, further experimental campaign will be performed on the complete structure. Anyway, the analysis of the data obtained by means of this experimental test campaign confirmed the reliability of the natural frequency values obtained with the numerical models presented in section 6.1.

6.2 Aerodynamic deck characterization

The aerodynamic behaviour of the bridge deck was tested in the wind tunnel boundary layer (WTBL) of the Polytechnic of Milan. Both cross sections (box section and girder deck) have been tested by means of a 1:30 scaled sectional models characterized by a total length of 2.95 m and a deck chord of 1.0 m. In Fig. 35 a picture of the sectional model of the girder deck placed in the wind tunnel is reported.

The experimental campaign was performed to investigate the deck aerodynamic characteristics. In particular the following aspects have been investigated:

- evaluation of the stationary aerodynamic behaviour of the deck through static coefficient measure;
- evaluation of flutter derivative values as a function of the reduced frequency and angle of attack.

Fig. 35: Girder deck sectional model tested on the Wind Tunnel Boundary Layer of the Polytechnic of Milan

Lift, Drag and Moment polar coefficients measured at different values of the angle of incidence, in a range between $\pm 10°$, were first carried out. The tests have been repeated at different wind velocity (at 7.7, 9.6, 11.6, 13.4 m/s for the box section, while at 4, 5, 8, and 10 m/s for the girder deck), in order to check any possible dependence of the coefficients due to Reynolds effect. For the tested cross sections a negligible influence of Reynolds number has been detected.

In Fig. 36 the value of the aerodynamic coefficients obtained from this test campaign are reported.

Looking the behaviour of the aerodynamic coefficients it is observed that:

- The drag coefficient presents different behaviour between the two sectional model, but in both cases it is always positive, this means that its contribution to the horizontal damping is always positive. It is worth noting that at strong negative value of the angle of attack the coefficients are almost similar to each other, while, as the angle of incidence increases, the girder section assumes higher value of the drag coefficient. This because the bottom part of the girder section is open, providing more surface which the flow can exert its action against, compared to the box section.
- The lift coefficients present similar behaviour in both sections, assuming higher values for the girder deck. For both cross sections the curve presents a positive slope, pointing out that galloping instability is always avoided.
- The moment coefficients present lower slope for the girder section. This means a lower reduction of the effective torsional stiffness due to aeroelastic load and smaller torsional forces due to vertical gust.
- The behaviour of both lift and moment coefficients, around a zero angle of incidence, are characterized by linear trend.

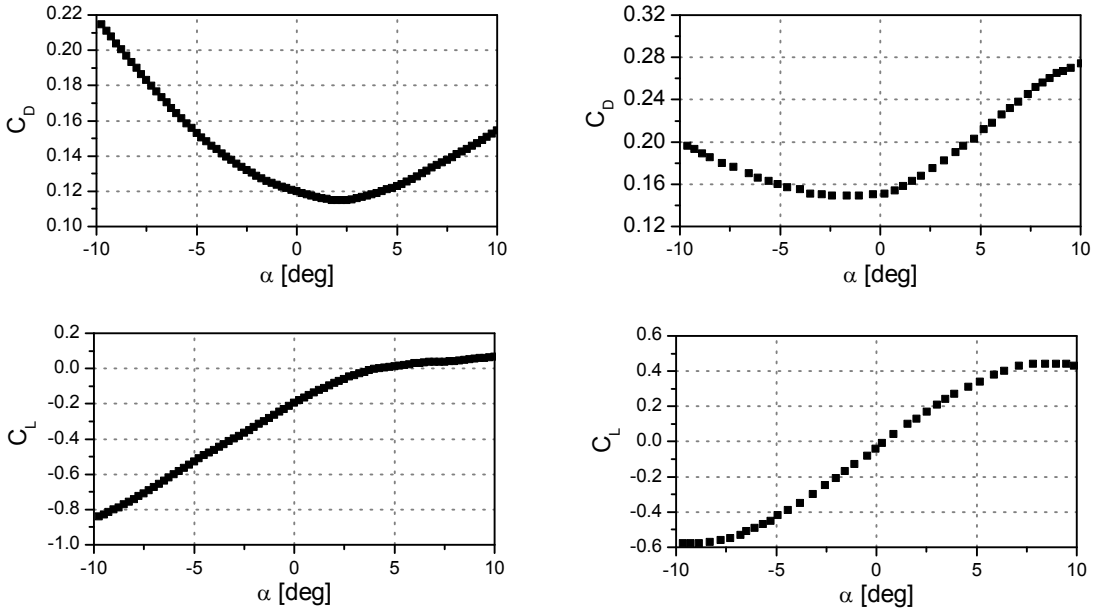

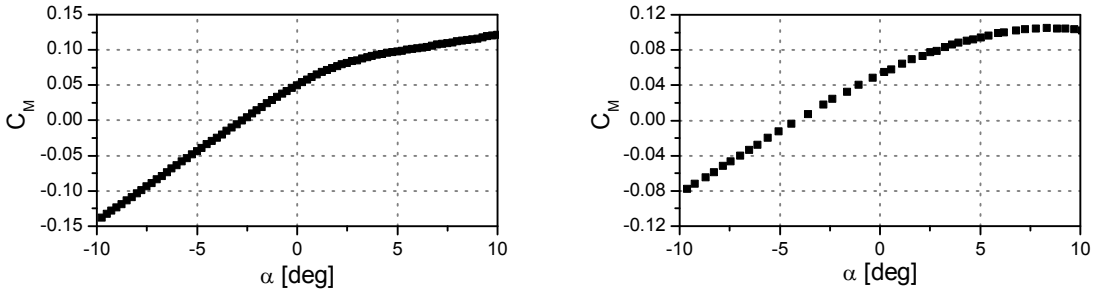

Fig. 36: Drag, Lift and Moment aerodynamic coefficients –box section on the left, girder section on the right

Flutter derivative values have been carried out by means of forced motion experimental test rig using three hydraulic actuators to support the model; this instrumentation enables the imposition of vertical, torsional and horizontal sinusoidal motions. The methodology used to assess the aerodynamic behaviour of the deck sections is fully described in (Cicada et al. 2001) and (Diana et al. 2004).

In Table 9 and in Table 10 frequency values of the imposed motion, wind tunnel velocity, and reduced velocity at which the test campaigns have been performed, are reported:

Frequency	**Velocity [m/s]**		
[Hz]	**8**	**10**	**14**
0.5	16.00	20.00	28.00
0.9	8.89	11.11	15.56
1.8	4.44	5.56	7.78
2.5	3.20	4.00	5.60
3.2	2.50	3.13	4.38
4.2	1.90	2.38	3.33

Table 9: Reduced velocity range investigated for the girder deck

Frequency	**Velocity [m/s]**			
[Hz]	**4**	**5**	**8**	**10**
0.5	--	--	--	20.0
1.0	--	--	8.0	10.0
1.5	--	3.3	5.3	6.7
2.4	1.7	2.1	3.3	4.2
4	1.0	1.3	2.0	2.5

Table 10: Reduced velocity range investigated for the box section

The two cross sections were tested at three different values of the angle of incidence: $\pm 3°$ and $0°$ for the box section, $\pm 2.5°$ and $0°$ for the girder deck.

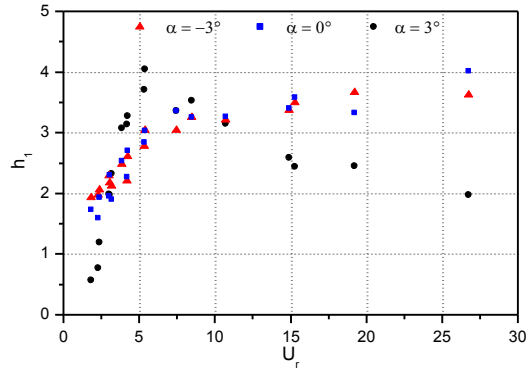
α = −3°
α = 0°
α = 3°
h1
Ur

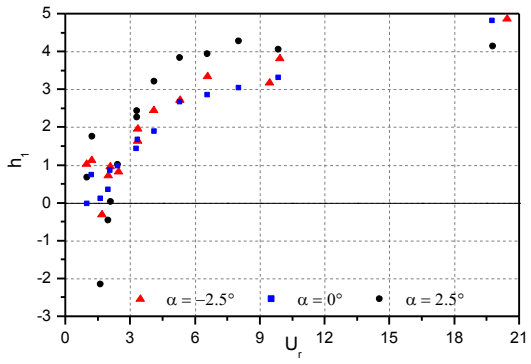
α = −2.5°
α = 0°
α = 2.5°
h1
Ur

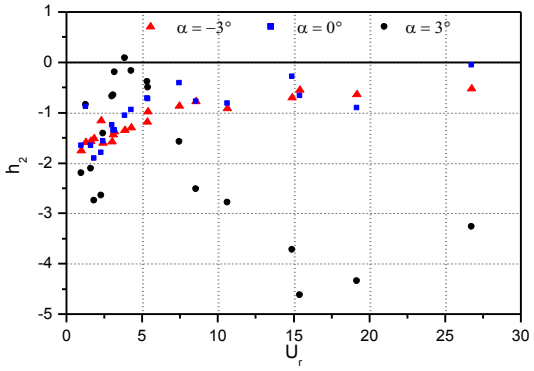
α = −3°
α = 0°
α = 3°
h2
Ur

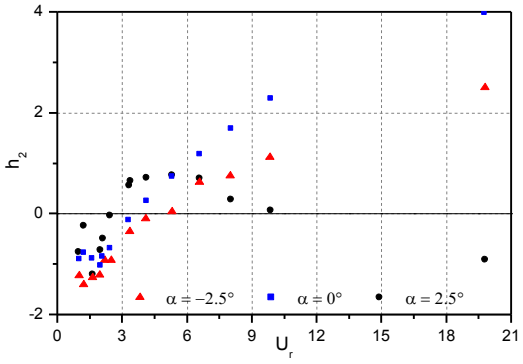
α = −2.5°
α = 0°
α = 2.5°
h2
Ur

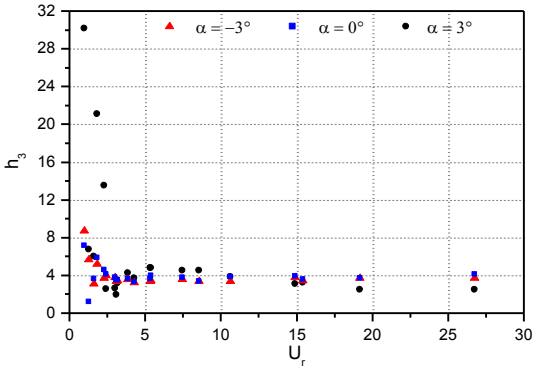
α = −3°
α = 0°
α = 3°
h3
Ur

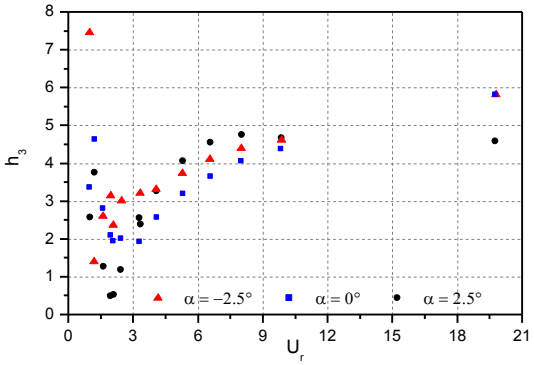
α = −2.5°
α = 0°
α = 2.5°
h3
Ur

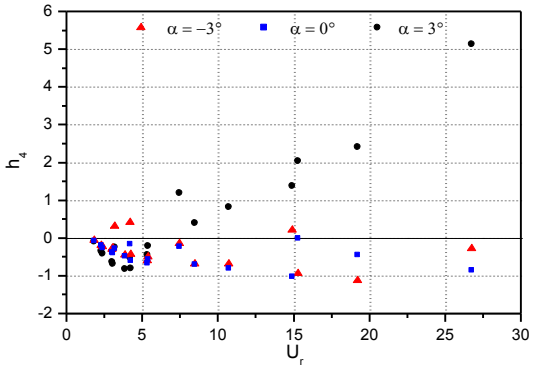
α = −3°
α = 0°
α = 3°
h4
Ur

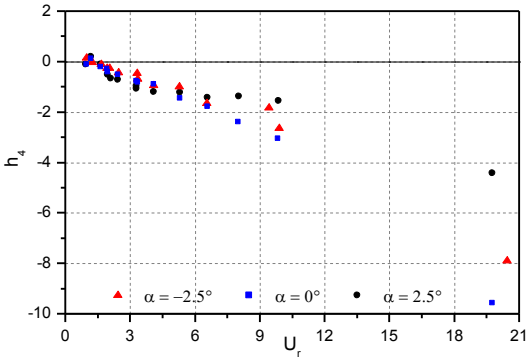
α = −2.5°
α = 0°
α = 2.5°
h4
Ur

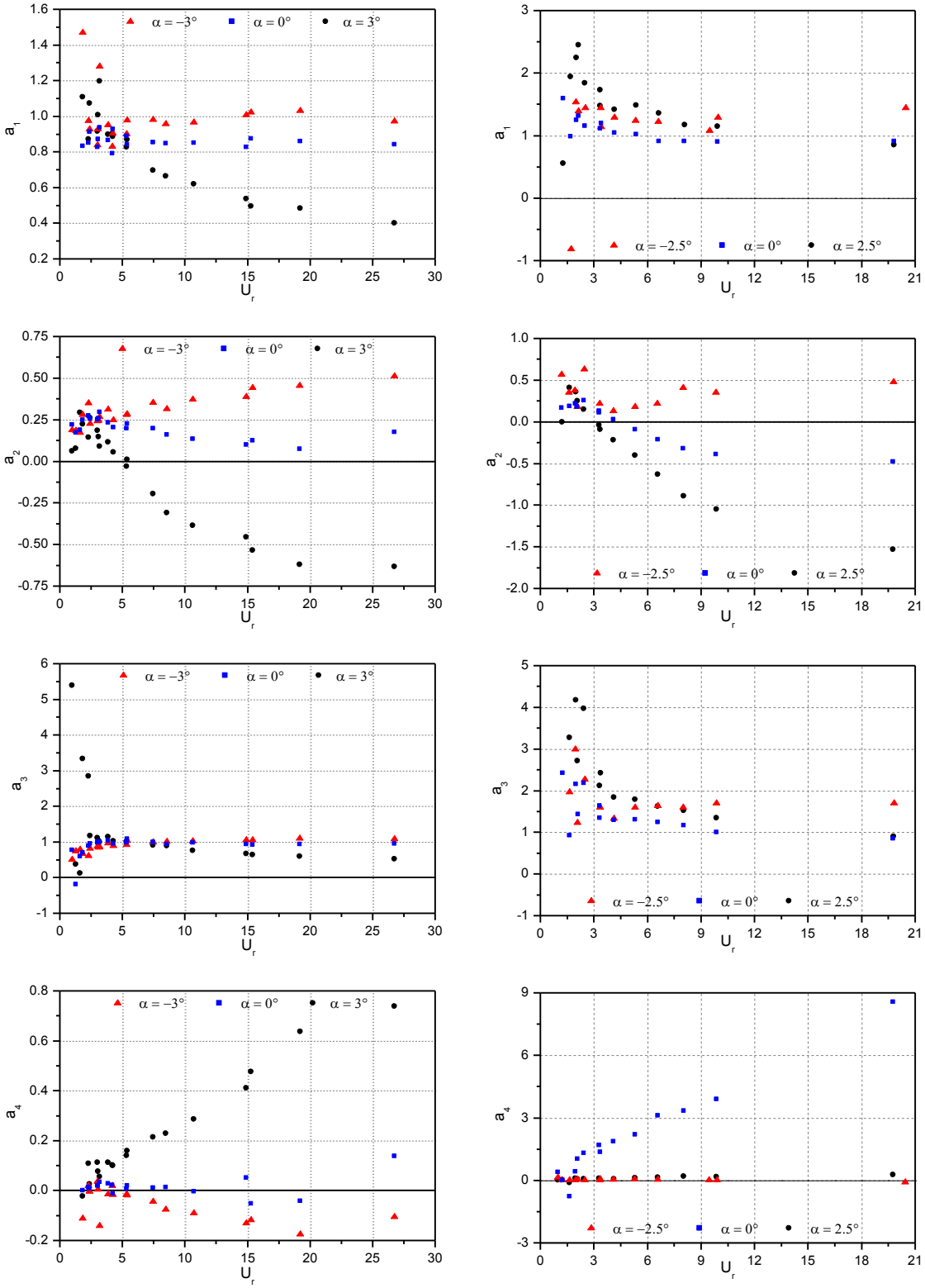

Fig. 37: Flutter derivatives Zasso convention –box section on the left, girder section on the right

The behaviour of the flutter derivatives suggests that:

- The coefficients h_1, h_3, a_1 and a_3, at higher values of the reduced frequency, approach the ones of the corresponding aerodynamic coefficients predicted by the quasi-steady theory, estimated at the same angle of incidence. In particular, comparing equation (4.16) with the aeroelastic force components in (4.28), the following relations stand:

$$h_1 = C_D + C_L' \qquad a_1 = C_M'$$
$$h_3 = C_L' \qquad a_3 = C_M'$$

In the following two tables the values of the above-mentioned coefficients are reported for both deck sections:

$\boldsymbol{\alpha}$	h_1	$C_D + C'_L$	h_3	C_L'	a_1	C_M'	a_3	C_M'
-3.0°	3.62	3.72	3.71	3.58	0.97	1.13	1.09	1.13
0.0°	4.02	4.03	4.10	3.91	0.82	0.92	0.96	0.92
3.0°	1.97	2.12	2.50	2.01	0.40	0.44	0.53	0.44

Table 11: Comparison between flutter derivatives and aerodynamic coefficients – Box section

$\boldsymbol{\alpha}$	h_1	$C_D + C'_L$	h_3	C_L'	a_1	C_M'	a_3	C_M'
-2.5°	4.87	4.78	5.82	4.64	0.91	0.74	1.07	0.74
0.0°	4.82	5.05	5.83	4.89	0.68	0.63	0.63	0.63
2.5°	4.13	4.56	4.58	4.39	0.42	0.49	0.44	0.49

Table 12: Comparison between flutter derivatives and aerodynamic coefficients – Girder deck

- The derivative h_1 evaluated for the girder deck shows a tendency to assume a negative value when the reduced frequency is around 1, especially when the mean angle of incidence assumes positive values. This means that the aerodynamic damping of the vertical motion becomes negative. This is a typical phenomena for bridge deck due to vortex shedding.
- The derivative a_2 represents the aerodynamic damping of the torsional motion. It assumes positive value for each reduced frequency when the mean angle of attach is of $-3°$ or $0°$ for the box section, or of $-2.5°$ for the girder deck, while, in the other cases, above a certain value of reduced frequency it becomes negative. The latter case means that the aerodynamic forces are introducing energy into the system, leading to a possible one degree of freedom instability. By means of (4.22) the wind velocity values which this type of instability arise at are calculated:

Section geometry	α	U_{cr}	U_{red}
Box section	3.0°	104.0	5.96
Girder deck	0.0°	92.4	5.29
	2.5°	68.7	3.94

Table 13: Torsional degree of freedom instability

6.3 Static wind load: bridge deck deformed configuration

Because of the presence of the mean wind velocity, a static wind force acts along the whole deck. In case of long-span bridges this load can lead to large deck deformations. It is very important to assess the amount of these deformations because they can affect both the dynamic and aerodynamic behaviour of the bridge. In fact, the aerodynamic shape can significantly change because of large rotations so that significant variation and non uniform distribution of the aerodynamic force acting on the deck can be observed. These effects will consequently influence the aerodynamic behaviour of the bridge (Zhang, Xiang, & Sun, 2002).

In this section the deck displacements due to structural weight and static wind component are calculated using the 3D bridge model called “MODEL 3”, described in Section 6.1.

The bridge displacements must be evaluated imposing to the whole structure a mean wind forces defined as follow:

$$\begin{aligned} L_{static} &= \frac{1}{2}\rho U^2 B L\, C_L(\alpha_s) \\ M_{static} &= \frac{1}{2}\rho U^2 B^2 L\, C_M(\alpha_s) \end{aligned} \tag{6.1}$$

Looking at the reported equation it is possible to observe that the aerodynamic coefficients must be assessed in correspondence of the static angle that is unknown. This means that an iterative procedure must be carried on. The aerodynamic coefficients can be initially evaluated in correspondence of a null value of the angle of attack. Once evaluated the static forces at the mean wind velocity of interest, a static analysis can be performed and a first approximation of the static angle α_s can be obtained. The procedure restarts with the identification of the aerodynamic coefficients using this approximated value of the static angle, and it is iterated until the stabilized configuration is reached.

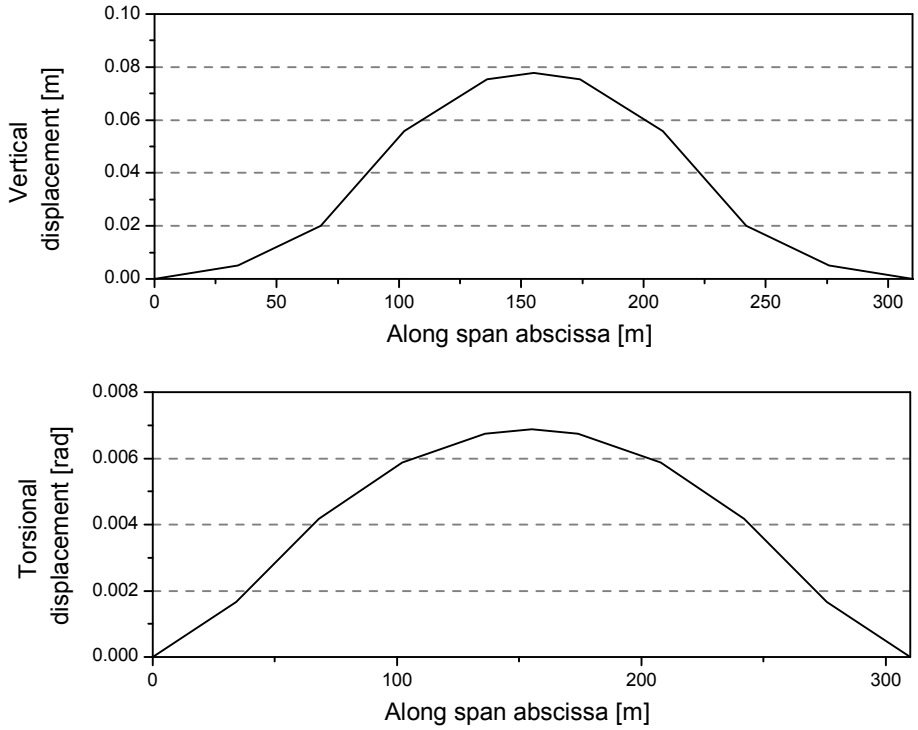

Fig. 38: Bridge deck deformed configuration due to static wind load $U = 80m/s$

In the case of the bridge under analysis the value of the mean wind velocity used to evaluate the static deck configuration is of $U = 80m/s$. This value has been selected in the range of the critical wind velocities reported in Fig. 42 at $\alpha = 0°$. In Fig. 38 the static deformed configuration of the bridge deck obtained considering the loads due to structural weight, cable pretension and aerostatic wind forces are depicted. The aerodynamic coefficients are evaluated assuming $\alpha = 0°$.

The obtained results highlight that the static deformed configuration reached by the deck can be considered small enough to avoid the adoption of the iterative procedure. Moreover, because of the small entities assumed by the deformed configuration, all future analysis are performed considering negligible their influence.

6.4 Flutter analysis in the frequency domain

As first step, in order to evaluate the flutter threshold of the bridge over the Adige river, a frequency analyses of the sectional model characterized by two degrees of freedom (vertical and torsional motion), is performed. All the detail about the numerical procedure can be found in (Dyrbye & Hansen, 1997).

Because flutter derivatives are known only at discrete values of the reduced frequency, an approximation using the rational function reported in (4.34) is performed. Not all the flutter derivatives obtained from wind tunnel test have taken into account in the approximation performed; in particular those evaluated in correspondence of the highest reduced velocity value are neglected. This allows a better approximation in the range where flutter instability occurs. In

particular, four poles have been chosen to perform the approximation whose values are: $d_i = [0.1\ \ 0.3\ \ 1.0\ \ 3.0]$ to approximate the derivatives of the box section and $d_i = [0.1\ \ 0.3\ \ 0.8\ \ 2.0]$ for those of the girder deck.

In Fig. 39 the comparison between the measured and fitted flutter derivatives $H_1, A_2 and\ A_3$, which, according to (Bartoli & Mannini, 2008) are the most important coefficients, are reported.

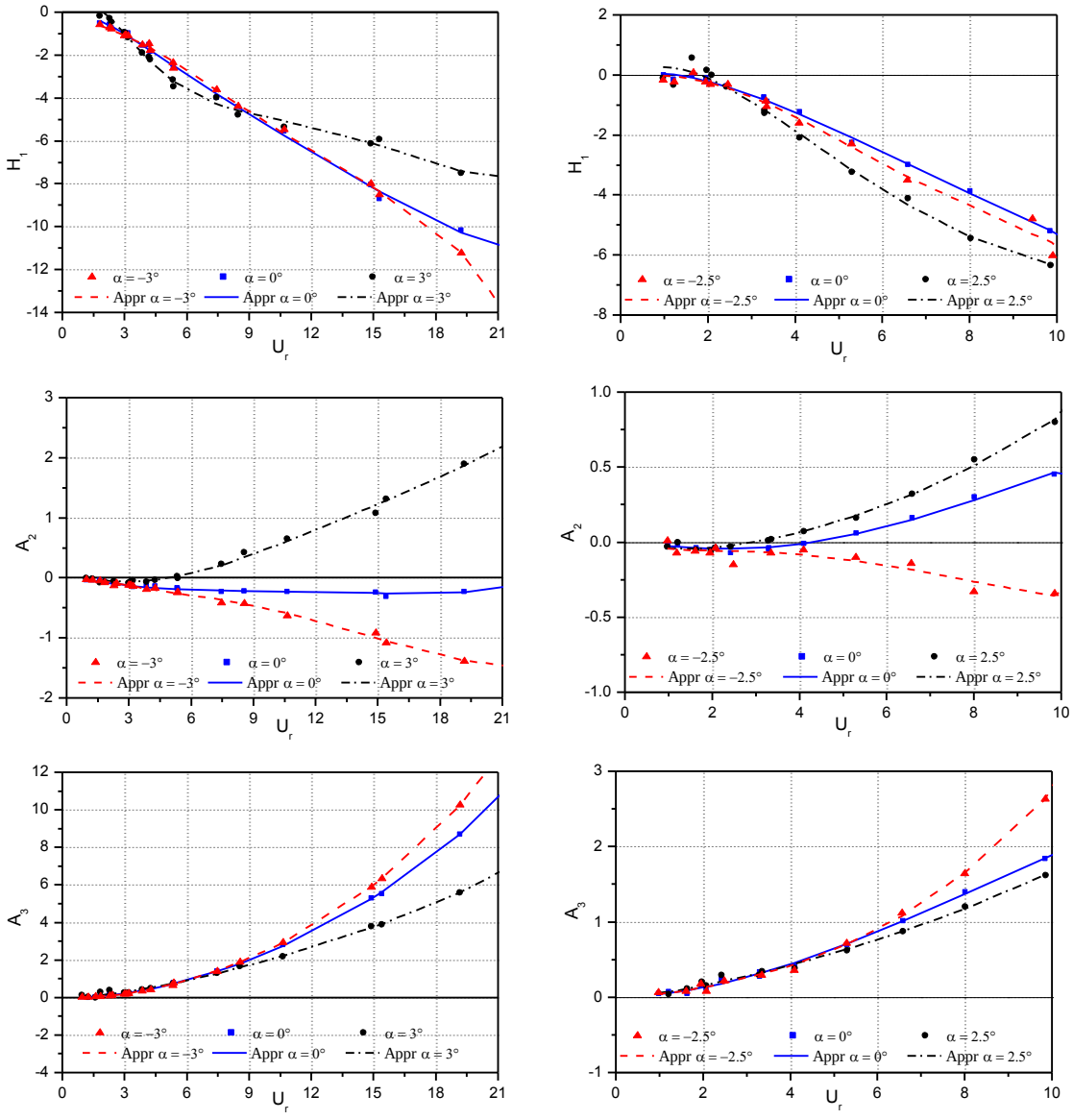

Fig. 39: Flutter derivatives Scanlan convention –box section on the left, girder section on the right

By means of the rational function approximation just introduced, the critical flutter velocity is here performed using the bimodal frequency approach. The solution is obtained plotting curves corresponding to the roots of the real and imaginary parts of the flutter determinant as a function of the reduced frequency. The intersection point between these curves with the lowest wind velocity value, defines the critical flutter threshold. The results obtained with aerodynamic parameters of the girder deck section are reported in Fig. 40.

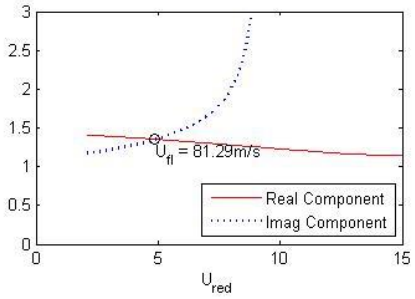

Flutter derivatives at $\alpha = 0.0°$

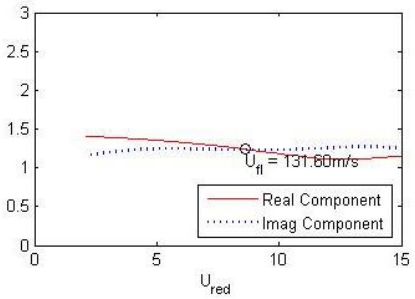

Flutter derivatives at $\alpha = -2.5°$

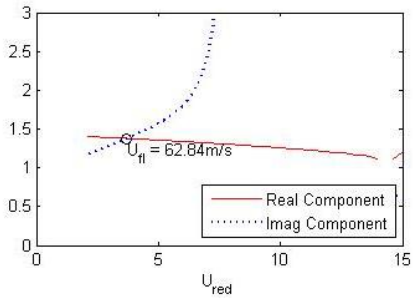

Flutter derivatives at $\alpha = 2.5°$

Fig. 40: Evaluation of the critical wind velocity in the frequency domain

As expected, the obtained results show that the structure is more stable when flutter derivatives are evaluated at negative values of the angle of incidence.

The structural damping used in all performed analysis is of $\xi_s = 0{,}5\%$. As already pointed out, this parameter is unknown during the design stage and, in some cases, it can strongly affect the analysis results. For this reason a sensitivity analysis of flutter threshold to damping is performed. The results obtained for both box section and girder deck are reported in Fig. 41 and Fig. 42 respectively.

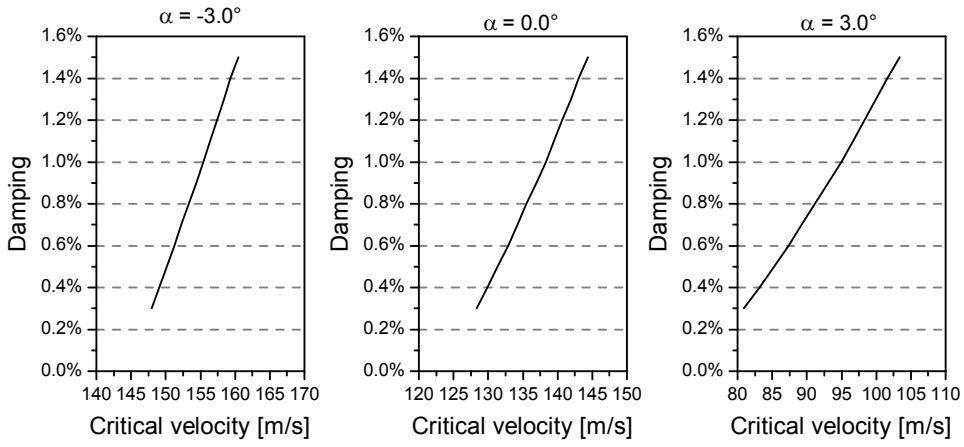

Fig. 41: Critical flutter velocity vs. Structural damping – Box section

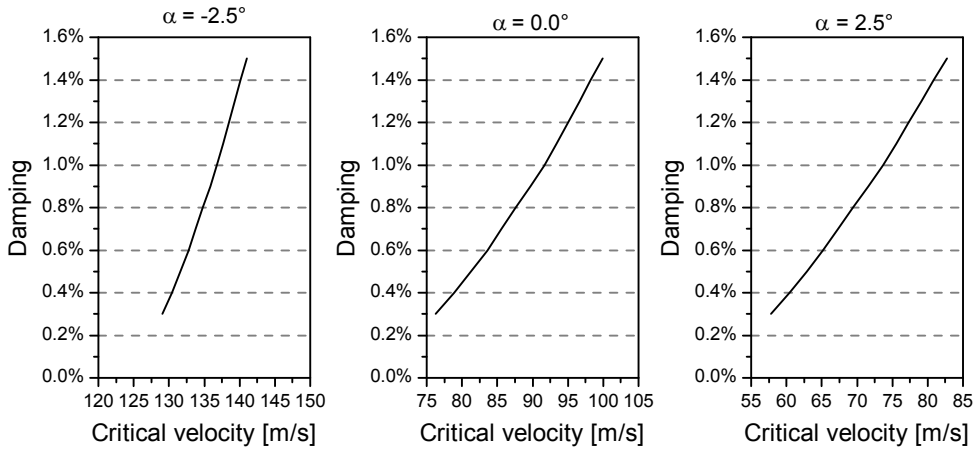

Fig. 42: Critical flutter velocity vs. Structural damping – Girder deck

It is worth noting that the slope of diagrams obtained using the set of flutter derivatives with coefficient a_2 that changes from positive to negative values (that means those evaluated at $\alpha = 0°$ and $\alpha = 2{,}5°$ in case of the girder deck solution and $\alpha = 3°$ in case of the box section) is lower than the one obtained in case its values are only negatives.

The results obtained by means of the frequency approach will be used as benchmark in future analysis performed by means of time domain formulations.

6.5 Flutter analysis in time domain

Sectional model

In this section the stability analysis performed in time domain using the linear model based on impulse functions is addressed. As reported in section 6.3, the deformed configuration due to static wind forces can be considered negligible so that the equation of motion can be linearized around the zero angle of incidence. In the following analysis, the sectional model described in section 6.1 have been adopted considering only the self-excited component of the wind load; for this reason in order to investigate the flutter threshold, an initial perturbation must be imposed to the system. The equation of motion are integrated using a time step value of $dt = 0{,}01s$ if the memory term of the aeroelastic load is evaluate by means of (4.38), otherwise if it is computed by means of (4.39) in order to guarantee a good level of approximation, the time step must be reduced up to $dt = 0{,}001s$. The structural response obtained calculating the memory term by means of (4.38) results to be the same of that obtained by means of (4.39).

In Fig. 43 it is possible to observe the structural response obtained in correspondence of three different wind velocities using the aeroelastic proprieties of the girder deck where the computation of the memory term is performed by means of (4.39).

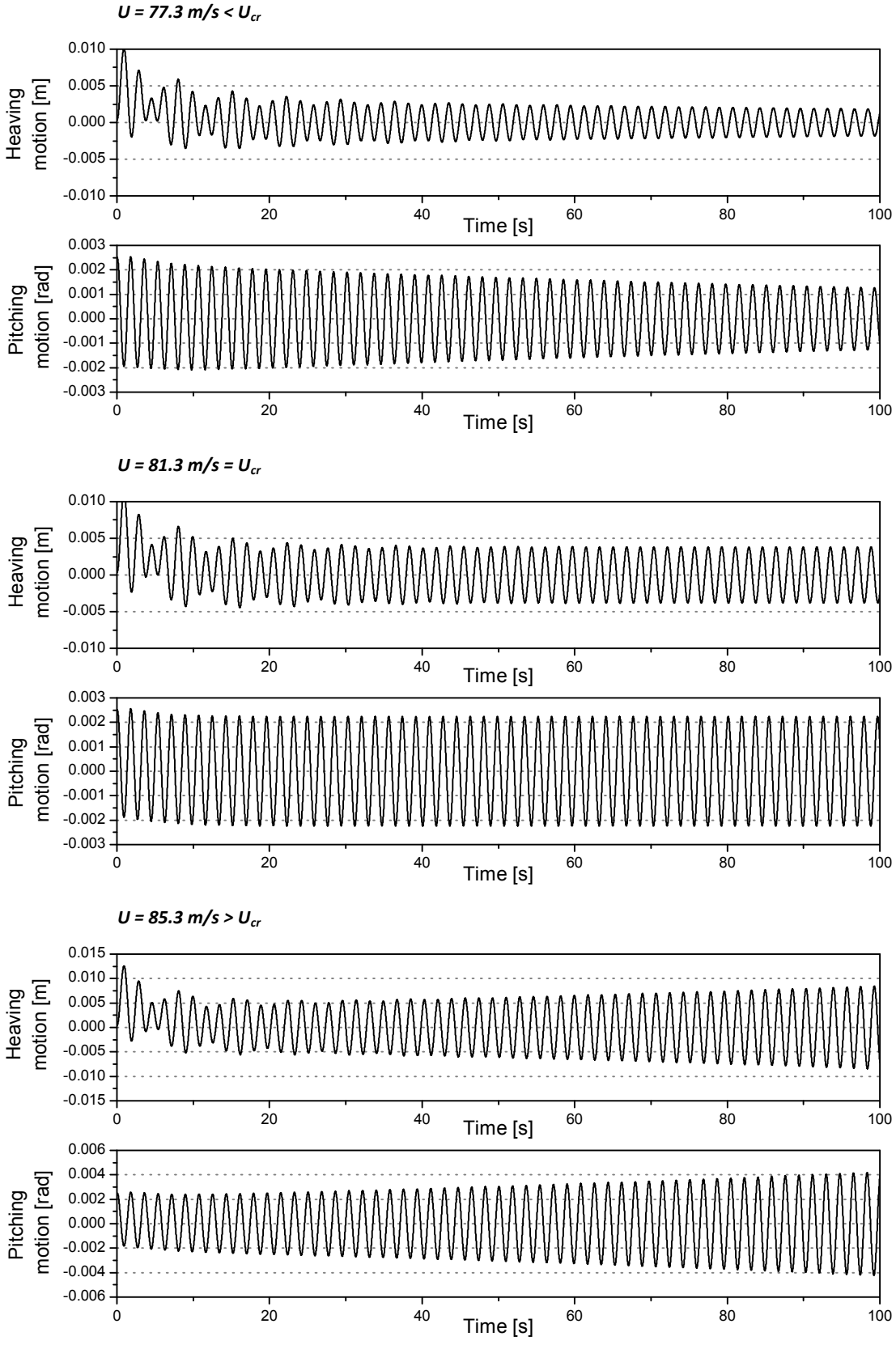

Fig. 43: Structural motion time history at different wind velocity– Girder deck

The values of the three wind velocity choices are respectively lower, equal and higher than the critical wind speed obtain by means of the frequency analysis presented in section 6.4. As expected, the results obtained are in good agreement with those reached in the frequency domain.

Similar analysis in the time domain are performed using the same structural proprieties but a different set of aerodynamic parameters evaluated at different angles of incidence. In Table 14 and Table 15 the critical wind speed, circular frequency and reduced velocity obtained for box section and girder deck respectively are reported.

Flutter angle	U_{cr} [m/s]	$\boldsymbol{\omega_{cr}}$ [rad/s]	U_{red}
$\alpha = -3.0°$	151.9	3.08	10.44
$\alpha = 0.0°$	124.7	3.30	8.00
$\alpha = 3.0°$	83.8	3.52	5.04

Table 14: Flutter analysis with sectional model in time domain – Box section

Flutter angle	U_{cr} [m/s]	$\boldsymbol{\omega_{cr}}$ [rad/s]	U_{red}
$\alpha = -2.5°$	131.6	3.20	8.69
$\alpha = 0.0°$	81.3	3.52	4.89
$\alpha = 2.5°$	62.8	4.01	3.69

Table 15: Flutter analysis with sectional model in time domain – Girder deck

It is worth noting that the box section presents higher value of the critical wind speed because of a better design of the deck shape that leads to a cross section more aerodynamically performant. This is mainly due to the different behaviour that the flutter derivative a_2 assume for the two sections. This explains why the flutter threshold presents higher values when aeroelastic parameters at negative value of the mean angle of incidence are considered. All the obtained results are perfectly in agreement with those calculated in the frequency domain. This confirms the good implementation of the force formulation in the time domain.

3D model

In this section the assessment of the critical wind velocity has been performed by means of a 3D model so that all the structural modes have been involved in the evaluation of the aeroelastic load. The analysis have been performed on both MODEL 3 and MODEL 4, see section 6.1. The main simplification introduced between these two models is about the schematization of the bridge deck that in the latter case is performed by means of only one equivalent cross section for the whole deck. The comparison of the obtained results allow to assess if the simplification introduced can be accepted. Moreover a qualitative idea of the reliability of results obtained by means of the sectional model can be addressed.

The assessment of the critical wind velocity is performed by means of the same procedure applied to the sectional model, that is by giving an initial impulse to the central point of the structure and by observing the trend of the structural response. The mean wind velocity in correspondence of which the structural displacements move from convergent to divergent motion represents the critical threshold. In Table 16 the obtained results are reported.

	U_{cr} [m/s]	$\boldsymbol{\omega_{cr}}$ [rad/s]	U_{red}
MODEL 3	84.3	3.61	4.94
MODEL 4	82.5	3.52	4.96

Table 16: Flutter analysis with 3D model in time domain (flutter derivatives evaluated at $\alpha = 0°$)

It is worth noting that the flutter threshold evaluated using MODEL 3 is higher than those obtained with MODEL 4. This means that the introduced simplification are not able to perfectly represent the real structural behaviour; anyway MODEL 4 is considered reasonably close to the preceding one and the results obtained are in favour of safety.

The results obtained using MODEL 4 pretty well collimate with the ones obtained with the sectional model. This means that the effects of both higher structural modes and structural nonlinearities are almost negligible. The small influence of structural nonlinearities is mainly due to the fact that the stays are connected in the central part of the deck so that their contribute to the total torsional stiffness is negligible. Since the aerodynamic instability of this structure is mainly torsionally-driven, structural nonlinearities results negligible in the evaluation of the flutter threshold.

In Fig. 44 and Fig. 45 the spectra analysis of the structural response evaluated at the critical wind velocity in correspondence of two different points on the deck span are reported.

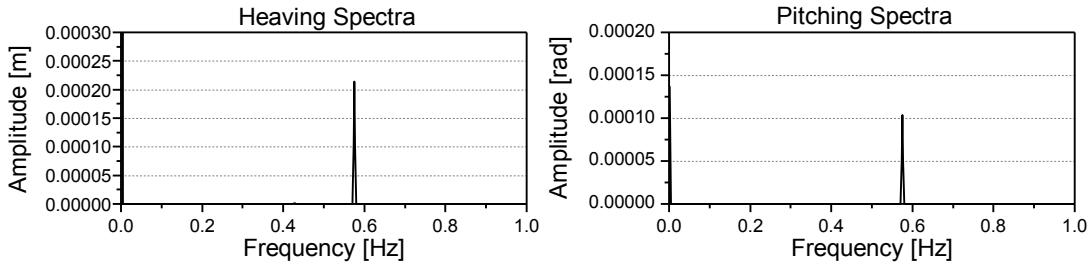

Fig. 44: Structural response spectrum of the central point – $\boldsymbol{U = U_{cr}}$

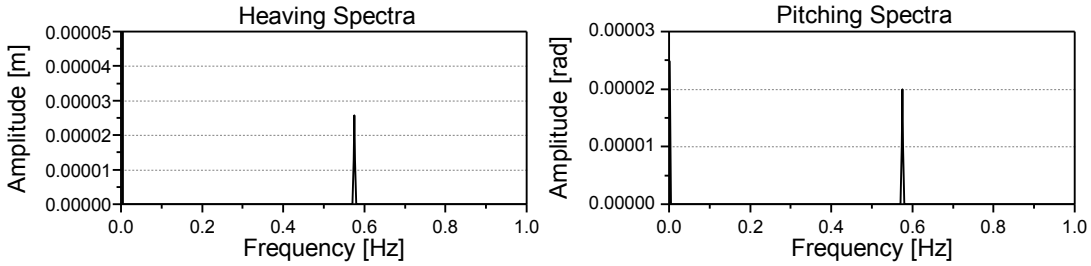

Fig. 45: Structural response spectrum of the point at 34m away from the pylon– $\boldsymbol{U = U_{cr}}$

Looking at graphs reported above it is possible to observe that, in both the monitored point, only one frequency component is present in the spectrum of the structural response. This underlines that the contribution of others modal shape is negligible so that the instability onset is due to the coupling between the first symmetric bending mode and the first symmetric torsional one. This result supports the previous evidence about the accuracy of results obtained by means of the sectional model. It can be considered a well suited tool for the investigation of the structural behavior with the advantages to be computationally more efficient.

On the basis of these evidences, I have decided to adopt the sectional model to investigate the structural response by means of the proposed nonlinear framework, as following presented in section 6.9.

6.6 Quasi steady analysis in time domain

A different approach to evaluate the critical wind speed is by means of the linearized quasi-steady force model, see section 4.3. As already mentioned, the assessment of the proper value of the coefficients m_h and m_α is a crucial point for the proper evaluation of the flutter threshold. In particular they are of difficult evaluation if wind tunnel tests are not performed in order to assess their values, as usually occurs. To remark how much these parameters can affect the structural response, a sensitivity analysis is here performed. In Fig. 46 the results obtained are reported.

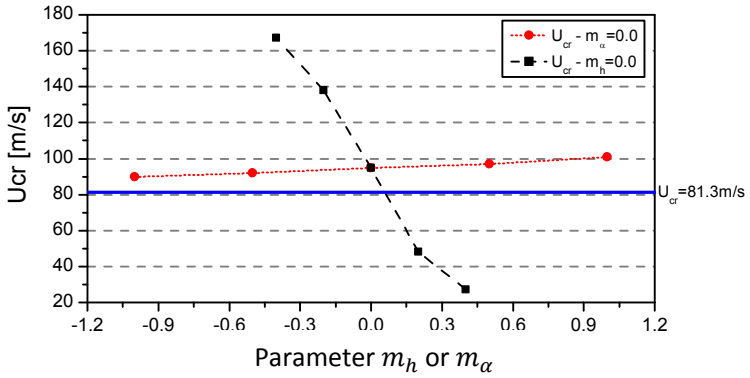

Fig. 46: Flutter wind speed evaluated by means of the quasi-steady theory using several values of the parameter m_h or m_α

The graph above is composed by three different curves. The dashed line represents how the flutter velocity change if $m_h = 0.0$ and m_α ranges between ± 0.4, while the dotted one is obtained keeping constant $m_\alpha = 0.0$ and ranging $m_h = \pm 1.0$. Finally, the solid line represents the flutter threshold obtained when aeroelastic forces are calculated by means of flutter derivatives instead of aerodynamic coefficients. It is worth noting that the results obtained with the quasi-steady theory are not so much sensitive to the parameter m_h while the influence of m_α is pretty strong.

Looking at Fig. 46 it is easy to see that the critical wind velocity that would be obtained using the values of parameters m set above, is really different from the one evaluated with aeroelastic derivatives. This underlies that the quasi-steady force model is not able to accurately predict the critical velocity because of its strong dependence on parameters m, which are of difficult identification. This remarks once again how important is the use of the unsteady load model in the evaluation of the flutter threshold.

6.7 Buffeting analysis

In preceding sections the analysis performed have been focused only on the definition of the critical wind speed. Since in future analysis the structural response due to both aeroelastic and buffeting loads will be investigated, in this section only the effects due to turbulent wind component are studied.

Turbulence generation

The spectral model proposed by Shinozuka, described in section 3.3, is used for the numerical generation of the time history of the turbulent wind component. Since the structure under analysis is located in Italy, the Italian code (CNR, 2008) has been here used to mathematically describe the wind velocity field.

Considering the specific characteristics of the area surrounding the bridge, the following parameters have been assumed to characterized the wind spectra:

Reference wind velocity	$v_r = 25m/s$
Terrain factor	$k_r = 0{,}19$
Roughness	$z_0 = 0{,}05$
Standard deviation	$\sigma_u = 4{,}75$
Turbulence intensity (z=15m)	$I_u = 0{,}175$
λ coefficient	$\lambda = 0{,}52$
Integral length scale	$L_u = 78$

Table 17: Wind turbulence spectra parameters

As an example in Fig. 47 the power spectral density of a generated time history is compared to the original target spectrum. The mean wind velocity used for the generated turbulence is of $U_m = 80m/s$.

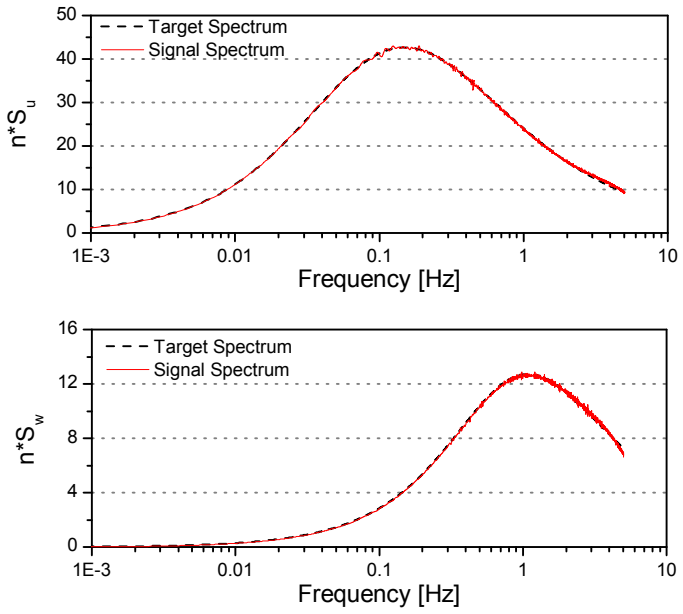

Fig. 47: Target and generated turbulent spectra comparison

Response analysis

In this section the analysis of the structural response, computed considering the sectional model, due to buffeting load is addressed. The force component due to the turbulent wind is here

evaluated by means of the linearized quasi-steady theory. For the sake of brevity only the results of one test performed using the sectional model and a mean wind velocity of $U = 80m/s$ are here addressed. In Fig. 48 the structural displacements and spectral response obtained at this wind velocity are reported. Anyway several analysis at different wind velocities have been performed, whose results will be showed in future sections.

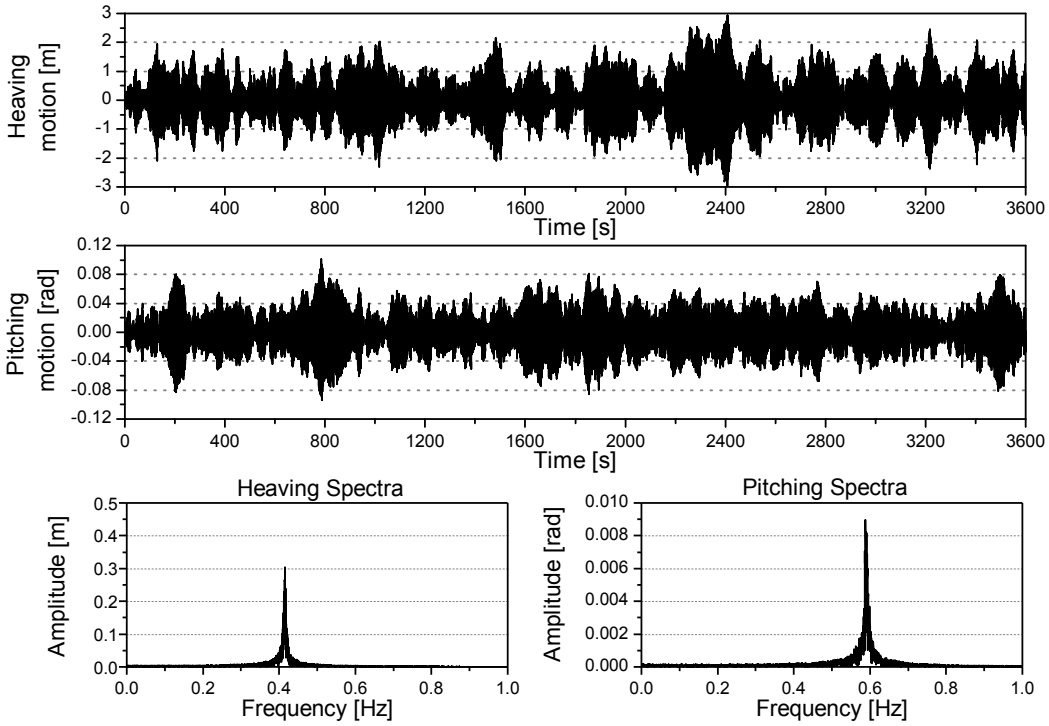

Fig. 48: Buffeting analysis: mean wind velocity of $U = 80m/s$ – Girder deck

Looking at the obtained results it is possible to observe that both vertical and torsional displacements have reached quite big values. This is here remarked to explain that in future analysis, when both self excited and buffeting load are considered, if only the flutter threshold is under investigation it will be not important the amount of displacement reached by the structure, but only the converging or diverging response trend will be considered.

6.8 Mixed problems: aeroelastic and buffeting forces

In this section the analysis of the bridge behaviour, represented by means of the sectional model, when excited by both self excited and buffeting forces is investigated. These analysis are conducted at several wind velocities ranging from $U = 27m/s$, that is the wind speed value related to a return period of 50 years, up to the critical one. A comparison between the response analysis of the bridge when excited only by buffeting forces and those obtained considering also self excited components is here performed. In this way it is possible to estimate how important are the aeroelastic wind components in the evaluation of the total response.

From Fig. 49 up to Fig. 54 the time history of the structural response and relative spectra are reported. The aerodynamic characteristics used to perform these analysis are those of the girder deck evaluated in correspondence of an angle of incidence of $\alpha = 0°$.

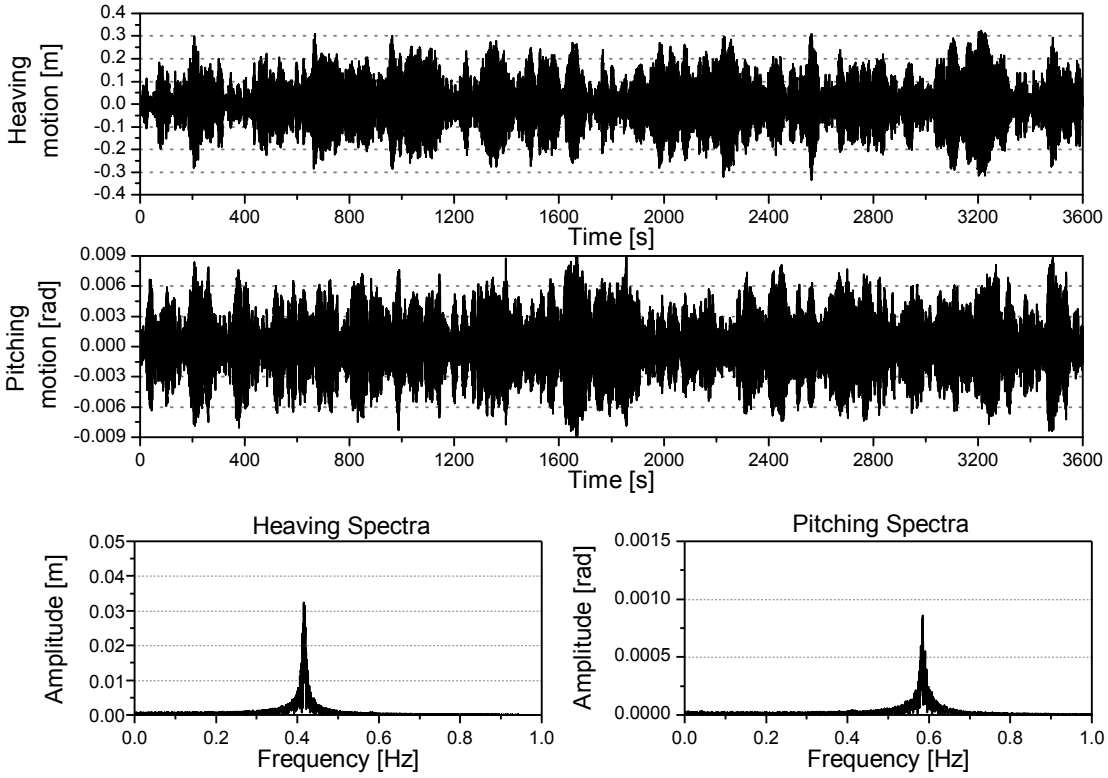

Fig. 49: Response analysis: mean wind velocity $U = 27m/s$

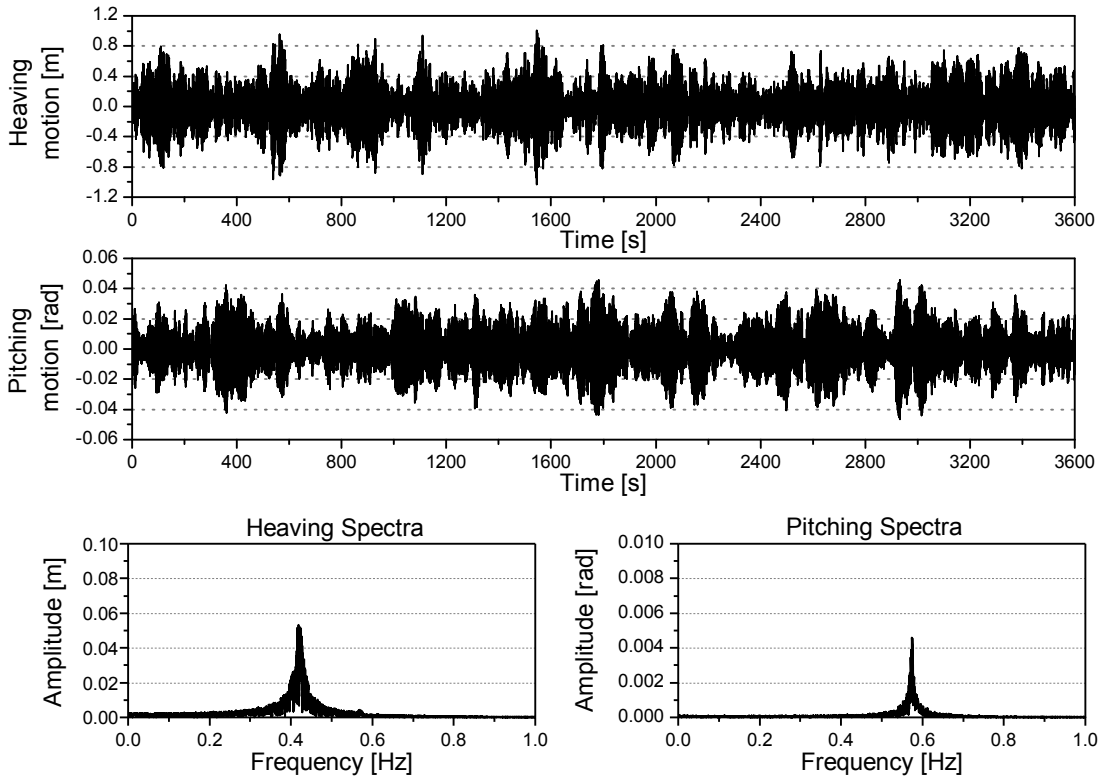

Fig. 50: Response analysis: mean wind velocity $U = 60m/s$

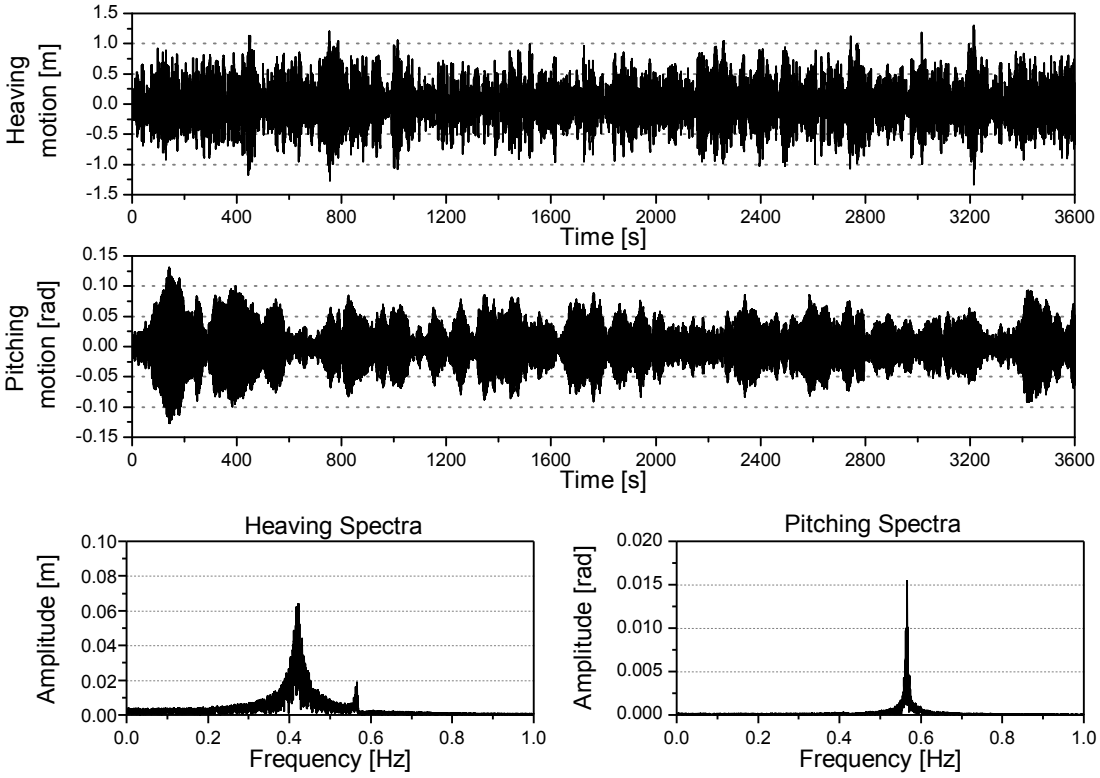

Fig. 51: Response analysis: mean wind velocity $U = 75m/s$

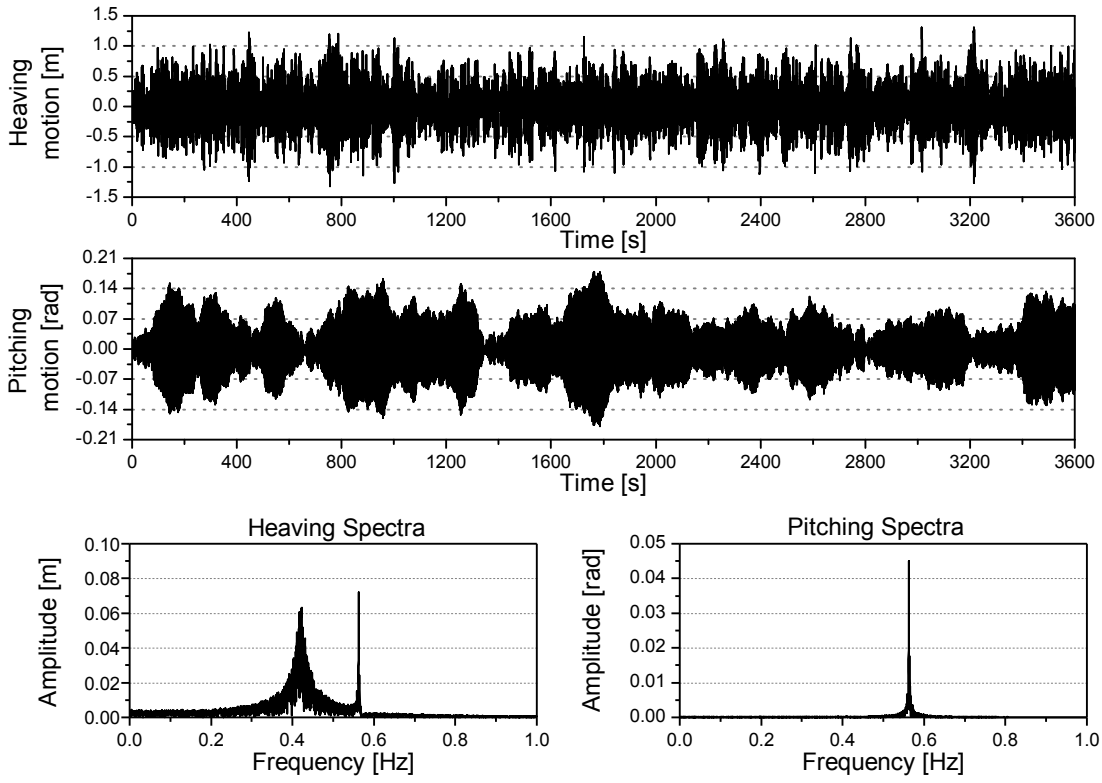

Fig. 52: Response analysis: mean wind velocity $U = 79m/s$

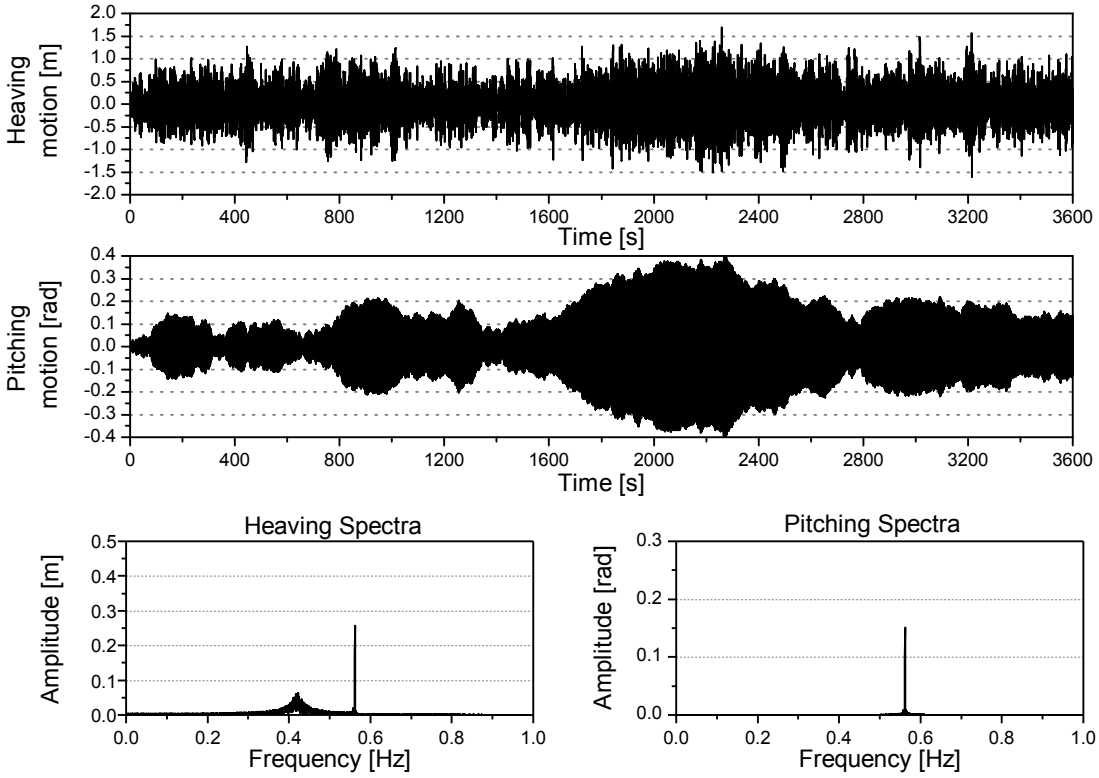

Fig. 53: Response analysis: mean wind velocity $U = 81m/s$

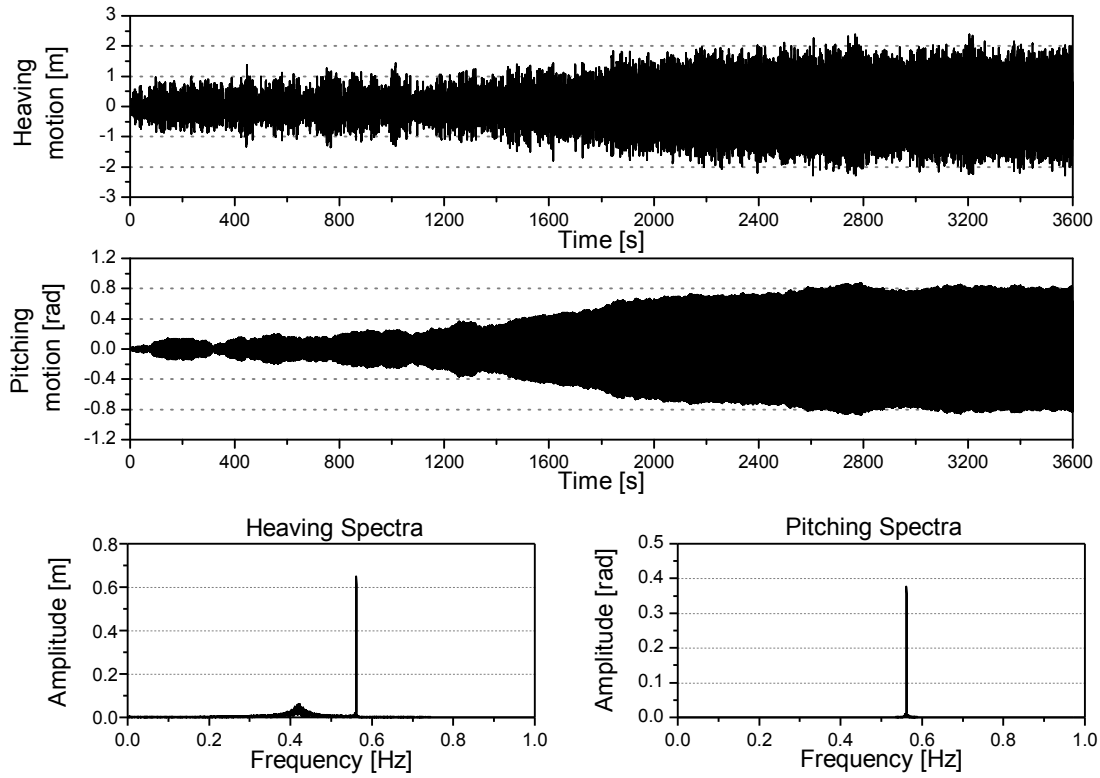

Fig. 54: Response analysis: mean wind velocity $U = 81.5m/s$

The reported results show that in the vertical spectra there is a second peak in correspondence of the frequency of the torsional response as the wind velocity is close to the critical one. The value of this peak is proportional to the intensity of the wind speed. This means that a coupling between vertical displacement and torsional motion is occurring.

Because the bridge is considered as a linear structure, the critical value of the mean wind velocity is not affected by the presence of turbulence.

6.9 Nonlinear model: flutter threshold identification

In this section the evaluation of the instability threshold is performed by means of the proposed nonlinear force model introduced in Section 4.7.

As first step, the definition of the cut-off frequency value, that will be used to decompose the turbulent wind velocity in both low and high frequency components, must be performed. The value of this frequency is evaluated by means of (4.55). In this equation the reduced velocity value above which the aeroelastic derivatives approach the quasi-steady behaviour must be used. The identification of this parameter is not an easy task since only its qualitative assessment can be performed. As previously observed from instabilities analysis carried out by means of the linear approach the aeroelastic load is highly sensitive respect to the flutter derivative a_2. So the assessment of the reduced velocity value is here performed just considering the behaviour of only this derivative. Moreover, it is well known that the trend of the derivative tends to reach a constant value when the reduced velocity value is high enough. In Fig. 55 is possible to observe the achievement of this constant trend looking at the behaviour of the flutter derivative obtained in correspondence of $\alpha = 0°$. This means that the quasi-steady behaviour is reached in a softening way, therefore the assessment of a definite value of the reduced velocity is not easy to perform. For this reason, several values of this parameter are here considered, so that a sensitivity analysis of flutter threshold can be carried out.

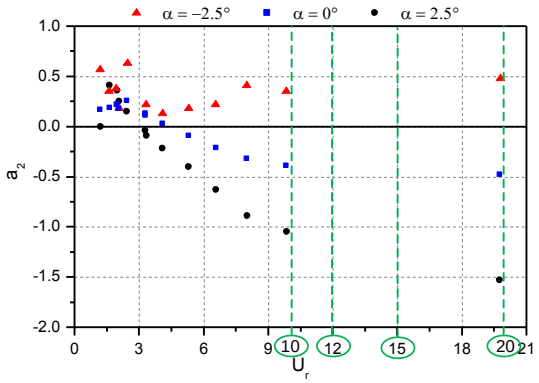

Fig. 55: Flutter derivative a_2

Because the flutter threshold obtained from linear analysis performed at a mean angle of attack of $\alpha = 0°$ is of $U_{cr} = 81.3m/s$, the cut-off frequency values reported in Table 18 are calculated with respect to a mean wind velocity of $U = 80m/s$.

Reduced velocity	Cut-off frequency
$U_{red} = 20$	$f_{cut-off} = 0.135Hz$
$U_{red} = 15$	$f_{cut-off} = 0.180Hz$
$U_{red} = 12$	$f_{cut-off} = 0.224Hz$
$U_{red} = 10$	$f_{cut-off} = 0.269Hz$

Table 18: Cut-off frequency values – $U = 80m/s$

In the following figures the angle of incidence obtained using only the low frequency turbulent component is compared with the total one.

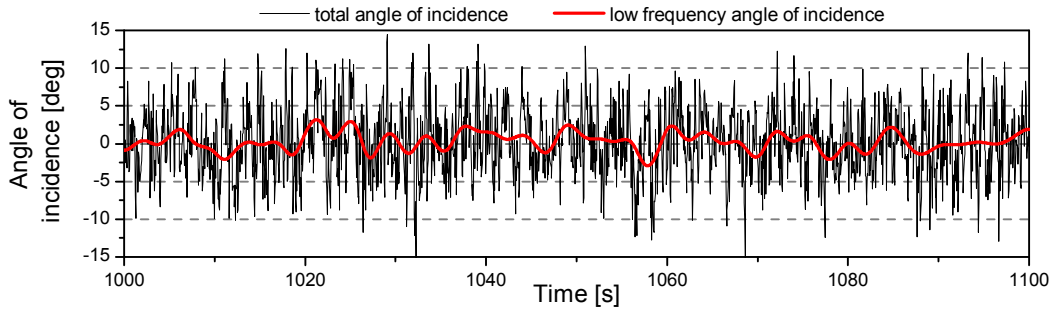

a) Cut-off frequency $f_{cut-off} = 0,135Hz$

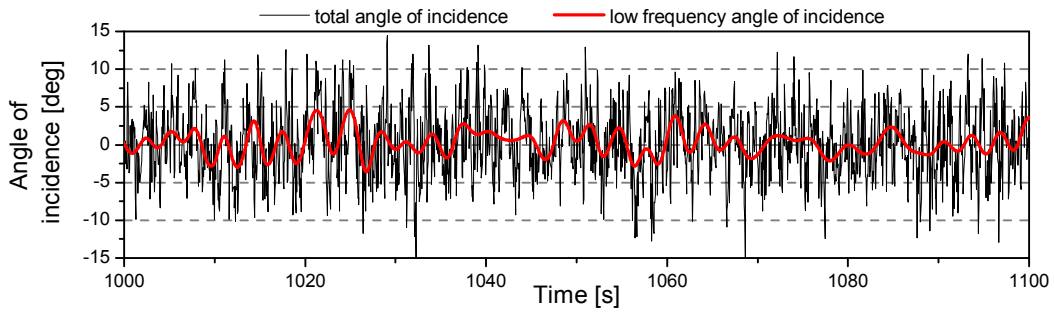

b) Cut-off frequency $f_{cut-off} = 0,180Hz$

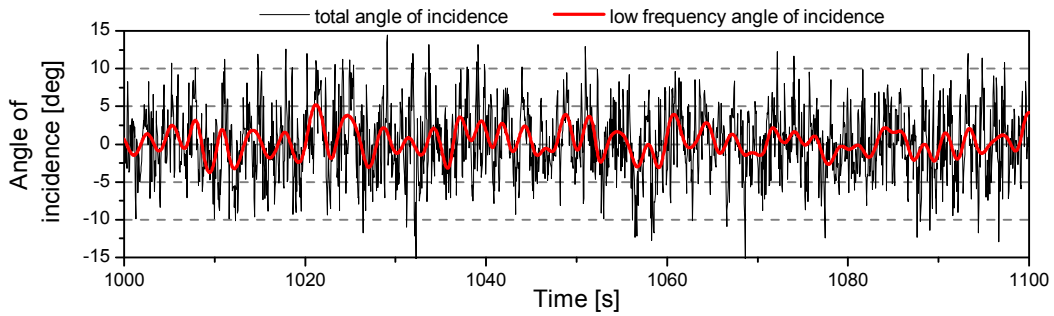

c) Cut-off frequency $f_{cut-off} = 0,224Hz$

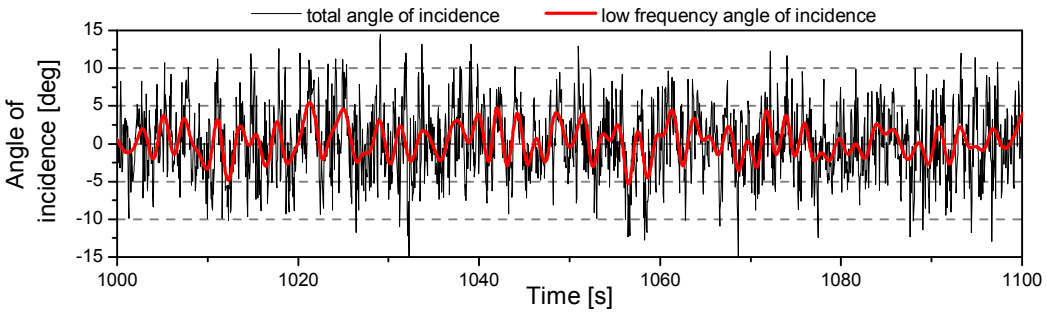

d) Cut-off frequency $f_{cut-off} = 0,269Hz$

Fig. 56: Comparison between total angle of incidence and low frequency one

It is worth noting that the angle of incidence evaluated with the low frequency turbulent component takes values that are out of the range of $\alpha = \pm 2.5°$, especially when higher cut-off frequency are considered. Since the experimental data was only available for a limited number of angles of incidence ranging between $\pm 2.5°$, the corresponding values for intermediate angles of incidence were interpolated, and the values for angles larger than 2.5° or smaller than $-2.5°$ were assumed to be the same as 2.5° or $-2.5°$, respectively.

In order to evaluate the flutter threshold by means of the proposed nonlinear approach, in correspondence of each value of the cut-off frequency several analysis have been performed with increasing wind speed. The investigation starts from a mean velocity value of $U = 80m/s$ and stops when a highly divergent oscillation behaviour arise. From Fig. 57 to Fig. 62 displacements and spectra results obtained using the sectional model and a cut-off frequency of $f_{cut-off} = 0{,}269Hz$ are reported. The first thing observed in the obtained results is that the amplitude of vertical and torsional displacements are quite high. This is due to both strong values of the buffeting load and aeroelastic load evaluated close to the critical wind velocity. Even if displacements reach high values, sometimes even greater than those accepted by the structure, it doesn't mean that the flutter threshold cannot be considered properly evaluated. In fact when flutter analysis is performed by means of the classical linear approach, the intensity of the initial impulse is arbitrary assumed. For this reason the assumption of small structural displacement is always verified. In case of the proposed nonlinear approach the aeroelastic forces depend on wind turbulence so that it is not possible evaluate the flutter threshold without the computation of buffeting forces.

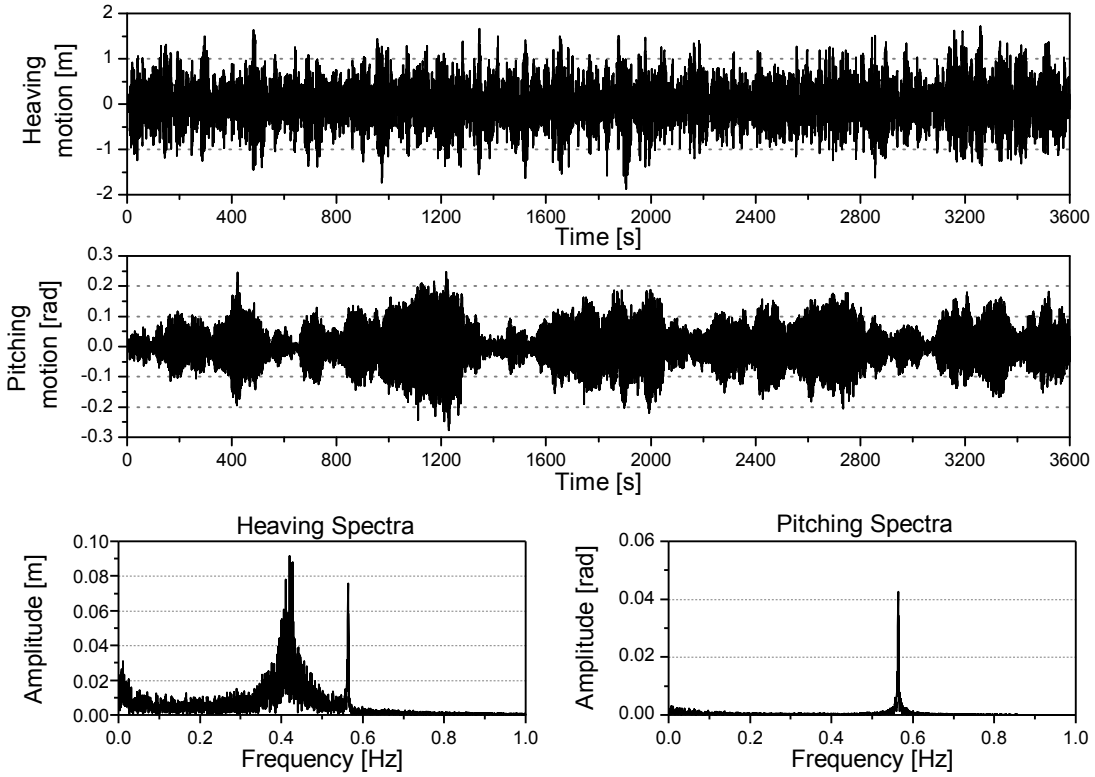

Fig. 57: Nonlinear analysis: mean wind velocity $U = 80\ m/s - f_{cut-off} = 0,269\ Hz$

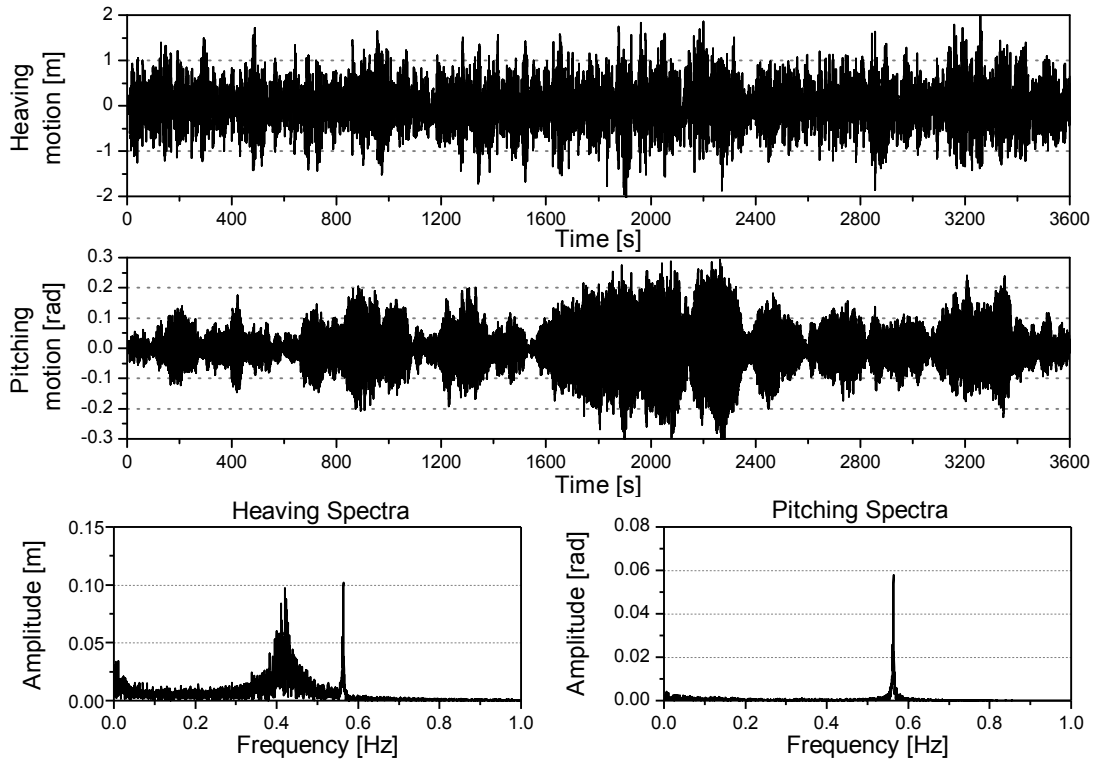

Fig. 58: Nonlinear analysis: mean wind velocity $U = 82\ m/s - f_{cut-off} = 0,269\ Hz$

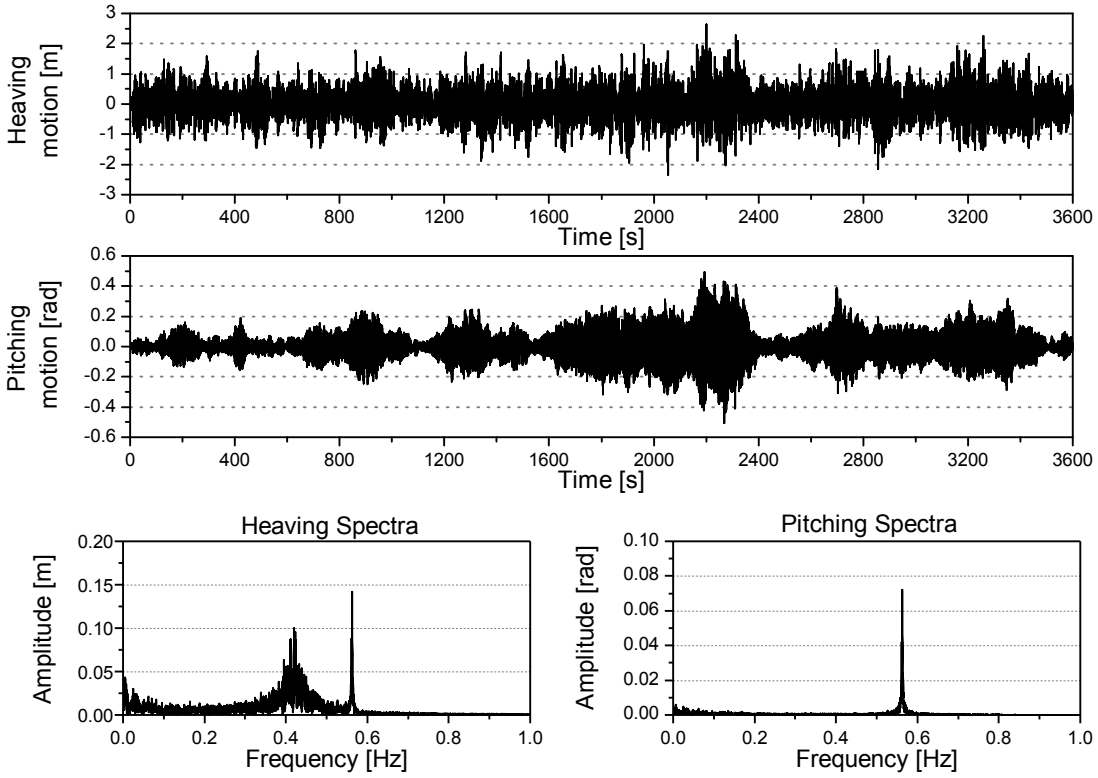

Fig. 59: Nonlinear analysis: mean wind velocity $U = 83\ m/s - f_{cut-off} = 0,269\ Hz$

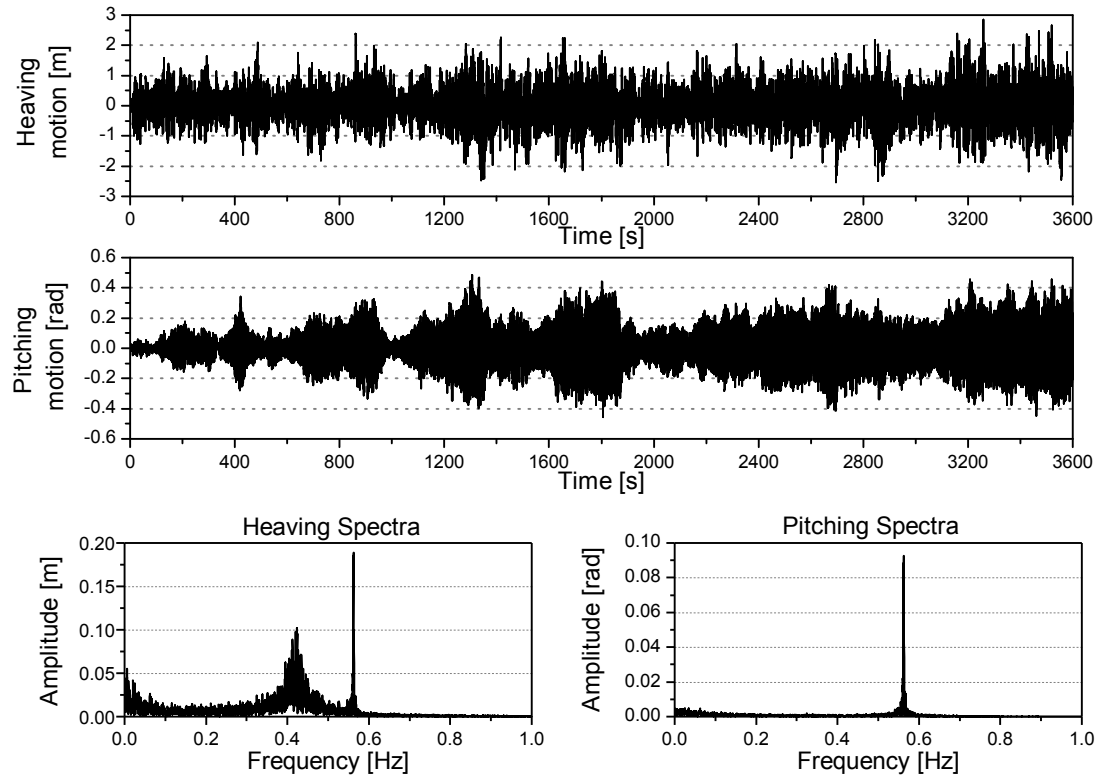

Fig. 60: Nonlinear analysis: mean wind velocity $U = 84\ m/s - f_{cut-off} = 0,269\ Hz$

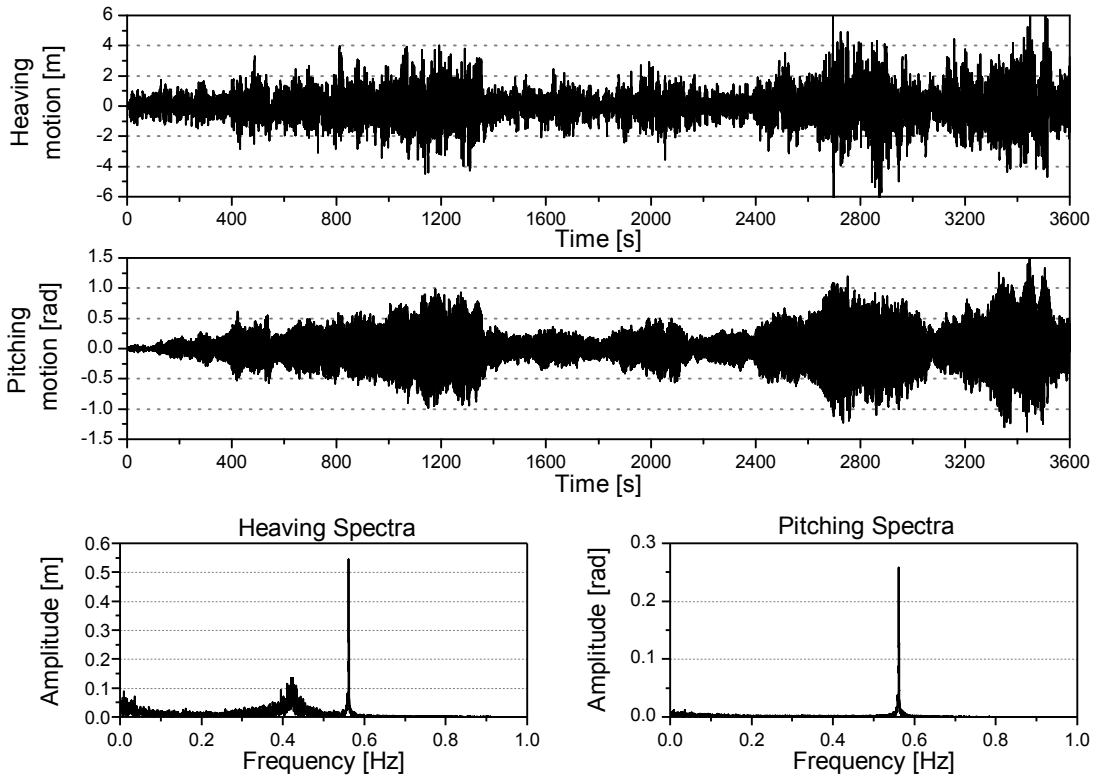

Fig. 61: Response analysis: mean wind velocity $U = 85\ m/s - f_{cut-off} = 0,269\ Hz$

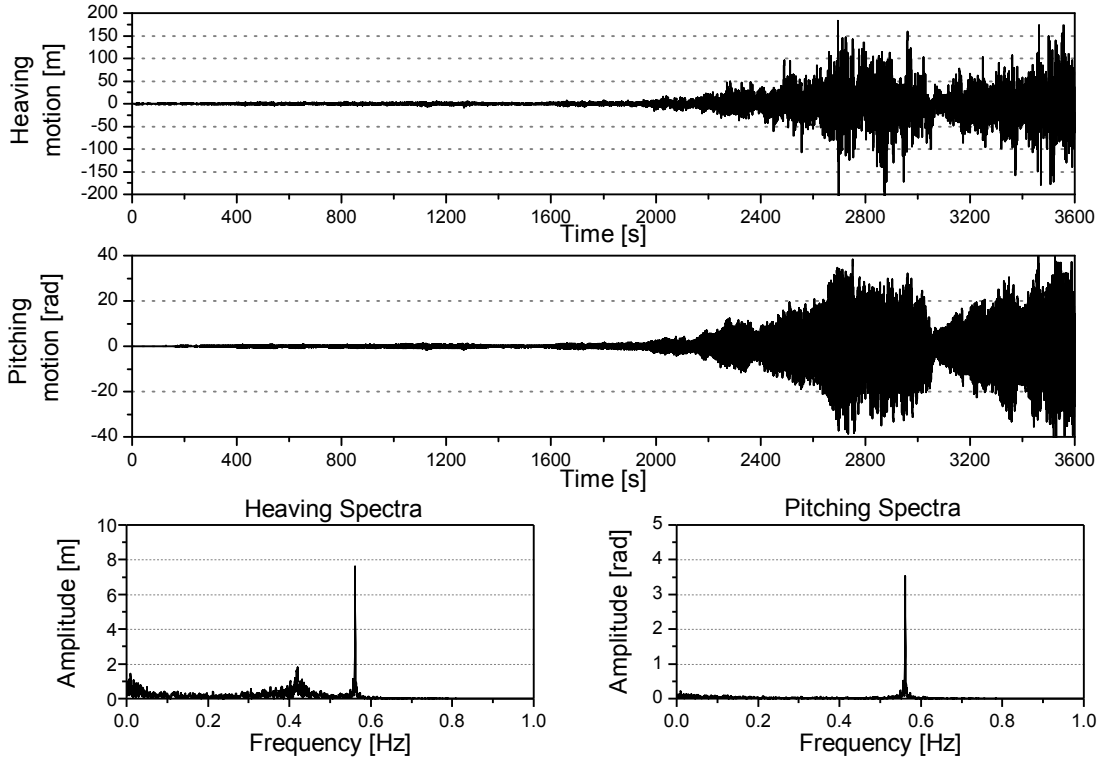

Fig. 62: Response analysis: mean wind velocity $U = 85.5\ m/s - f_{cut-off} = 0,269\ Hz$

Similar analysis have been conducted in correspondence of each cut-off frequency value previously assessed. The results obtained by all these analysis are reported in Appendix I. Looking at the results reported it is difficult to identify a definite value of flutter velocity. In fact, because of the presence of the buffeting load, it is hard to evaluate at which wind speed the structural response in time domain becomes unstable. Only a possible range of wind velocity values at which flutter occurs can be defined. Also the spectral analysis of structural displacements can be of help to better assess the flutter range. In particular it is possible to observe that close to the critical wind speed the vertical displacement is strongly affected by torsional motion, but nothing can be said about the exact wind velocity value at which flutter arise.

In order to compare in an effective manner the results obtained using different cut-off frequency, the whole structural response has been resumed with its RMS values. In Fig. 63 and Fig. 64 the RMS of respectively vertical and torsional displacements are reported.

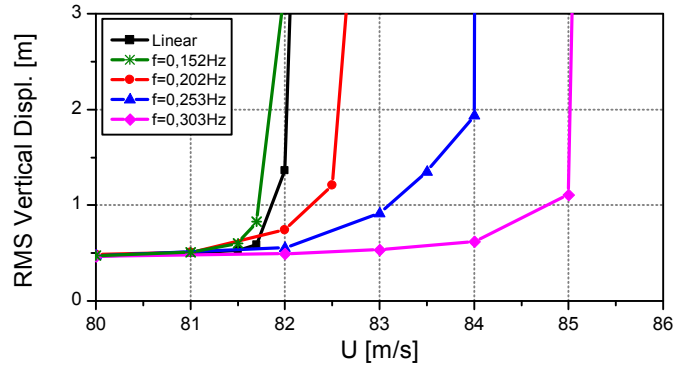

Fig. 63: RMS Vertical displacement – $\xi_{cr} = 0,5\%$ - Girder deck

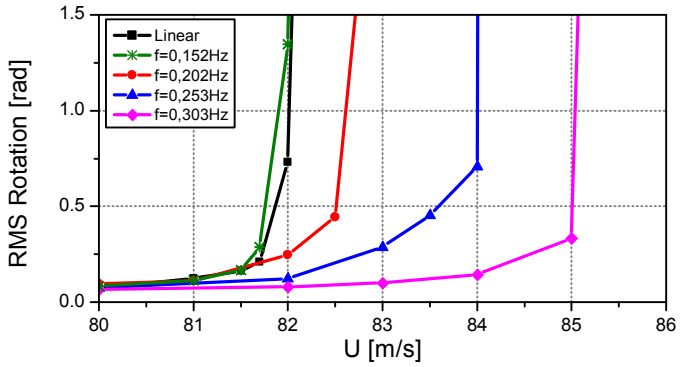

Fig. 64: RMS Torsional displacement – $\xi_{cr} = 0,5\%$ - Girder deck

It is evident from the above reported results how sensitive the system is to the cut-off frequency value. In particular, if a low value of this parameter is chosen, the structural response obtained with the nonlinear force model is almost close to the linear one, while as the cut-off frequency value increases, also the critical wind speed move towards higher values. This implies the impossibility to identify a defined and stable flutter threshold using the proposed approach. Anyway, the nonlinear model gives important information about the trend of flutter threshold to move over or under the one calculated by means of the linear approach. Moreover it is worth

underlining that the critical wind velocity calculated using the nonlinear force model is not so different from that obtained by means of the linear approach when the set of flutter derivatives used are those calculated in correspondence of the static angle. The case study here proposed presents negligible deformation under static loads so a direct comparison with results obtained in preceding sections with the classical approach linearized around a mean angle of $\alpha = 0°$ can be performed. The agreement between the two approaches is not surprising because even if the set of flutter derivatives used to define the aeroelastic load changes at each time step, when the nonlinear approach is used, their values always fluctuate around the static ones. This means that also the flutter threshold must be close to each other.

As illustrated in section 6.1, the cross section shape initially chosen for this bridge was different. In order to investigate the differences between the two proposed sections, and to better understand the effects of turbulence on the flutter instability, similar analysis as above have been performed using the aerodynamic proprieties of the box section. The deck stiffness of the box section is higher than the one evaluated for the girder deck. Anyway, in order to investigate only the differences due to the changed aerodynamic behaviour, the same structural characteristics used in previous analysis are here adopted. Also the critical wind velocity evaluated with classical approach is higher for the box section than for the girder deck. Despite this fact, the values of the cut-off frequency used in the following nonlinear analysis are the same used in preceding ones.

In Fig. 65 and Fig. 66 the RMS of respectively vertical and torsional displacements are reported.

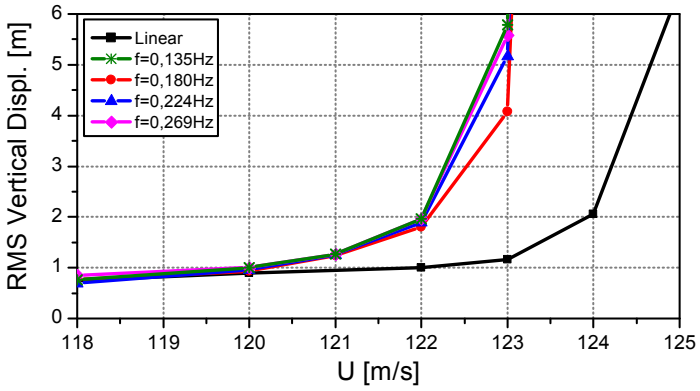

Fig. 65: RMS Vertical displacement – $\xi_{cr} = 0,5\%$ - Box section

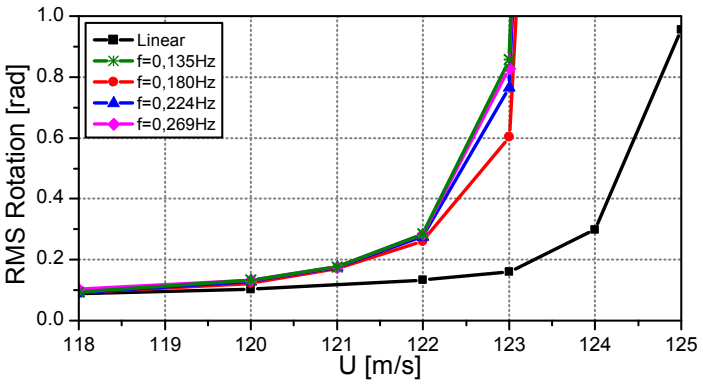

Fig. 66: RMS Torsional displacement – $\xi_{cr} = 0,5\%$ - Box section

Looking at the obtained results, it is worth pointing out that the trend of the critical flutter velocity calculated with the nonlinear approach is independent from the choice of the cut-off frequency value. This means that, in this case, it is not only possible to assess the trend of flutter threshold, but also evaluate its value in a precise way.

While the girder deck almost presents an increase of the critical wind velocity as the cut-off frequency arise, the box section presents an opposite trend. This means that in the first case the flutter threshold calculated with the linear approach is safer than the one obtained with the nonlinear model, while in the second case the flutter wind speed calculated with the linear approach cannot be considered reliable. The different behaviour observed can be mainly attributed to the different trend the derivatives $A_2(\alpha_s)$,with $\alpha_s = 0°$, presents between the two sections. In fact this parameter for the box section assumes always negative values; this means that the sum of the aeroelastic damping and the structural one rise to an enhance of the structural stability. Conversely, the derivative A_2 of the girder deck assumes positive or negative values depending on whether it refers to higher or lower value of the reduced velocity than $U_{red} \cong 4.3$. As reported in Table 15 the reduced velocity value when flutter occur is close to this particular transient value, so that the flutter phenomenon is almost torsionally driven. This explains why the aerodynamic proprieties of the girder deck leads to the evaluation of a critical wind speed more sensitive to the cut-off frequency value than the box section.

Another interesting analysis to perform is about the structural response sensitivity related to the structural damping coefficient. As already stated, the latter is a parameter difficult to evaluate at the design phase, but its value is sometimes strongly affecting the analysis results. For these reasons it has been decided to investigate what happens if a different value of this parameter is chosen. In particular, the second damping value considered, of 1%, is that assumed by the structural designers. On the other hand, since the values assumed by the designers looks to be too much higher for this type of structure, all the previously illustrated analysis have been performed considering a damping of 0.5%. This has been subsequently confirmed by the in situ experimental campaign, previously presented, by means of which it has been obtained a structural damping of about 0.3%.

Because the flutter threshold obtained from linear analysis performed considering the aerodynamic characteristics of the girder deck refers to a mean angle of attack of $\alpha = 0°$ is of $U_{cr} = 91.6 m/s$, the evaluation of the cut-off frequency parameter, reported in Table 18, is performed by means of (4.55) considering a mean wind velocity value of $U = 90 m/s$.

Reduced velocity	Cut-off frequency
$U_{red} = 20$	$f_{cut-off} = 0.152 Hz$
$U_{red} = 15$	$f_{cut-off} = 0.202 Hz$
$U_{red} = 12$	$f_{cut-off} = 0.253 Hz$
$U_{red} = 10$	$f_{cut-off} = 0.303 Hz$

Table 19: Cut-off frequency values – $U = 90 m/s$

For the sake of brevity, diagrams of displacements and of their relative spectra are here omitted and in Fig. 67 and Fig. 68 only the graphs of RMS values are reported.

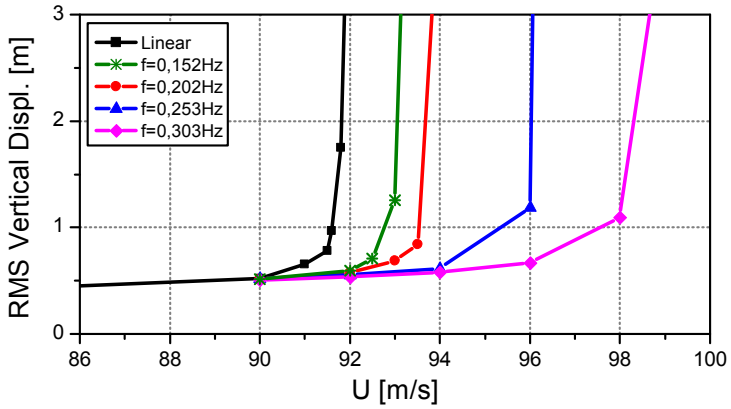

Fig. 67: RMS Vertical displacement – $\xi_{cr} = 1\%$ - Girder deck

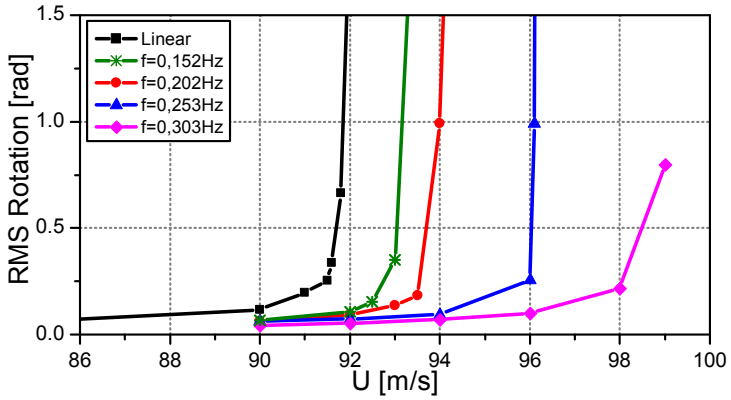

Fig. 68: RMS Torsional displacement – $\xi_{cr} = 1\%$ - Girder deck

As already seen when a damping coefficient of $\xi = 0{,}5\%$ has been assumed, also in this case the critical wind velocity evaluated using the nonlinear approach is strongly affected by the choice of the cut-off frequency value. In particular, the flutter threshold obtained with the proposed approach assumes higher values than the one calculated with the classical linear model. It is worth underlining that the results obtained with the nonlinear approach and a structural damping of $\xi = 1\%$ lead to a shift of the flutter threshold always towards higher values than the one obtained with the linear model. This has not happened for each value of the cut-off frequency when a structural damping of $\xi = 0{,}5\%$ has been assumed. The outlined differences probably depend on the strong sensitivity of the structural response with respect to the flutter derivatives A_2. In particular the value of the structural damping leads the system to be more or less sensitive respect to the aerodynamic damping, that is the structural damping value emphasize or reduce the effects due to the self excited forces.

Similar analysis have been performed considering the aerodynamic characteristics of the box section and structural damping of $\xi = 1\%$. The obtained results are reported in Fig. 69 and Fig. 70.

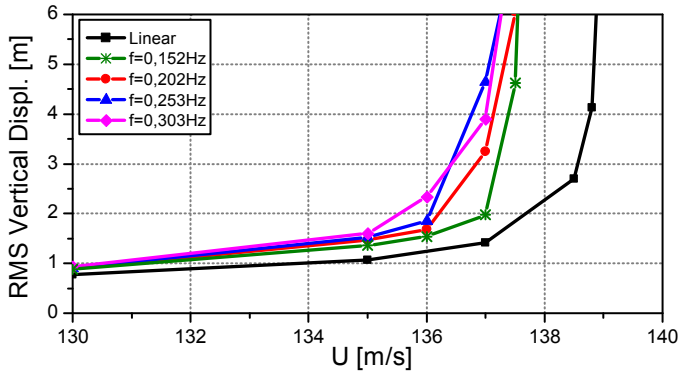

Fig. 69: RMS Vertical displacement – $\xi_{cr} = 1\%$ - Box section

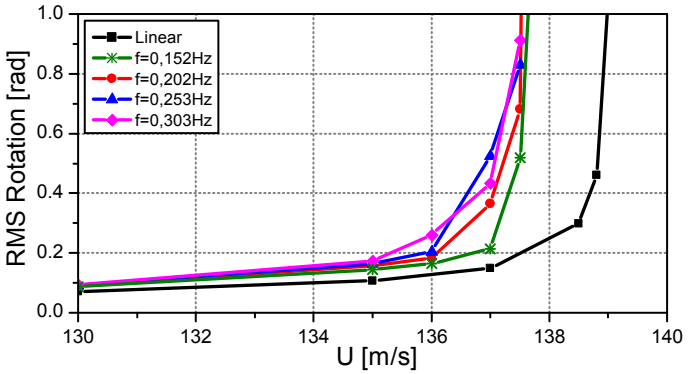

Fig. 70: RMS Torsional displacement – $\xi_{cr} = 1\%$ - Box section

In this case the results obtained assuming a structural damping of $\xi = 1\%$ present similar trend of those obtained with $\xi = 0{,}5\%$. In fact, in both cases the flutter threshold evaluated with the nonlinear approach is always smaller than the one calculated with the linear model. Moreover, using the proposed approach it is possible to define a unique value of the critical wind velocity since it does not depend on the choice of the cut-off frequency value.

A very important remark that can be carried out comparing the behaviour of the two different deck solution, is about the effects of turbulence on flutter stability. In fact it is possible to observed that for the girder solution the flutter thresholds tends to move towards higher, and so safer values; while in the second case the critical wind velocity assumes a lower value than that obtain with the linear approach. Even if it is not always possible to identify just one single value of the flutter wind velocity, the nonlinear model gives important information about the trend of the flutter threshold to move over or under the one calculated by means of the linear approach. In other word, this means that the effects of turbulence can be either stabilizing or destabilizing, and only the analysis performed by means of the nonlinear framework allow to understand which is the behaviour assumed by the structure under investigation.

6.10 Response analysis: 2D and 3D Models

In this section the differences between the results obtained using the sectional model and those obtained by means of the 3D model (MODEL 4) at several wind velocities are extensively investigated.

As first step, only buffeting loads are considered. The two following aspects have been investigated:

- comparison between 2D and 3D models in order to check the effects of higher structural modes on the global response;
- comparison between fully and partially correlated flow field by means of 3D analysis. Several authors have observed that buffeting forces are generally more correlated than the incident turbulent wind, anyway the span wise correlation of buffeting forces has been here assumed to be the same as the wind fluctuations in the approaching flow.

In Fig. 71 and Fig. 72 the RMS values of displacements obtained by means of sectional model analysis are compared with those obtained using the 3D model considering both fully and partially correlated buffeting load.

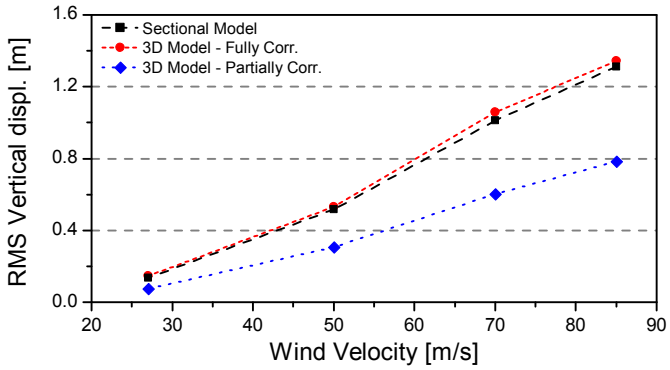

Fig. 71: RMS Vertical displacement – 2D vs. 3D Models – Buffeting load

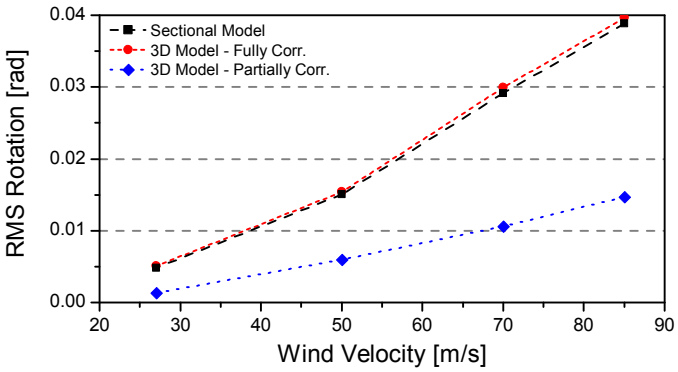

Fig. 72: RMS Torsional displacement – 2D vs. 3D Models – Buffeting load

The obtained results highlight the good agreement between 2D and 3D response analysis. A slightly higher response is detected for the 3D model, mainly due to the contribution of higher modes. This can be also detected looking at the spectral analysis of the structural response reported in Fig. 73 and Fig. 74 (these graph referred to a mean wind velocity of $U = 50m/s$ but similar results have been obtained also in correspondence of the other tested values). In particular in the spectral analysis of the structural response of the central point of the 3D model it is observed the presence of the second symmetric vertical mode in the global response. Anyway its contribution slightly influence the final results that can be well evaluated by means of the sectional model. This is mainly due to the fact that fully correlated flow excited only symmetrical modes, as can be observed looking at Fig. 74 and Fig. 76. Moreover, since the stays have been placed at the mid-point of the cross section, the effects of structural nonlinearities, in particular for the torsional motions are vanished.

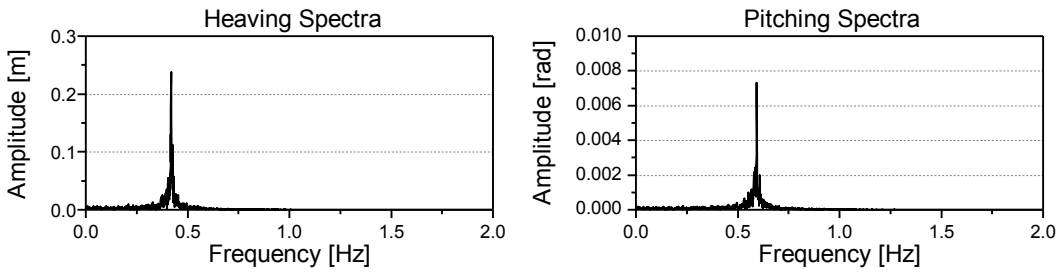

Fig. 73: Spectral response – Only buffeting load - Sectional model

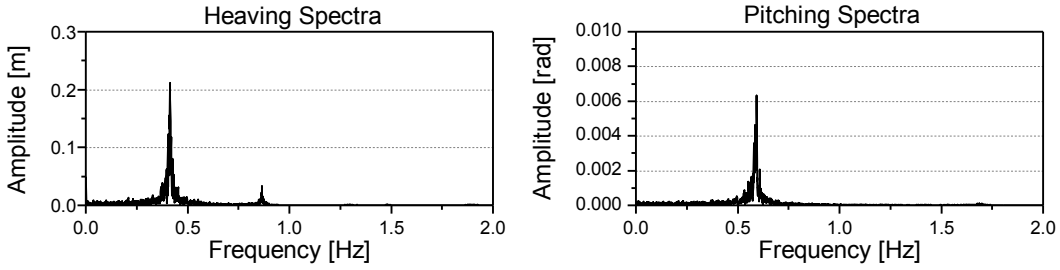

Fig. 74: Spectral response – 3D model fully correlated – Only buffeting load - Central point

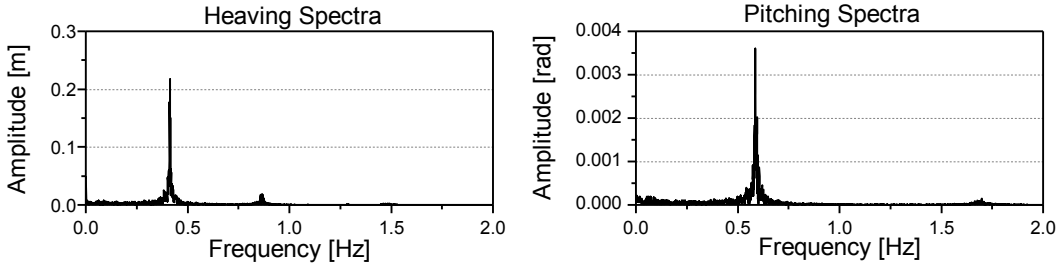

Fig. 75: Spectral response – 3D model partially correlated – Only buffeting load - Central point

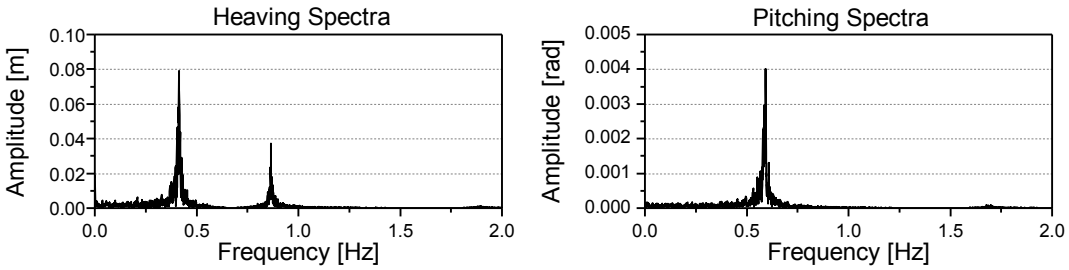

Fig. 76: Spectral response – 3D model fully correlated – Only buffeting load - Lateral point

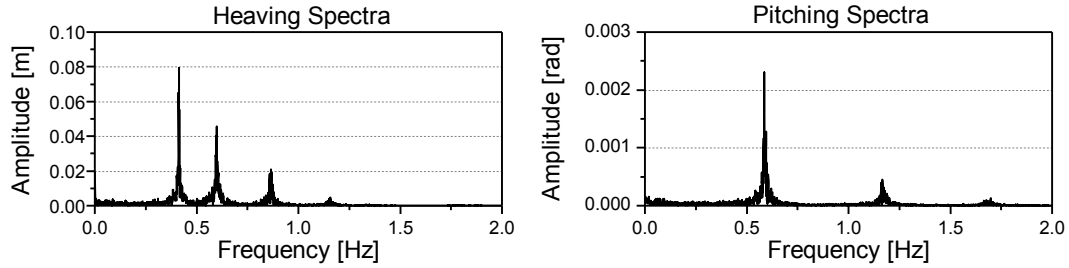

Fig. 77: Spectral response – 3D model partially correlated – Only buffeting load - Lateral point

Looking at Fig. 71 and Fig. 72 it is also possible to observe the differences between fully and partially correlated response analysis. In particular results with partial correlation of the flow exhibit slower displacement than those obtained when fully correlation is assumed. Looking at Fig. 74, Fig. 75 and Fig. 76, Fig. 77 a comparison between the spectral analysis of the structural response obtained with both fully and partially correlated flow ($U = 50m/s$) can be performed respectively for the central point of the bridge and the one placed at about a quarter of the span length (in correspondence of the second stay far from the pylons). Focusing on spectral graphs reported for the lateral point, it is possible to observe that the partially correlated flow excites not only the symmetric modes but also all the skew-symmetric ones. This results in a reduction of the total amount of structural displacements.

All the results above reported have been carried out considering only buffeting load. In the following analysis also the effects of aeroelastic forces are taken into account. In particular in Fig. 78 and Fig. 79 the RMS of displacements recorded at the mid-point of the bridge span are plotted when both fully and partially correlated wind flow are considered.

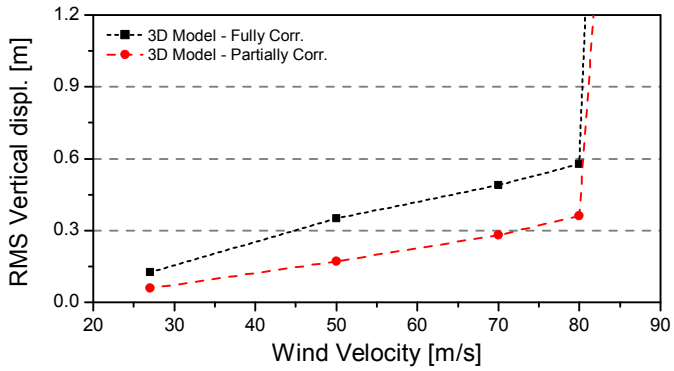

Fig. 78: RMS Vertical displacement – 2D vs. 3D Models – Aeroelastic and buffeting load

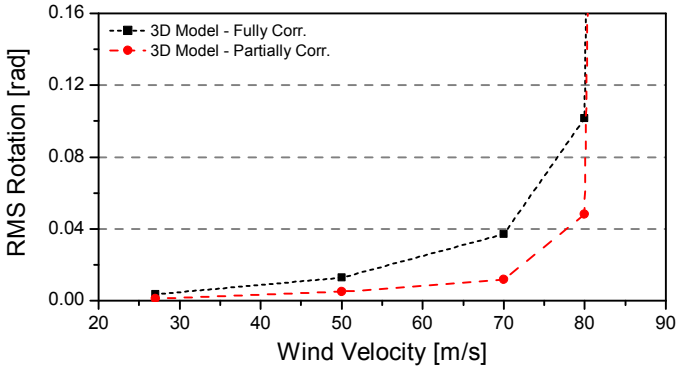

Fig. 79: RMS Torsional displacement – 2D vs. 3D Models – Aeroelastic and buffeting load

Also in this case the structural response obtained considering the flow partially correlated results lower than the one obtained with fully correlated field. The motivations are the same observed in the previous case when only buffeting load were considered, as can be checked looking at Fig. 80 until Fig. 83.

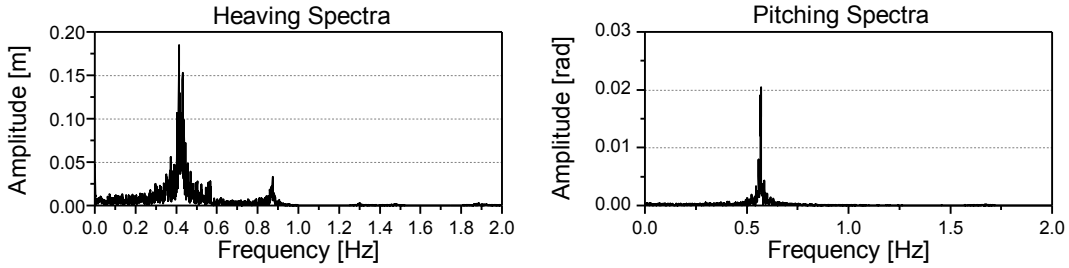

Fig. 80: Spectral response – 3D model fully correlated – Self-excited and buffeting load - Central point

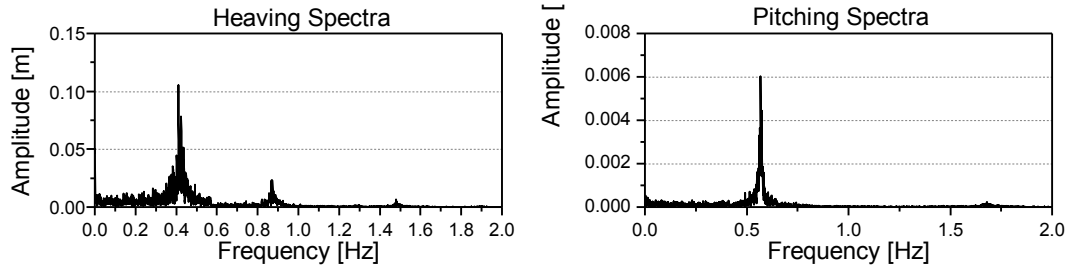

Fig. 81: Spectral response – 3D model partially correlated – Self-excited and buffeting load - Central point

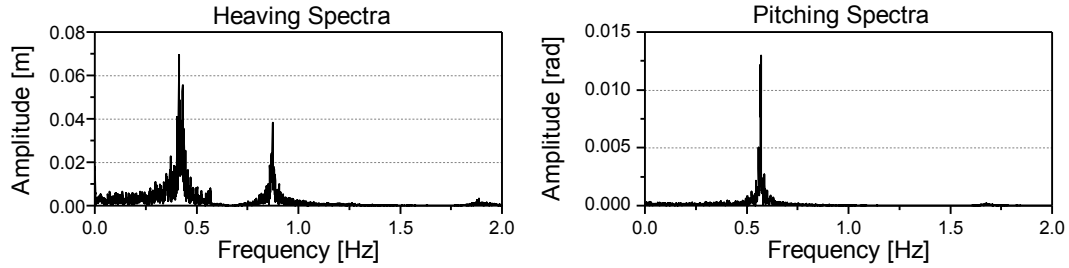

Fig. 82: Spectral response – 3D model fully correlated – Self-excited and buffeting load - Lateral point

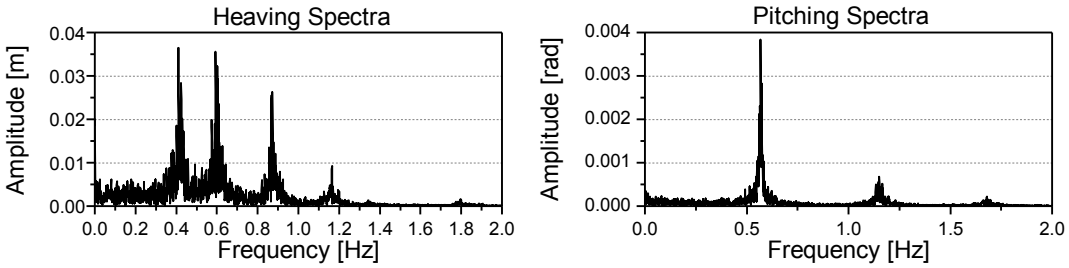

Fig. 83: Spectral response – 3D model partially correlated – Self-excited and buffeting load - Lateral point

Looking at the spectral graph above reported it is observed that fully correlated flow excites only symmetrical modes, while if partially correlated field is assumed, also the skew-symmetric modes are excited and this leads to a lower global response.

6.11 Nonlinear model: mixed problems

An interesting aspect which have been here investigated, is the evaluation of the structural response for wind velocity values lower than the critical one when load nonlinearities are taken into account.

For each wind velocity tested, the following three analysis have been performed:

- response analysis: only buffeting load
- mixed problems: buffeting and self-excited load
- mixed problems: buffeting load and self-excited forces evaluated by means of the proposed nonlinear model.

The main goal pursued is the investigation of possible differences between the linear and nonlinear approach when flutter condition is not yet developed. All the performed analysis have been carried out using the sectional model with the aerodynamic characteristics of the girder deck and a structural damping of $\xi_{cr} = 0.5\%$. Even if higher structural modes are not take into account, as pointed out in section 6.10 the obtained results can be considered representative of the global structural behaviour.

In Fig. 84 and Fig. 85 the RMS of vertical and torsional displacements of the analysis performed for the girder deck are reported.

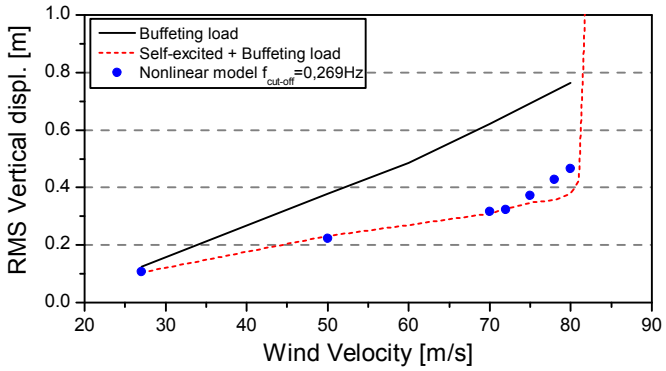

Fig. 84: RMS Vertical displacement – $\xi_{cr} = 0.5\%$ - Girder deck

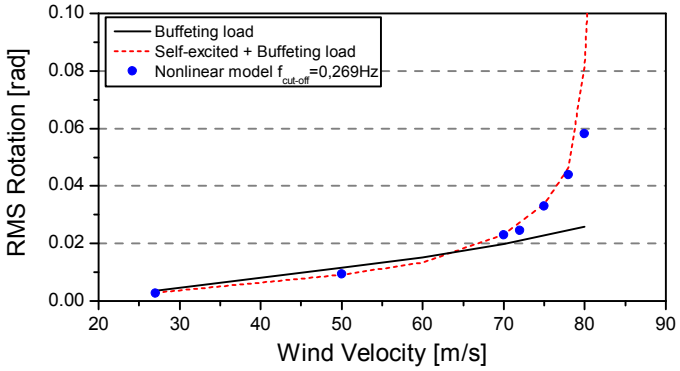

Fig. 85: RMS Torsional displacement – $\xi_{cr} = 0.5\%$ - Girder deck

The above reported graphs allow to compare the structural response obtained from the three different analysis carried out. In particular, it is possible to observed that, when the mean wind velocity value is small enough respect to the flutter wind speed, the vertical displacements are higher if only buffeting loads are considered. Conversely, the torsional displacement is a little bit higher if only buffeting load is adopted until when the wind velocity value becomes higher enough to make self excited forces predominant with respect to the buffeting ones.

Finally, it is observed that the results obtained evaluating the self-excited force components by means of the proposed nonlinear model are almost equal to those obtained using the linear approach.

The same analysis have been performed using the data of the box section and are reported in Fig. 86 and Fig. 87.

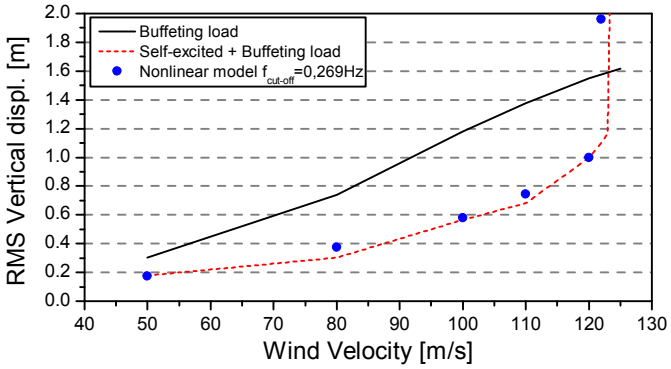

Fig. 86: RMS Vertical displacement – $\xi_{cr} = 0.5\%$ - Box section

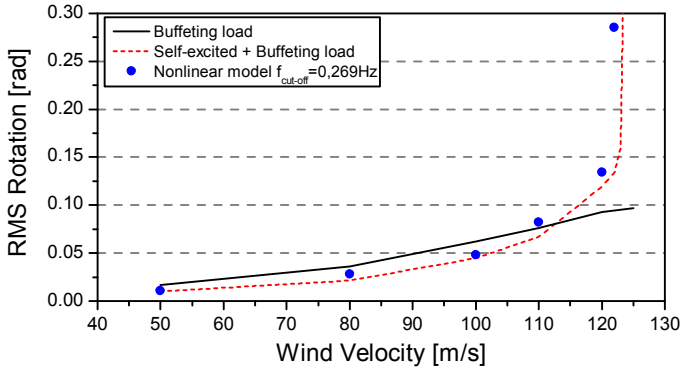

Fig. 87: RMS Torsional displacement – $\xi_{cr} = 0.5\%$ - Box section

Looking at the reported graph, the same consideration already reported for the case of the girder deck can be done. In particular it is remarked that the nonlinearities of self-excited forces do not affect too much the structural response when the mean wind velocity is lower enough than the critical one.

Chapter 7

Conclusions

In this work, the problem of the Aeolian risk assessment of long-span bridges has been investigated focusing on the structural vulnerability analysis. The main topic of the thesis is the development of an effective and reliable numerical model for the evaluation of wind induced loads. Among all of them, particular attention has been paid to the simulation of self-excited forces, whose knowledge is the basis for the investigation of the structural safety.

Afterwards, a comprehensive literature review of the most commonly adopted aeroelastic models is dealt with. In particular, two basic aspects have been highlighted: the first is the importance of modelling the frequency dependence of forces, the other is the strong sensitivity of flutter derivatives values with respect to the effective angle of incidence. In light of the current state of the art, an innovative nonlinear aerodynamic force model has been proposed. Its main attractive is the capability to take into consideration the dependence of the aeroelastic loads on both the aforementioned parameters. This issues may not be addressed by utilizing the previously presented classical linear aerodynamic force model.

Subsequently, a complete description of the computational framework developed to analyse the effects of wind load on bridges is addressed. In particular a three dimensional FE model is implemented allowing to take into account also of structural nonlinearities.

All the presented enhancements are applied to a real case study that is the bridge recently built in Italy over the Adige river in order to investigate the effects of loads nonlinearities on the overall bridge response. At first the evaluation of the flutter threshold has been performed, estimating the aeroelastic loads by means of classical linear force models. The comparison between results obtained in the frequency domain with those obtained in the time domain, as well as between 3D and 2D models have been carried out, observing a good agreement with each other. Then the nonlinear aeroelastic force model has been adopted to investigate the bridge deck stability by means of the sectional model. The aerodynamic behaviour of two different cross-sections are considered and a sensitivity analysis of the flutter threshold with respect to the cut-off frequency

parameter is investigated. Looking at the obtained results, it is observed a different trend of the critical wind velocity respect with the two considered sections: in one case the nonlinear approach leads to a reduction of flutter wind speed with a fixed value independent on the cut-off frequency ones; in the other instead, the structural stability shows its dependence on the choice of the cut-off frequency parameter with the tendency towards higher values of the flutter threshold. The different behaviour detected between the two cases analyzed can be mainly attribute to the particular trend of the derivative A_2, which, in the second case, exhibit a change from positive to negative values. This remark is confirmed by the results obtained in relation to different values of the structural damping. The obtained results have highlighted that the flutter threshold could move towards higher as well as lower values than that obtained with the classical linear model underling that the effects of turbulence on flutter stability can be both stabilizing or destabilizing. Moreover, even if it is not always possible to define a unique value of the critical wind velocity because of the sensitivity of results respect to the cut-off frequency parameter, it is always possible to get important information about the trend of flutter threshold to move or not towards safer values.

Subsequent to the assessment of the bridge stability, the evaluation of the structural response due to both self-excited and buffeting loads at not critical wind velocity values has been carried out. In this case the differences between results obtained with linear and nonlinear approach are negligible underlying the effectiveness of the classical linear approach for the investigation of the serviceability conditions.

The analysis of the aerodynamic behaviour of a bridge deck depends on both structural and aeroelastic parameters, as well as on their inter-relationship. In other words, the results obtain from the analysis of one specific structure are difficult to extend in a straightforward manner to other similar structures. However, based on the knowledge gained from the case study analyzed, some general conclusion can be drawn. The critical wind speed value estimated by classical linearized methods is generally quite reliable from a qualitative point of view. Nevertheless, when the aerodynamic characteristics of the bridge deck exhibit considerable sensitivity with respect to the effective angle of incidence the nonlinear aerodynamics may become significant. Particular care has to be given to those deck sections which presents the sign changing of the torsional aeroelastic damping coefficient.

Because of the particular case study investigated, the nonlinear model has been implemented and adopted only in the numerical framework of the sectional model. Anyway, in case of structures with a remarked nonlinear structural behaviour, the nonlinear load model can be easily introduced also in the three-dimensional framework.

Appendix I

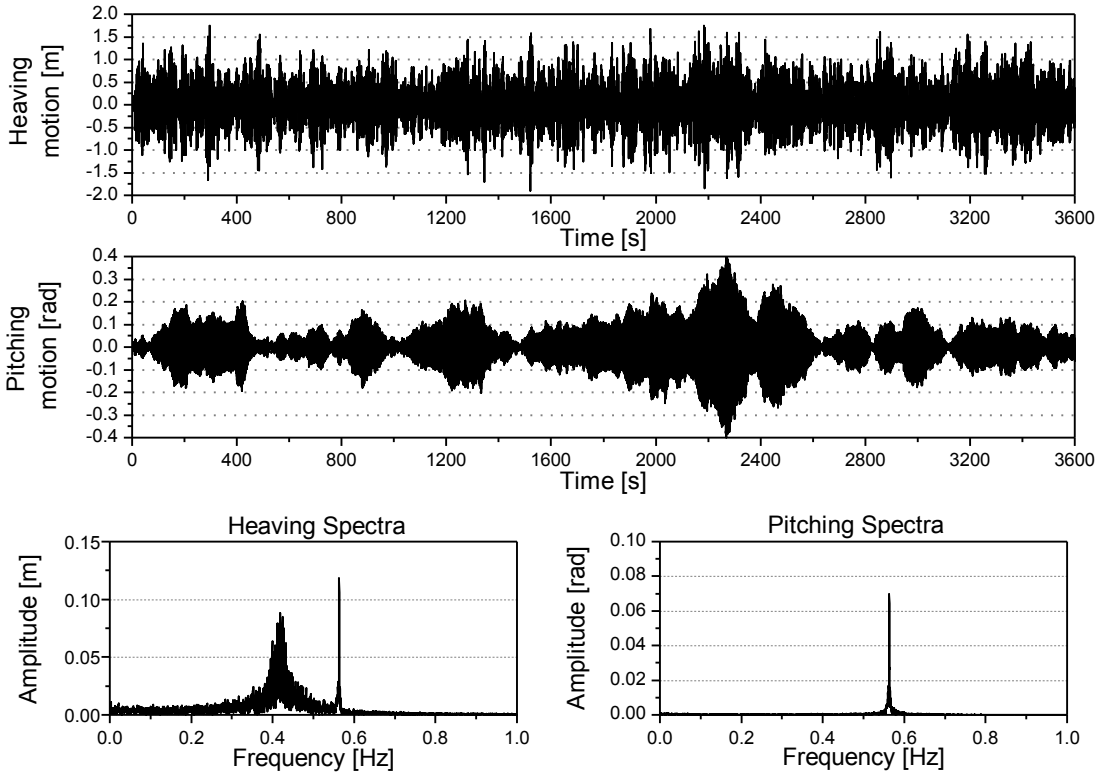

Fig. 88: Nonlinear analysis: mean wind velocity $U = 80\ m/s - f_{cut-off} = 0,135\ Hz$

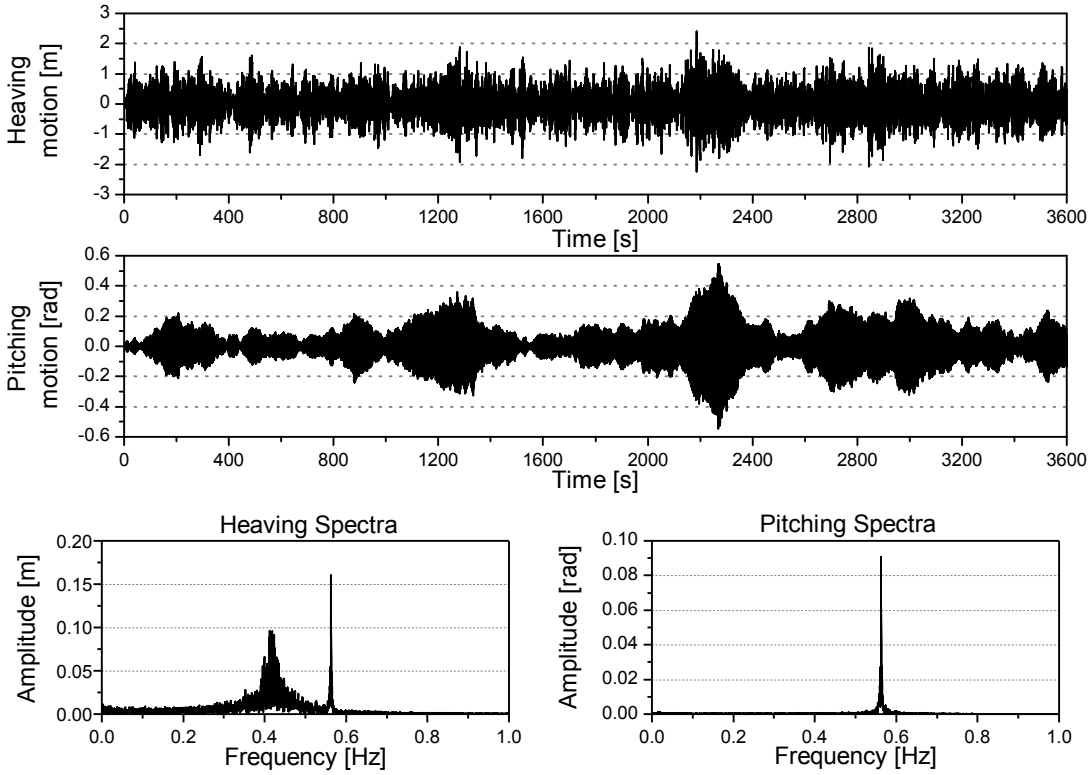

Fig. 89: Nonlinear analysis: mean wind velocity $U = 81\ m/s - f_{cut-off} = 0,135\ Hz$

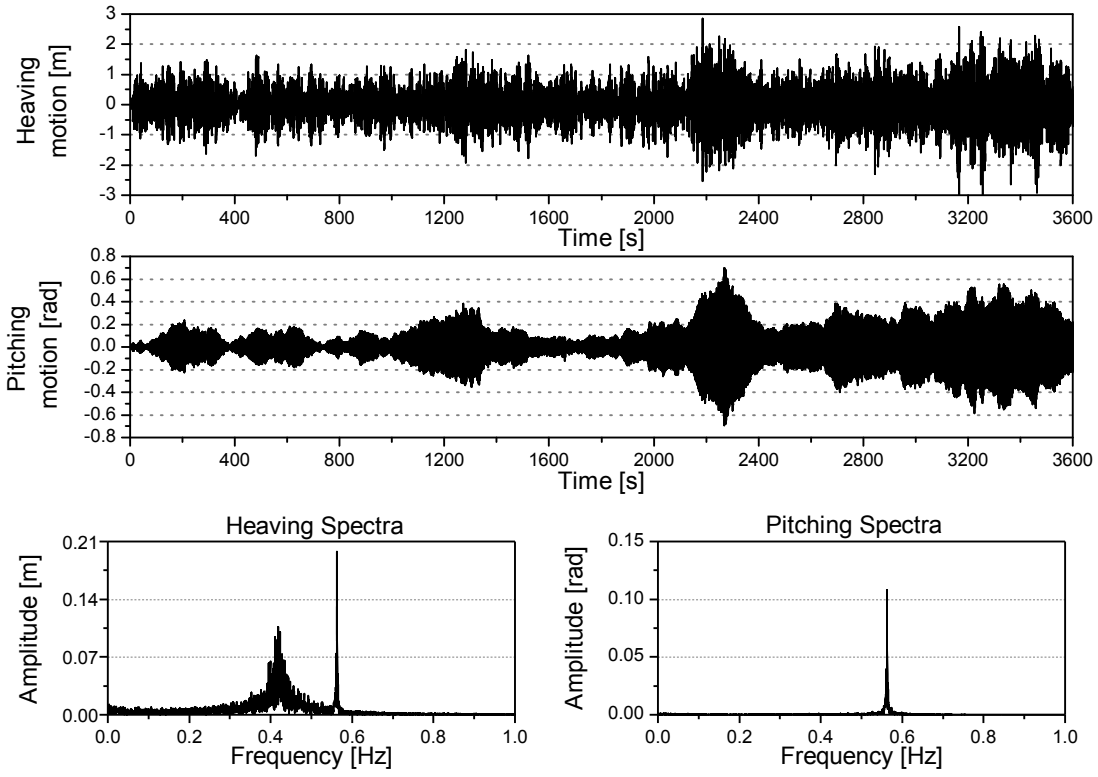

Fig. 90: Nonlinear analysis: mean wind velocity $U = 81.5\ m/s - f_{cut-off} = 0,135\ Hz$

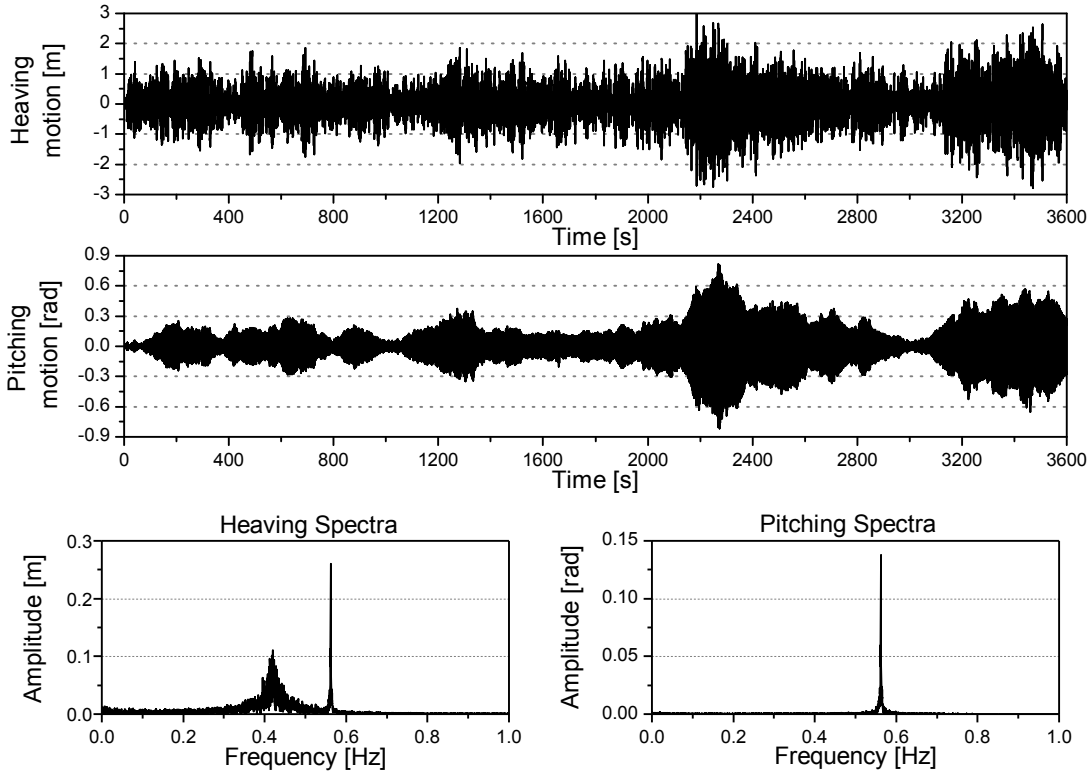

Fig. 91: Nonlinear analysis: mean wind velocity $U = 82\ m/s - f_{cut-off} = 0,135\ Hz$

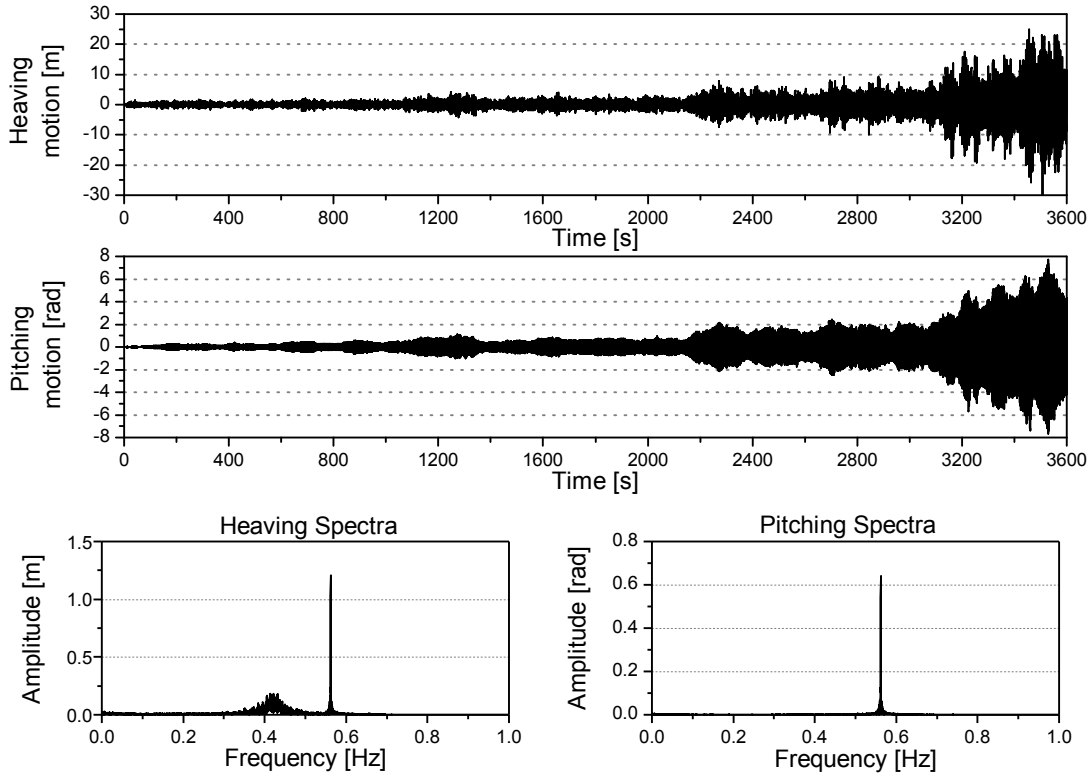

Fig. 92: Nonlinear analysis: mean wind velocity $U = 82.5\ m/s - f_{cut-off} = 0,135\ Hz$

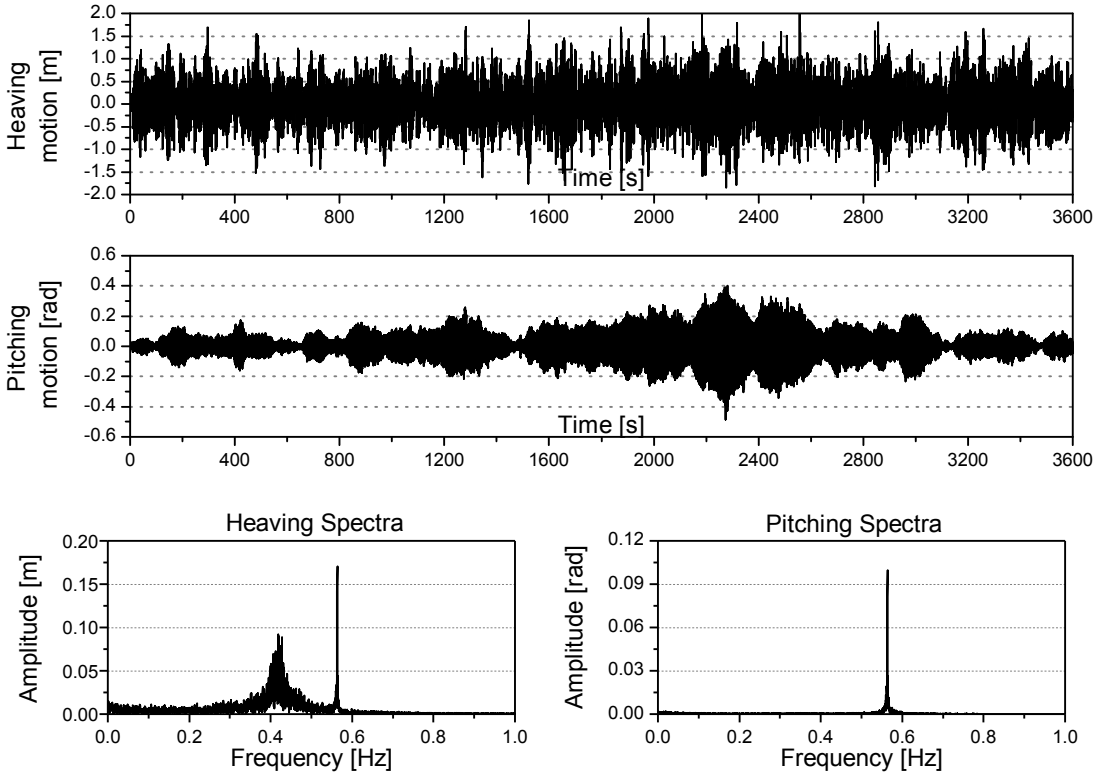

Fig. 93: Nonlinear analysis: mean wind velocity $U = 80\ m/s - f_{cut-off} = 0,135\ Hz$

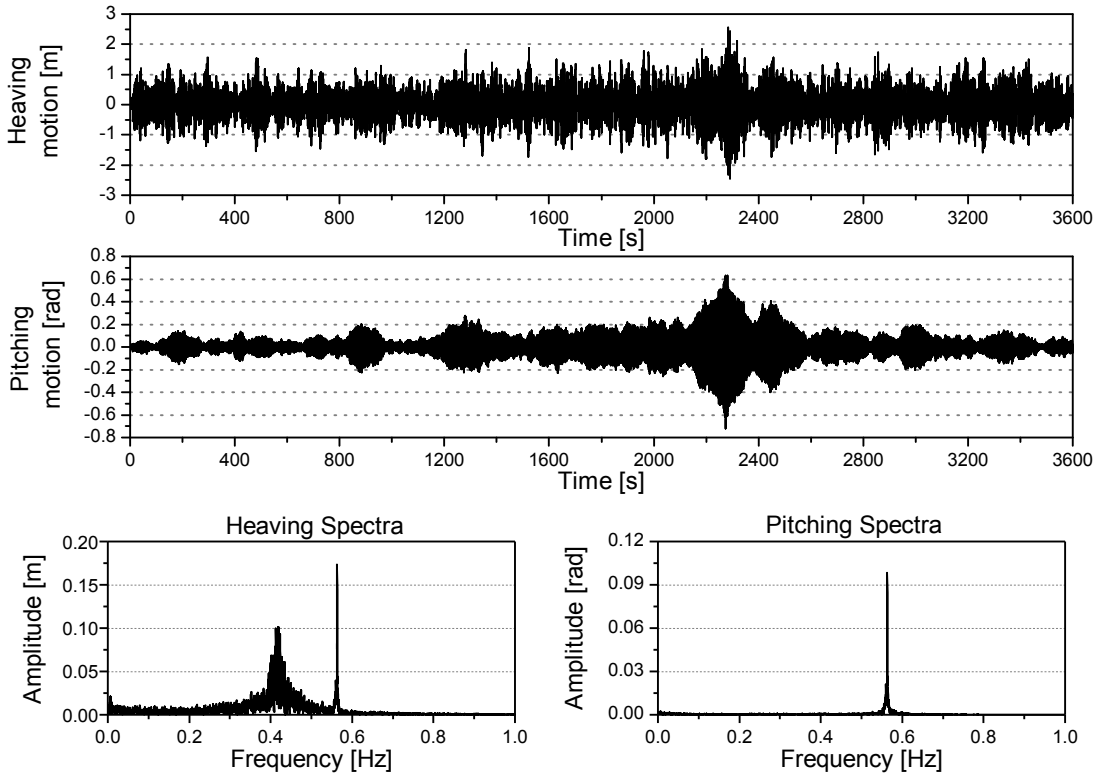

Fig. 94: Nonlinear analysis: mean wind velocity $U = 81\ m/s - f_{cut-off} = 0,180\ Hz$

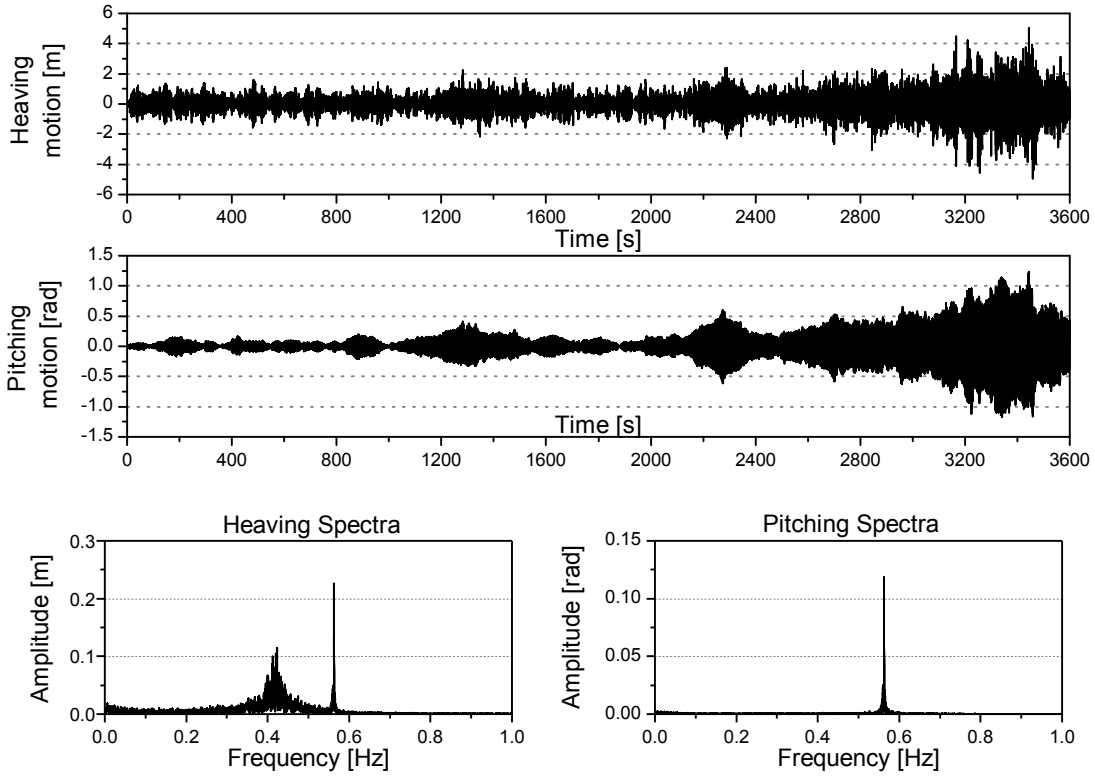

Fig. 95: Nonlinear analysis: mean wind velocity $U = 82\ m/s - f_{cut-off} = 0,180\ Hz$

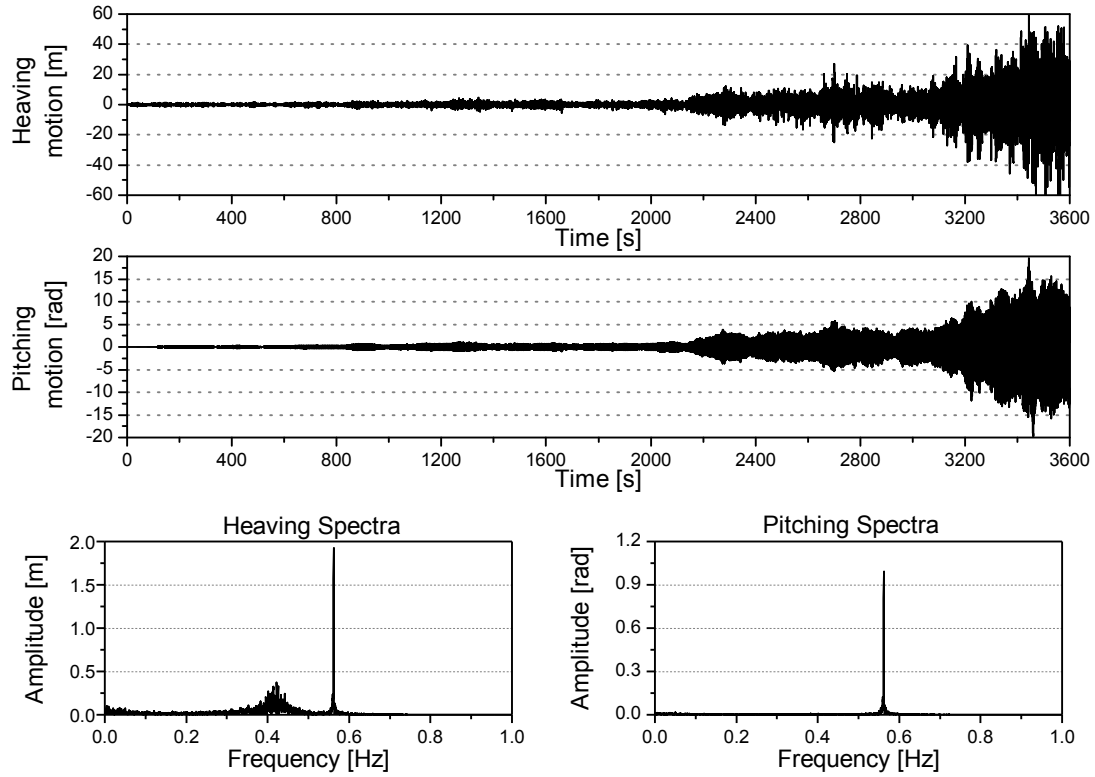

Fig. 96: Nonlinear analysis: mean wind velocity $U = 83\ m/s - f_{cut-off} = 0,180\ Hz$

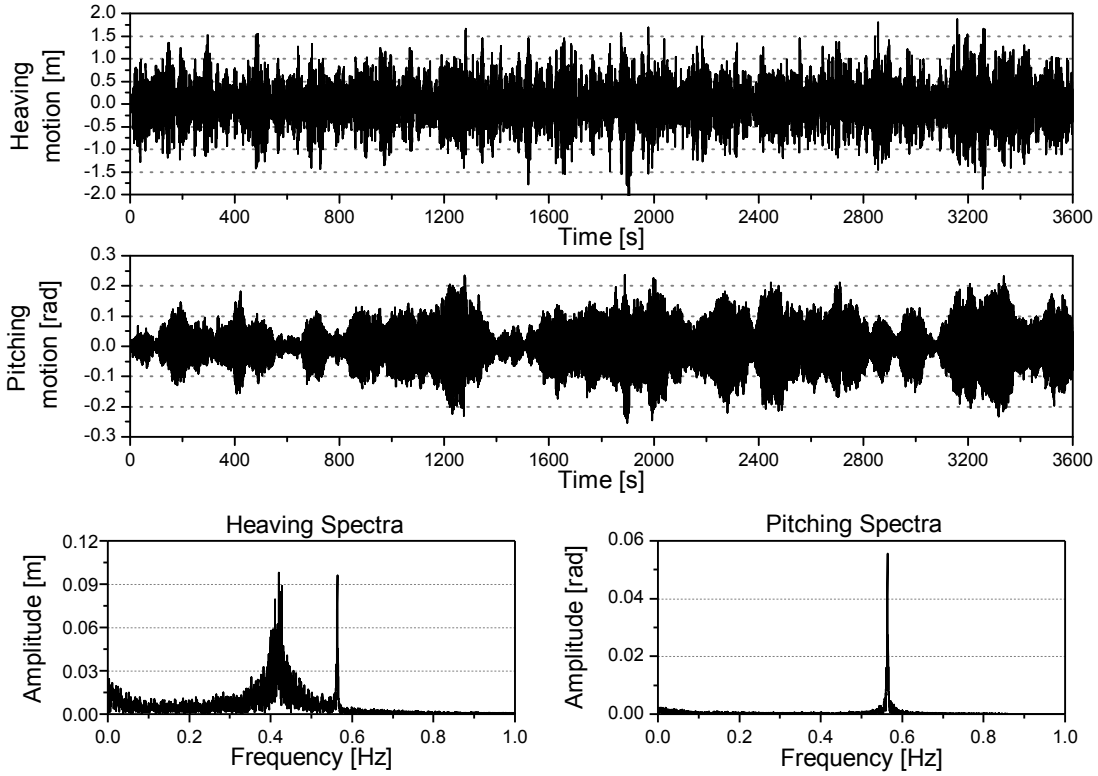

Fig. 97: Nonlinear analysis: mean wind velocity $U = 80\ m/s - f_{cut-off} = 0,224\ Hz$

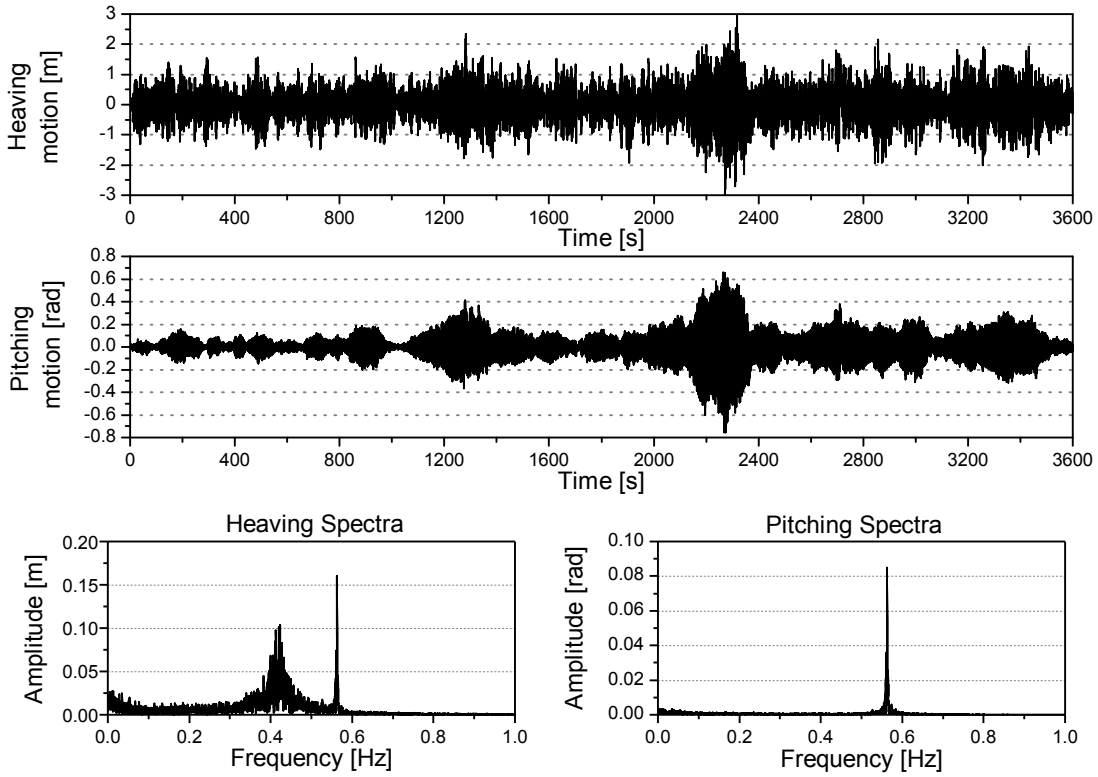

Fig. 98: Nonlinear analysis: mean wind velocity $U = 82\ m/s - f_{cut-off} = 0,224\ Hz$

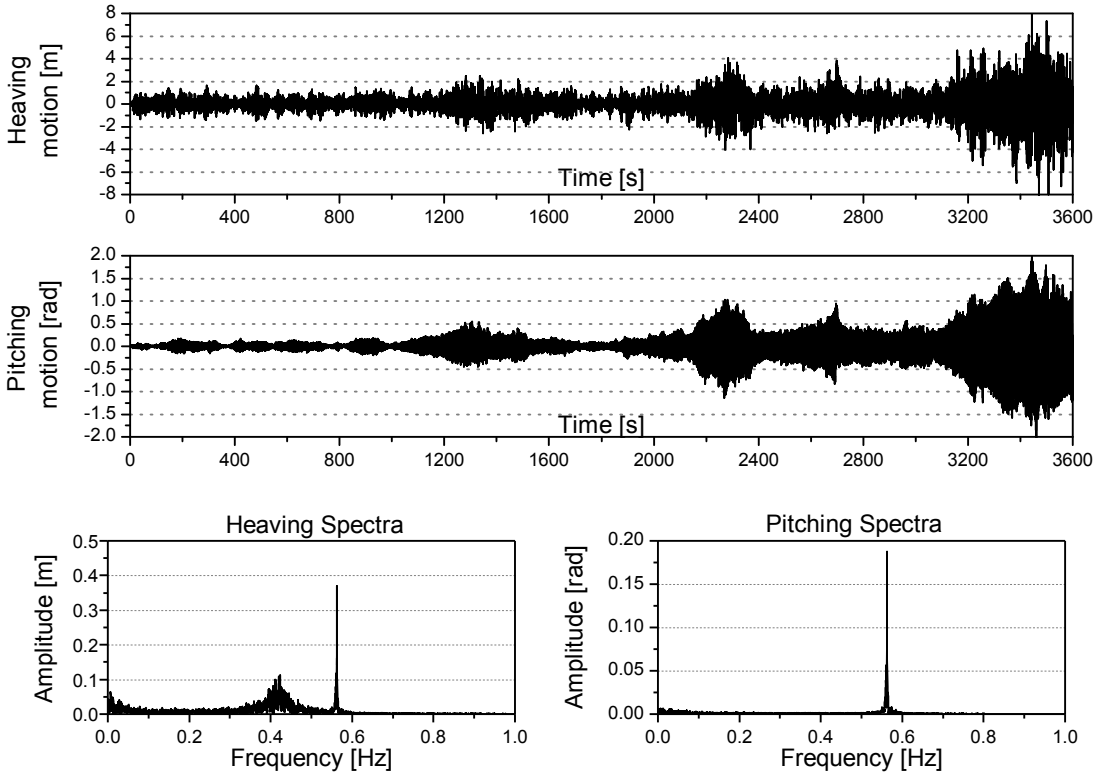

Fig. 99: Nonlinear analysis: mean wind velocity $U = 83\ m/s - f_{cut-off} = 0,224\ Hz$

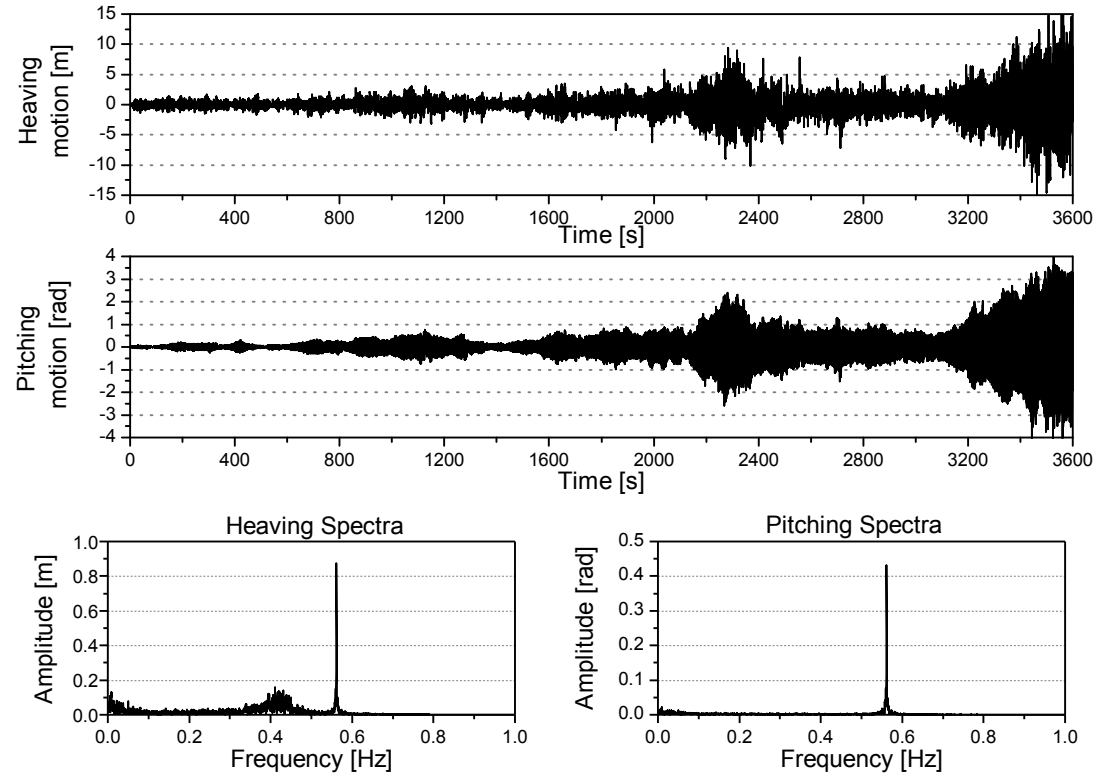

Fig. 100: Nonlinear analysis: mean wind velocity $U = 84\ m/s - f_{cut-off} = 0,224\ Hz$

Chapter 8

References

Agar. (1989). Aerodynamic flutter analysis of suspension bridges by a modal technique . *Engineering structures* , 75-82.

Augusti, Borri, & Niemann. (2001). Is aeolian risk as significant as other environmental risks? *Reliability Engineering & System Safety, 74* , 227-237.

Bartoli, & Mannini. (2008). A simplified approach to bridge deck flutter. *Journal of Wind Engineering and Industrial Aerodynamics, 96* , 229-256.

Bartoli, & Mannini. (2005). From multimodal to bimodal approach to flutter. *Proceedings of the 6th European Conference on Structural Dynamics*, (pp. 349-354). Rotterdam.

Bartoli, & Righi. (2006). Flutter mechanism for rectangular prism in smooth and turbolent flow. *Journal of Wind Engineering and Industrial Aerodynamics 94* , 275-291.

Bartoli, Borri, & Gusella. (1997). On the influence of wind turbulence on bridge deck flutter. In *Aspects in modern computational analysis* (pp. 3-17). Rotterdam: Meskouris & Wittek.

Berz. (2005). Windstorm and storm surges in Europe: loss trends and possible counter-actions from the viewpoint of an international reinsurer. *Philosophical transactions royal society of London series a mathematical physical and engineering science* , 1431-1440.

Bocciolone, Cheli, Curami, & Zasso. (1992). Wind measurements on the humber bridge and numerical simulations. *Journal of Wind Engineering and Industrial Aerodynamics, 41-44* , 165-173.

Borri, & Costa. (2004). Quasi-steady analysis of a two-dimentional bridge deck element. *Computers and Structures, 82* , 993-1006.

Bucher, & Lin. (1988). Stochastic stability of bridges considering coupled modes. *Journal of Engineering Mechanics, ASCE 114* , 2055–2071.

Cao, Xiang, & Zhou. (2000). Simulation of stochastic wind velocity field on long-span bridges. *Journal of Engineering Mechanics (ASCE), 126* , 1-6.

Caracoglia. (2008). Influence of uncertainty in selected aerodynamic and structural param on buffeting. *Journal of Wind Engineering and Industrial Aerodynamics, 96* , 327–344.

Caracoglia, & Jones. (2003b). A methodology for the experimental extraction of indicial functions for streamlined and bluff deck sections. *Journal of Wind Engineering an Industrial Aerodynamics, 91* , 371–402.

Caracoglia, & Jones. (2003a). Time domain vs. frequency domain characterization of aeroelastic forces for bridge deck sections. *Journal of Wind Engineering and Industrial Aerodynamics, 91* , 371–402.

Chen, & Kareem. (2002). Advances in modeling of aerodynamic forces on bridge deks. *Journal of Engineering Mechanics* , 1193-1205.

Chen, & Kareem. (2003). Aeroelastic analysis of bridges: effects of turbulence and aerodynamic nonlinearities. *Journal of engineering mechanics, 129* , 885-895.

Chen, & Kareem. (2001). Nonlinear responce analysis of long-span bridges under turbulent winds. *Journal of Wind Engineering and Industrial Aerodynamics* , 1335-1350.

Chen, Kareem, & Haan. (2000). Nonlinear aerodynamic analysis of bridges under turbulent winds: the new frontier in bridge aerodynamics. *Proceedings of the international conference on advances in structural dynamics*, (pp. 475-482). Hong Kong.

Chen, Matsumoto, & Kareem. (2000b). Time domain and buffeting response analysis of bridges. *Journal of Engineering Mechanics, 126* , 7-16.

Chen, Matzumoto, & Kareem. (2000a). Aerodynamic Coupling Effects on Flutter and Buffeting of Bridges. *Journal of Engineering Mechanics, ASCE* , 17-26.

Cicada, Falco, & Zasso. (2001). Development of new systems to measure the aerodynamic forces in section models in wind tunnel testing. *Journal of Wind Engineering and Industrial Aerodynamics 89* , 725-746.

Cigada, Diana, & Zappa. (2002). On the response of a bridge deck to turbulent wind: a new approach. *Journal of Wind Engineering and Industrial Aerodynamics, 90* , 1173-1182.

Clough, & Penzien. (1993). *Dynamics of Structures.* New York: McGraw-Hill.

CNR, I. (2008). *Istruzioni per la valutazione delle azioni e degli effetti del vento sulle costruzioni.*

Costa, Borri, Flamand, & Grillaud. (2007). Time-domain buffeting simulations for wind-bridge interaction. *Journal of Wind Engineering and Industrial Aerodynamics, 95* , 2073–2086.

Counihan. (1975). Adiabatic atmospheric boundary layers: a review and analysis of data from the period 1880-1972. *Atmospheric Environment 9* , 871-905.

CRED. (n.d.). Retrieved from CRED - Centre for Research on the Epidemiology of Disasters: http://www.cred.be/

Dadvand. (2007). *"A framework for developing finite element codes for multi-disciplinary applications.* UPC Barcelona: doctoral thesis.

Davenport. (1962). Buffeting of a suspension bridge by storm winds. *Journal of Structural Engineering, ASCE 88* , 233-268.

Davenport. (1961). The application of statistical concepts to the wind loading of structures. *Proceedings of Institution of civil engineers* , 449-472.

Deodatis. (1996). Simulation of ergodic multivariate stochastic processes. *Journal of Engineering Mechanics (ASCE), 122* , 778-787.

Diana, Bruni, & Rocchi. (2005). A numerical and experimental investigation on aerodynamic non linearities in bridge response to turbulent wind. *The Fourth European & African Conference on Wind Engineering, EACWE4*, (pp. 1-10). Prague.

Diana, Bruni, Cigada, & Zappa. (2002). Complex aerodynamic admittance function role in buffeting response of a bridge deck. *Journal of Wind Engineering and Industrial Aerodynamics, 90* , 2057-2072.

Diana, Cheli, Bruni, Collina, & Larose. (1993). Compairson between wind tunnel test on a full aeroelastic model of the proposed Messina Bridge and numerical results: Part II. *Proceeding of the 3rd Asia-Pacific Symposium on Wind Engineering*, (pp. 137-142). Hong Kong.

Diana, Cheli, Zasso, Collina, & Brownjohn. (1992). Suspension bridge parameter identication in full-scale tests. *Journal of Wind engineering and Industrial Aerodynamcis, 41-44* , 165-176.

Diana, Cheli, Zasso, Collina, & Bruni. (1998). Aerodynamic design of very long-span suspension bridges . *IABSE Symposium*, (pp. 115-128). Kobe.

Diana, Falco, Bruni, Cigada, & Collina. (1994). Risposta di un ponte a grande luce al vento turbolento: confronto tra simulazioni numeriche e risultati sperimentali. *Proceedings of the third IN-VENTO congress.* Rome.

Diana, Resta, & Rocchi. (2008). A new numerical approach to reproduce bridge aerodynamic non-linearities in time domain. *Journal of Wind Engineering and Industrial Aerodynamics, 96* , 1871-1884.

Diana, Resta, Zasso, Belloli, & Rocchi. (2004). Forced motion and free motion aeroelastic tests on a new concept dynamometric section model of the Messina suspension bridge. *Journal od Wind Engineering and Industrial Aerodynamics 92* , 441-462.

Diana, Rocchi, Argentini, & Muggiasca. (2010). Aerodynamic instability of a bridge deck section model: Linear and nonlinear approach to force modeling. *Journal of Wind Engineering and Industrial Aerodynamics, 98* , 363-374.

Dung, Miyata, & Yamada. (1998). Flutter response in long-span bridges with wind-induced displacement by the mode tracing method. *Journal of Wind Engineering and Indistrial Aerodynamics 77-78* , 367-379.

Dyrbye, & Hansen. (1997). *wind loads on structures.* John Wiley & Sons, First Edition.

Ehsan, & Bosch. (1989). Modelling of the effect of spanwise coherence of aerodynamic forces on full-bridge response. *Proceedings of the 20th Joint Meeting of the US-Japan Cooperative Program in Natural Resources Panel on Wind and Seismic Effects*, (pp. 3–17). Washington.

Ehsan, & Scanlan. (1990). Vortex-induced vibrations of flexible bridges. *Journal of Engineering Mechanics ASCE 116* , 1392–1411.

Falco, Gasparetto, & Scaramelli. (1978). *Ricerca sul comportamentoaeroelastico dei ponti sospesi a grande luce.*

Garrick. (1938). *some reciprocal relations in the theory of nonstationary flows.* (NACA) Technical Report 629.

Ge, & Tanaka. (2000). Aerodynamic flutter analysis of cable-supported bridges by multi-mode and fullmode approaches. *Journal of Wind Engineering and industrial Aerodynamics, 86* , 125-153.

GID. (n.d.). Retrieved from GID - The personal pre e post processor: http://gid.cimne.upc.es/

Haan, & Kareem. (2009). Anatomy of turbulence effects on the aerodynamics of an oscillating prism. *Journal of Engineering Mechanics, ASCE,* , 987-999.

Haan, Kareem, & Szewczyk. (1998). The e¤ects of turbulence on the pressure distribution around a rectangular prism. *Journal of Wind Engineering and Industrial Aerodynamics, 77&78* , 381-392.

Hann. (2000). *The effects of turbulence on the aerodynamics of long-span bridges.* University of Notre Dame: PhD Dissertation.

Harris. (1968). *On the spectrum and auto-correlation function of gustiness in high winds.* Electrical Research Association - Report 5273.

Hatanaka, & Tanaka. (2002). New estimation method of aerodynamic admittance function. *Journal of Wind Engineering and Industrial Aerodynamics, 90* , 2073–2086.

Holmes. (2001). *Wind loading of structures.* Taylor & Francis.

Irwin. (1978). *Further investigations of a full aeroelastic model of Lions' Gate Bridge, Report LTR-LA-221.* Ottawa: National Research Council of Canada.

Jones. (1940). *The unsteady lift on a wing of finite aspect ratio.* (NACA) Technical Report 681.

Jones, & Scanlan. (2001). Theory and full-bridge modelling of wind response of cable-supported bridges. *Journal of Bridge Engineering, ASCE 6* , 365-375.

Kaimal, & Finnigan. (1995). *Atmospheric boundary layer flows, their structure and measurement.* Oxford University press.

Kaimal, Wyngaard, Izumi, & Coté. (1972). Spectral characteristics of surface-layer turbulence. *Quarterly journal of surface-layer turbulence, 98* , 563-589.

KRATOS-Wiki. (n.d.). Retrieved from Free multiphysic finite element method C++ open source code.: http://kratos.cimne.upc.es/kratoswiki/index.php/Main_Page.

Larose. (1999). Experimental determination of the aerodynamic admittance of a bridge deck segment. *Journal of Fluids and Structures, 13* , 1029-1040.

Larose, & Mann. (1998). Gust loading on streamlined bridge decks. *Journal od fluids and Structures, 12* , 511-536.

Lazzari. (2005). Time domain modeling of aeroelastic bridge decks: a comparative study and an application. *International Journal for Numerical Methods in Engineering 62* , 1064-1104.

Li, & Kareem. (1990). ARMA representation of wind field. *Journal of wind engineering and industrial aerodynamics, 36* , 415-427.

Lin, & Yang. (1983). Multimode bridge responce to wind excitations. *Journal of Engineering Mechanics, ASCE, 109* , 586-603.

Mannini. (2006). *Flutter vulnerability assessment of flexible bridges.* University of Florence: PhD Dissertation.

Matsumoto, Yagu, Ishizaki, Shitato, & Chen. (1998). Aerodynamic stability of 2-edge girders for cable-stayed bridge. *Proceedings of 15th National Symposium on Wind Engineering*, (pp. 389-394). Tokyo.

Miyata, Yamada, Boonyapinyo, & Santos. (1995). Analytical investigation on the responce of a very long suspension bridge under gusty wind. *Proceedings of Ninth ICWE, Vol.2*, (pp. 1006-1017). New Delhi.

Nakamura. (1993). Bluff-body aerodynamics and turbulence. *Journal of Wind Engineering and Industrial Aerodynamics, 49* , 65-78.

Namini. (1992). Finite element-based flutter analysis of cable-suspended bridge. *Journal of Structural Engineering, ASCE 118* , 1509-1526.

Olesen, Larsen, & Hojstrup. (1984). Modelling velocity spectra in the lower part of the planetary boundary layer. *Boundary-Layer Meteorology 29* , 285-312.

Olivato. (2010). *Managing wind risk on long span roofs.* University of Florence: PhD Dissertation.

Oudheusden, v. (2000). Aerodynamic stiffness and damping effects in the rational galloping of a rectangular cross-section. *Journal of Fluids Structures* , 1119-1144.

Panofsky, & Dutton. (1984). *Atmospheric Turbolence, models and methods for engineering applications.* Wiley International.

Parry. (2007). *Climate Change 2007: impacts, adaptation and vulnerability.* Cambridge University Press.

Paulotto, Ciampoli, & Augusti. (2004). Some proposal for a first step towards a Performance Based Wind Engineering. *Proceedings of 1st International Forum in Engineering Decision Making*, (pp. 5-9). Stoos, Switzerland.

Peil, & Kirch. (2008). Approximation of unsteady aerodynamic derivatives by rational function. *EURODYN - 7th European Conference on Structural Dynamics.* Southampton.

Petrini. (2009). *A probabilistic approach to Performance-Based Wind Engineering (PBWE).* University of Rome "La Sapienza": PhD Dissertation.

Petrini, Giuliani, & Bontempi. (2007). Comparison of time domain techniques for the evaluation of the response and stability in long span suspension bridges. *Computer and Structures 85* , 1032-1048.

Pliefke, Sperbeck, Urban, Peil, & Budelmann. (2007). A standardized methodology for managing disaster risk - An attempt to remove ambiguity. *5th International Probabilistic Workshop.* Ghent, Belgium.

RIANOVOSTI. (2010, 05 25). *Signs of oscillation keep Russia's wobbling bridge closed.* Retrieved from http://en.rian.ru/russia/20100525/159143749.html

Ricciardelli, & Marra. (2008). Sectional aerodynamic forces and their longitudinal correlation on a vibrating 5:1 rectangular cylinder. *6th International Colloquium On Bluff Body Aerodynamics & Applications.* Milan.

Ricker. (2003). *Echo Signal Processing.* Massachusetts.

Rossi, Lazzari, & Vitaliani. (2004). Wind field simulation for structural engineering purposes. *International Journal for Numerical Methods in Engineering, 61* , 738-763.

Salvatori, & Borri. (2007). Frequency- and time-domain methods for the numerical modeling of full-bridge aeroelasticity. *Computers and Structures, 85* , 675-687.

Samaras, Shinozuka, & Tsurui. (1983). ARMA representation of random processes. *Journal of Engineering Mechanics, 111* , 449-461.

Sarpkaya. (1979). Vortex-induced oscillations; a selective review. *Journal of Applied Mechanics, ASME, 46* , 241–258.

Scanlan. (1993). Problematics in formulation of wind-force models for bridge decks. *Journal of Engineering Mechanics Division, ASCE 119* , 1353–1375.

Scanlan, & Jones. (1990). Aeroelastic analysis of cable-stayed bridge. *Journal of Structural Engineering, ASCE, 116* , 279-297.

Scanlan, & Lin. (1978). Effects of turbulence on bridge flutter derivatives. *Journal of Engineering Mechanics, ASCE, 104* , 719-733.

Scanlan, & Tomoko. (1971). Airfoil and bridge deck flutter derivatives. *Journal of Engineering Mechanics, ASCE 97* , 1717-1737.

Scanlan, Béliveau, & Budlong. (1974). Indicial aerodynamic functions for bridge decks. *Journal of Engineering Mechanical Division, ASCE 100* , 657/673.

Shahrzad, & Mahzoon. (2002). Limit cycle flutter of airfoils in steady and unsteady flows. *Journal of Sound and Vibration, 256* , 213-225.

Shinozuka. (1974). Digital simulation of random processes in engineering mechanics with the aid of FFT technique. *Stochastic problems in mechanics* , 277-286.

Shinozuka. (1970). Simulation of multivariate and multidimentional random processes. *Journal of Acoustic Society of America, 49* , 357-368.

Shinozuka, & Deodatis. (1991). Simulation of stochastic processes by spectral representation. *Applied Mechanics Reviews,44* , 191-204.

Shinozuka, & Jan. (1972). Digital simulation of random processes and its applications. *Journal of Sound and Vibration, 25* , 111-128.

Simiu, & Scanlan. (1996). *Wind effects on Structures.* New York.

Solari. (1987). Turbulence modelling for gust loading. *Journal of Structural Engineering ASCE, vol. 113, no 7* , 1550-1569.

Stecca. (2008). *Aeroelastic study of a bridge cross-section.* University of Padua: Master thesis.

Stoyanoff. (2001). A unified approach for 3D stability and time domain response analysis with application of quasi-steady theory. *Journal of Wind engineering and Industrial Aerodynamics, 89* , 1591-1606.

Su, Fan, & He. (2007). Wind-inuced vibration analysis of a cable-stayed bridge during erection by a modified time-domain method. *Journal of Sound and Vibration, 303* , 330-342.

Tanaka, Yamamura, & Tatsumi. (1992). Coupled mode flutter analysis using flutter derivatives. *Journal of Wind Engineering and Industrial Aerodynamics 41-44* , 1279-1290.

Theodorsen. (1935). *General theory of aerodynamic instability and the mechanism of flutter.* NACA, Technical Report 496.

Tiffany, & Adams. (1988). *Nonlinear programming extensions to rational function approximation methods for unsteady aerodynamic forces.* NASA Technical Paper 2776.

Tubino. (2005). Relationships among aerodynamic admittance functions, flutter derivatives and static. *Journal of Wind Engineering and Industrial Aerodynamics, 93* , 929–950.

Van der Hoven. (1957). Power spectrum of horizontal wind speed in the frequency range 0.0007 to 900 cycles per hour. *Journal of meteorology 14* , 160-164.

von Karman. (1948). Progress in the statistical theory of turbulence. *Proceedings of the National Academy of Sciences 34* , 530-539.

Vos, Rodriguez, Below, & Guha-Sapir. (2010). *Annual Disaster Statistical Review 2009.* Brussels.

Zasso. (1996). Flutter derivatives: Advantages of a new representation convention. *Journal of Wind Engineering and Industrial Aerodynamics 60* , 35-47.

Zhang, Xiang, & Sun. (2002). Nonlinear aerostatic and aerodynamic analysis of long-span suspension bridges considering wind-structure interactions. *Journal of Wind Engineering and Industrial Aerodynamics, 90* , 1065–1080.